Modeling Fiber Orientation using Empirical Parameters Obtained from Non-Lubricated Squeeze Flow for Injection Molded Long Carbon Fiber Reinforced Nylon 6,6

Kennedy Rose Boyce

Dissertation submitted to the faculty of the Virginia Polytechnic Institute and State University in partial fulfillment of the requirements for the degree of

Doctor of Philosophy

in

Chemical Engineering

Donald G. Baird, Chair
Michael J. Bortner
Stephen M. Martin
Scott W. Case

10 February 2021
Blacksburg, VA

Keywords: Long Carbon Fiber, Fiber Aspect Ratio, Fiber Orientation, Squeeze Flow, Injection Molding

Modeling Fiber Orientation using Empirical Parameters Obtained from Non-Lubricated Squeeze Flow for Injection Molded Long Carbon Fiber Reinforced Nylon 6,6

Kennedy Rose Boyce

Abstract

Long fiber reinforced thermoplastic composites are used for creating lightweight, but mechanically sound, automotive components. Injection molding is a manufacturing technique commonly used for traditional thermoplastics due to its efficiency and ability to create complex geometries. Injection molding feedstock is often in the form of pellets. Therefore, fiber composites must be chopped for use in this manufacturing method. The fibers are cut to a length of 13 mm and then fiber attrition occurs during processing. The combination of chopping the fibers into pellets and fiber breakage creates a distribution of mostly short fiber lengths, with some longer fibers remaining. Discontinuous fiber reinforcements are classified as long for aspect ratios greater than 100. For glass fibers, that distinction occurs at a length of 1 mm, and for carbon fibers 0.5 mm. Traditional composite materials and manufacturing processes utilize continuous fibers with a controlled orientation and length. The use of chopped discontinuous fibers requires a method to predict the orientation of the fibers in the final molded piece because mechanical properties are dependent on fiber length and orientation. The properties and behavior of the flow of a fiber reinforced polymer composite during molding are directly related to the mechanical properties of the completed part. Flow affects the orientation of the fibers within the polymer matrix and at locations within the mold cavity. The ability to predict, and ultimately control, flow properties allows for the efficient design of safe parts for industrial uses, such as vehicle parts in the automotive industry.

The goal of this work is to test material characterization techniques developed for measuring and predicting the orientation of fiber reinforced injection molded thermoplastics using commercial grade long carbon fiber (LCF) reinforced nylon 6,6 (PA 6,6). Forty weight percent LCF/PA 6,6 with a weight averaged fiber length of 1.242 mm was injection molded into center gated disks and the orientation was measured experimentally. A Linux based Numlab flow simulation process that utilizes the finite element method to model the flow and orientation of fiber reinforced materials
was tested and modified to accurately predict the orientation for this composite and geometry. Fiber orientation models used for prediction require the use of empirical parameters. A method of using non-lubricated squeeze flow as an efficient way to determine the strain reduction factor, α, and Brownian motion like factor, C_I, parameters for short glass fiber polypropylene orientation predictions using the strain reduction factor (SRF) model was extended to use with the LCF/PA 6,6 composite. The 40 weight percent LCF/PA 6,6 material was compression molded and underwent non-lubricated squeeze flow testing. The flow was simulated using finite element analysis to predict the fiber orientation using the SRF model. The empirical parameters were fit by comparing the simulated orientation to experimentally measured orientation. This is a successful method for predicting orientation parameters that is significantly more efficient than optimizing the parameters based on fitting orientation generated in injection molded pieces. The determined orientation parameters were then used to reasonably predict the fiber orientation for the injection molded parts. The authors proved that the experimental and simulation techniques developed for the glass fiber reinforced polypropylene material are valid for use with a different, more complex material.

Modeling Fiber Orientation using Empirical Parameters Obtained from Non-Lubricated Squeeze Flow for Injection Molded Long Carbon Fiber Reinforced Nylon 6,6

Kennedy Rose Boyce

General Audience Abstract

Fibers reinforce thermoplastic polymers to create lightweight, but mechanically sound, automotive parts. Thermoplastics flow when heated and harden when cooled. This work compares two of the commonly used thermoplastics, polypropylene (plastic grocery bags, food storage containers) with a glass fiber reinforcement and a form of nylon called PA 6,6 with a carbon fiber reinforcement. Injection molding is a manufacturing technique commonly used for un-reinforced thermoplastics due to its efficiency and ability to create complicated shapes. Injection molding feedstock is often in the form of pellets. Therefore, fiber composites must be chopped for use in this manufacturing method. The fibers are cut to a length of 13 mm and then fiber breakage occurs in the injection molder. The combination of chopping the fibers into pellets and fiber breakage creates a range of lengths. This distribution consists of mostly short fiber lengths, with some longer fibers remaining. Discontinuous fiber reinforcements are classified as long for aspect ratios (the ratio of length over diameter) greater than 100. For glass fibers, that distinction occurs at a length of 1 mm, and for carbon fibers 0.5 mm. Traditional composite materials and manufacturing processes utilize continuous fibers with a controlled orientation and length, such as the weave pattern one might see in a carbon fiber hood. The use of chopped fibers requires a method to predict the orientation of the fibers in the final molded piece because mechanical properties are dependent on fiber length and orientation. The way

that the plastic flows during molding is directly related to the mechanical properties of the completed part because flow affects the way that the fibers arrange. The ability to predict, and ultimately control, flow properties allows for the efficient design of safe parts for industrial uses, such as vehicle parts in the automotive industry.

The goal of this work is to test the techniques developed for measuring and predicting the orientation of fiber reinforced injection molded thermoplastics using commercial grade long carbon fiber (LCF) reinforced nylon 6,6 (PA 6,6). LCF/PA 6,6 with an average fiber length of 1.242 mm was injection molded into a disk and the orientation was measured experimentally. A computer flow simulation process that utilizes the finite element method to model the flow and orientation of fiber reinforced materials was tested and modified to accurately predict the orientation for this composite and geometry. Fiber orientation models used for prediction require the use of parameters. There is no universal method for determining these parameters. A method of using non-lubricated squeeze flow as an efficient way to determine the parameters for short glass fiber polypropylene orientation predictions was extended to use with the LCF/PA 6,6 composite. The LCF/PA 6,6 material was compression molded and underwent non-lubricated squeeze flow testing. The flow was modeled to predict the fiber orientation. The empirical parameters were fit by comparing the simulated orientation to experimentally measured orientation. This is a successful method for predicting orientation parameters. The determined orientation parameters were then used to reasonably predict the fiber orientation for the injection molded parts. The authors proved that the experimental and simulation techniques developed for the glass fiber reinforced polypropylene material are valid for use with a different, more complex material.

Acknowledgements

I would like to begin by thanking my advisor Dr. Donald Baird. It has been an honor to work under his tutelage. I have gained immeasurable insight into polymer processing and non-Newtonian fluids and developed into a skilled researcher. Not only has Dr. Baird shared his intellectual knowledge, it has also been a true joy to hear of his adventures while traveling the world and sharing stories of our favorite destinations. Furthermore, it is imperative to thank my advising committee members, Dr. Michael Bortner, Dr. Scott Case, and Dr. Stephen Martin for their guidance and direction. Their classes were enriching and the additional notes and resources have been invaluable throughout this process. Next, I extend my gratitude to Dr. Peter Wapperom from the mathematics department for his patience and extended support with the extensive amount of simulation work needed for this project.

This research required many pieces of tooling and used multiple instruments and equipment. Mike Vaught and Kevin Holshouser in the chemical engineering machine shop were irreplaceable members of the team by helping me to keep things moving forward and fixing any issues that occurred. The research that we do as graduate students would also not be possible without the support of the chemical engineering staff that manage and structure the countless administrative tasks. To the other members of the Baird research group, “Thank You”! We have kept each other sane, lent a helping hand, brainstormed, and been true teammates throughout this process.

At last, I would like to thank my incredible support system. I greatly appreciate their prayers, encouragement, and willingness to help!

Original Contributions

This work contributes to the overall body of literature on fiber reinforced composites in the following ways:

1.) Non-lubricated squeeze flow (NLSF) was extended as a method for determining the empirical parameters used in modeling the orientation of injection molded fiber reinforced thermoplastics. The rheology of the matrix is used for modeling the flow parameters during NLSF testing. Previous work was conducted with a short glass fiber reinforced polypropylene (SGF/PP) and assumed a Newtonian model for the matrix viscosity. The author used a long carbon fiber reinforced polyamide 6,6 (LCF/PA 6,6) composite to further the research on using NLSF to determine empirical parameters. The simulation was improved to account for the non-linear rheological behavior of a polymer matrix. The nylon 6,6 viscosity was represented using the Carreau-Yasuda model.

2.) The process of using NLSF to optimize empirical model parameters for the simulation of fiber orientation in injection molded reinforced composites was expanded for use with long fibers. Discontinuous fibers are classified as long when the aspect ratio (L/D) is greater than 100. Using a LCF/PA 6,6 material allowed for the NLSF method to be tested and adapted for a composite with a fiber aspect ratio of 248. The method had previously only been used for short fibers (aspect ratio of 53). Using NLSF with long fibers allowed for fiber bending and was able to be extended as an efficient manner for determining the parameters needed for adequate long fiber orientation simulation.

Format of Dissertation

Chapter one of this dissertation describes the problems that this work aimed to answer and a look into the general concepts behind that work. The motivation behind why the work is important along with the applications are explained to set the stage for the remainder of the chapters. Chapter two goes into greater detail with a review of the current body of literature on thermoplastic composites, rheology, and other topics critical to this research. Chapters three and four are in the form of manuscripts that will be submitted for publication in the Polymer Composites journal at a later date. Chapter six contains the conclusions drawn from this work and proposes a direction for future exploration.

3.) A long carbon fiber reinforced polyamide 6,6 material was used to injection mold center-gated disk samples with an aspect ratio of 248. The small diameter of the carbon fiber allowed for the material to have long fiber characteristics despite the breakage that occurs during injection molding. Previously long glass fiber material was used for testing of the experimental methods and the Linux based Numlab low simulation process that utilizes the finite element method to model the flow and orientation of fiber reinforced materials. The aspect ratio of this LGF/PP material was 120. The author expanded all previous work with a much "longer" fiber material. Fiber properties, orientation and length, were experimentally determined for this new aspect ratio range. The experimentally measured parameters were used in conjunction with the empirical parameters determined from NLSF as inputs for the Numlab flow simulation to model the flow and fiber orientation for the commercial grade LCF/PA 6,6. The fiber orientation compared well to that which was experimentally measured.

Table of Contents

List of Figures

List of Tables

Chapter 1: Introduction

Current trends in the automotive industry show an increased focus on engineering new materials to create lighter vehicles. Like many trends we see in our cars, carbon fiber composites began in limited-production, high-cost, high-performance sectors of the industry. These composites have been a major component for racing and super car design. Carbon fiber based composites account for 85% of the volume of a Formula 1 car, yet only 25% of its weight [1]. However, light weighting not only affects a vehicle's performance, it is a vital factor in fuel efficiency. As legislation demands higher environmental standards and individuals are becoming increasingly aware of their carbon footprint, fuel efficiency becomes an ever more important factor for economy car production and sales. According to a Department of Energy study conducted by West Virginia University [2], a 10% decrease in vehicle weight should result in a 6.6% increase in fuel efficiency. Materials such as carbon fiber and other polymer based composites, when utilized in place of traditional materials, have the ability to reduce vehicle weight up to 70%, while light weighting efforts conducted by engineering and design improvements for traditional steel materials can only reduce the weight by a maximum of 25% [2].

In order to obtain the mechanical properties needed for automotive and aerospace applications, polymers are reinforced with fibers, often glass or carbon. Glass-based and carbon-based fibers are added to polymers to increase the stiffness and strength. Continuous fiber reinforced materials have strands of fibers that run the length of the material, often as a woven mat, and are impregnated with a thermoplastic

or thermoset resin [3] . These materials are used for large parts with flat or simple geometries. The length and processing of continuous fibers restrict the complexity of the part.

High material and manufacturing costs have traditionally restricted applications to low volume high-cost applications, usually in the form of prepregs and semi-pregs [4]. The material cost of carbon fiber has decreased in recent years, but the production of reinforcement fabrics requires high labor costs, and has a large percentage of waste [4]. Figure 1.1 illustrates a cost comparison for a generic mass produced fender constructed with steel, semi-preg carbon fiber material, and a DCFP material [5]. DCFP (directed carbon fiber preforming) is a technique developed by Ford Motor Company [5] that uses a robot-mounted mechanical chopper head to spray fibers and a polymeric binder onto a perforated tool; after spraying a punch tool is lowered to compress the preform. Figure 1.1 indicates that this level of automation has significantly decreased the cost per piece at higher production numbers compared to traditional semi-preg materials. A completely automated injection molding process further decreases the cost per piece, making the mass production of automobile parts feasible [7].

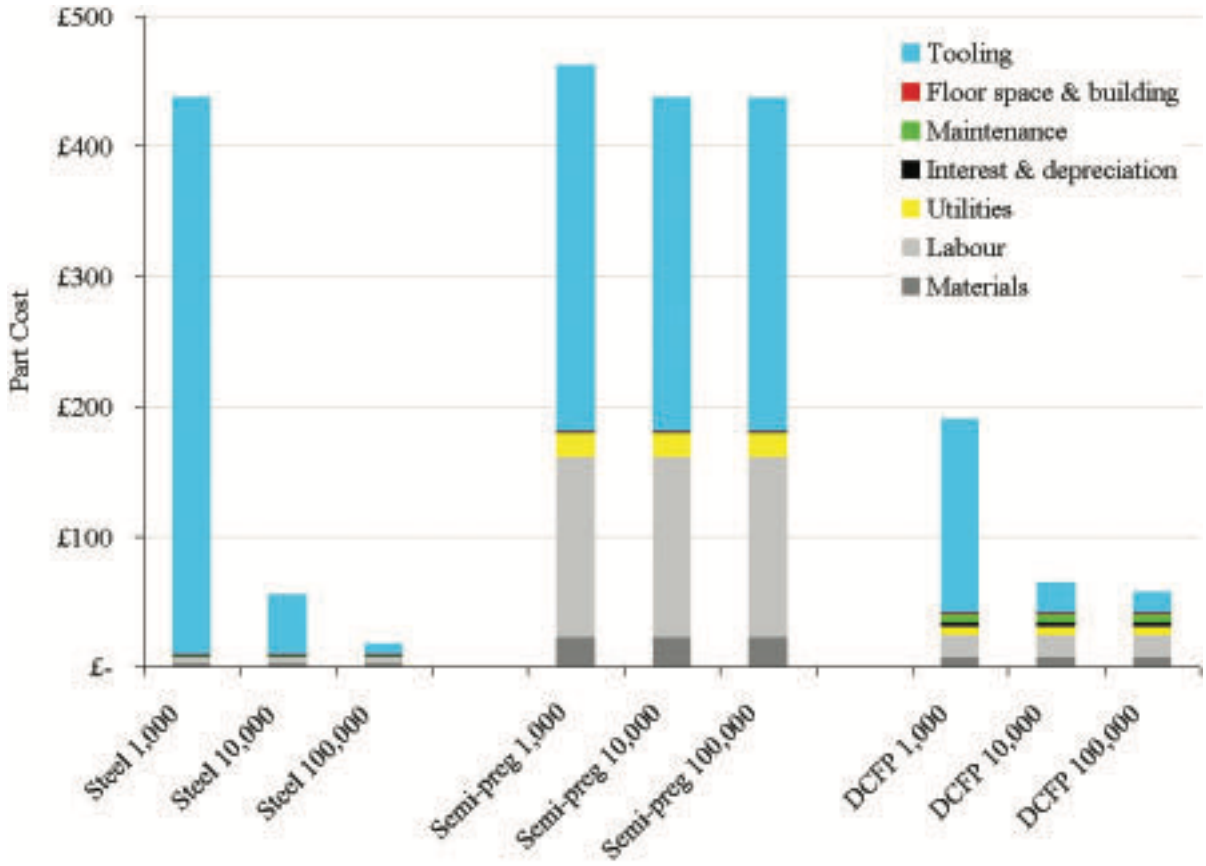

Figure 1.1: Cost comparison for steel, semi-preg, and DCFP materials for mass-produced fenders at three volume levels 1,000, 10,000, and 100,000 parts annually [5]. Reproduced with permission from the Journal of Automotive Engineering.

Injection molding provides an alternative, fast, and efficient method for the mass production of complicated geometries [6]. In order to injection mold fiber reinforced materials, the fibers are chopped. The smaller fiber lengths allow for more intricate part geometries. The process of injection molding, discussed in greater detail in Section 1.1, also aids in the development of complex parts compared to sheet molding composites or pre-pregs, because the composite material is melted and then pushed into a mold cavity [6, 7].

A downside of injection molding is that feed stock needs to be in a form that is compatible with the injection molder, such as pellets. The pellets are fed into the

injection molder where breakage and mixing occurs, resulting in a final piece that has fibers of varying lengths arranged in different orientations throughout the part. The mechanical properties of the final part are dependent on the length and orientation of the fibers.

Traditional composite materials are reinforced with glass or carbon fibers and are cut into 10-13 mm long pellets. Long fiber thermoplastic (LFT) materials are pultruded so the fibers are continuous throughout the pellet resulting in an initial fiber length of 10-13 mm as opposed to short fibers that are 0.2-0.4 mm long regardless of the pellet length [8]. Within the discontinuous fiber literature, “short” refers to fibers that are less than 1 mm in length (usually around 0.2-0.4 mm), and “long” refers to fibers that are 1 mm or longer [9]. The longer the fiber lengths, the better the material properties that can be expected from the final part. Figure 1.2 reveals that modulus, strength, and impact resistance all increase and eventually plateau with increasing fiber length; a glass fiber wet lay material was used to allow fiber lengths up to 100 mm [7].

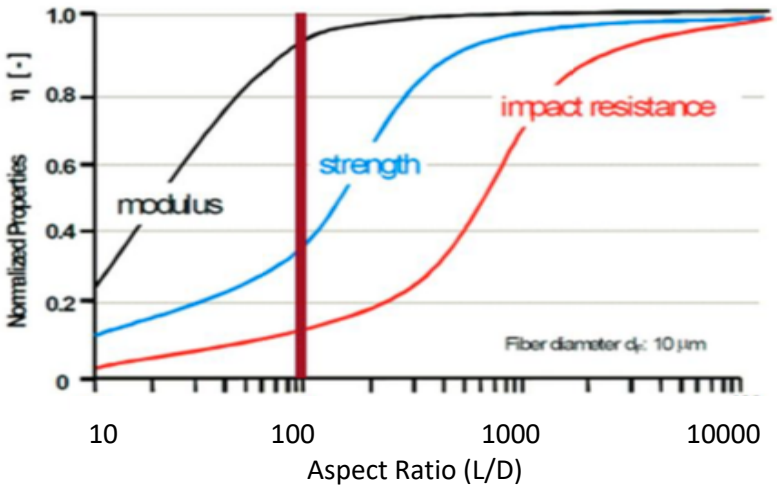

Figure 1.2: Dependence of composite mechanical properties on fiber aspect ratio for a glass fiber material processed using a wet lay procedure [7]. Reproduced and altered with permission from author and Virginia Tech.

In order to efficiently injection mold LFT parts for industrial use, it is imperative to be able to understand the orientation evolution of the fiber reinforcement. Mechanical performance is also dependent upon fiber orientation. The ability to model and predict fiber orientation during mold filling provides engineers with the ability to tailor mold design for preferred orientation and therefore mechanical properties. Figure 1.3 uses test strips cut from a unidirectional fiber reinforced composite material to demonstrate the effect of fiber orientation on tensile strength and elastic modulus; fiber reinforcement is more effective when the fibers are aligned in the direction that the load is applied [10].

(a)

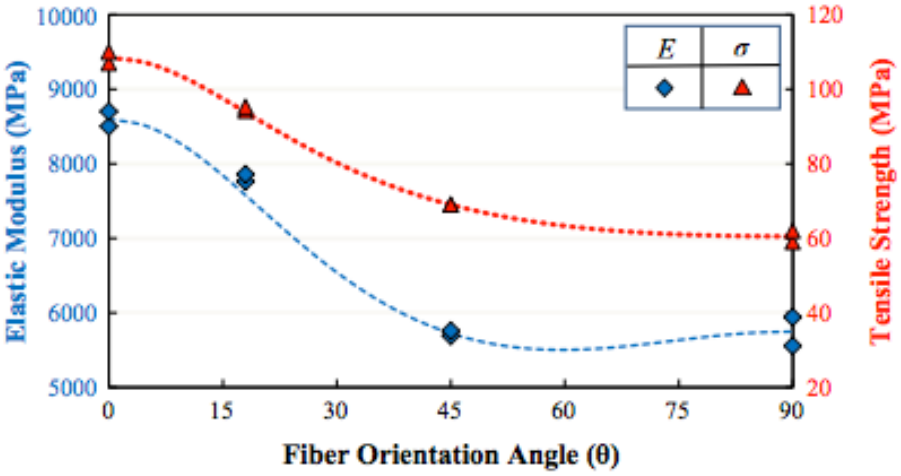

(b)

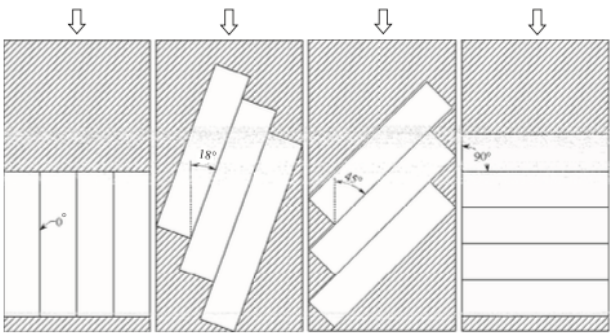

Figure 1.3: (a) Elastic modulus and tensile strength for test strips with various fiber orientations. The strips are cut from a unidirectional material, shown in (b), in the direction of flow, transverse to flow, and two angles (18 & 45) in between [10]. Reproduced with permission from Composites, Part B.

The proposed research aims to apply work previously conducted by Baird and coworkers [7, 11-18] to new materials. Prior research has been conducted using glass reinforced polypropylene to predict the fiber length and orientation distributions in injection molded parts. The work was successful in center-gated disk geometries, matching well the predicted orientation to experimentally obtained data [11]. The fiber orientation distribution throughout the part controls the mechanical properties of the part. Fiber orientation is dependent on the flow of the suspension and fiber interactions [19].

Fiber orientation and suspension flow are heavily coupled. The fibers are oriented by the flow patterns of the suspension, and the flow changes when fibers are introduced due to their interactions with one another and the matrix [7]. Stress tensors are used to model flow properties and couple the flow of the suspension to the fiber orientation. Due to the complexity of a concentrated non-Newtonian fluid with flexible fibers, there have been many attempts to improve these stress models [7, 16, 20-23]. The work done by Baird and coworkers [7, 13-17, 24, 25] has been influential on the development of rheologically determined orientation parameters. Due to the connection of fiber orientation and flow patterns, research has been done to derive the empirical orientation model parameters from rheological flows. The current work examines the ability to use non-lubricated squeeze flow to induce fiber flexing in a controlled flow system that has shear and extensional flow and is simpler than injection molding. This method has been developed and tested by Lambert [7].

1.1 Injection Molding

Injection molding is considered to most likely be the most popular cyclic process for manufacturing thermoplastic parts [6]. Injection molding is fast, automatic, and can be used for complex geometries, thus making it cost effective and efficient. Pellets are fed into the hopper, then melted and mixed in the barrel with a screw. There are three zones in the barrel: the feed zone, or solids conveying, in which pellets are compressed and dragged forward, they then melt as they enter the transition zone and undergo mixing. They are further mixed as they approach the end of the barrel in the metering zone where they are pushed forward. The screw then acts as a plunger and pushes the plug of now liquid polymer forward through the nozzle into the mold cavity. The mold consists of a sprue that aids in lowering the resistance to flow and providing a smooth transition to the mold, and if multiple parts are being made in the same mold, a runner connects the parts.

Two mold geometries will be used in the proposed research, a center-gated disk (CGD) and an end-gated plaque (EGP). Figure 1.4 and 1.5 illustrate a CGD and EGP along with the respective coordinate systems and the dimensions used for this work.

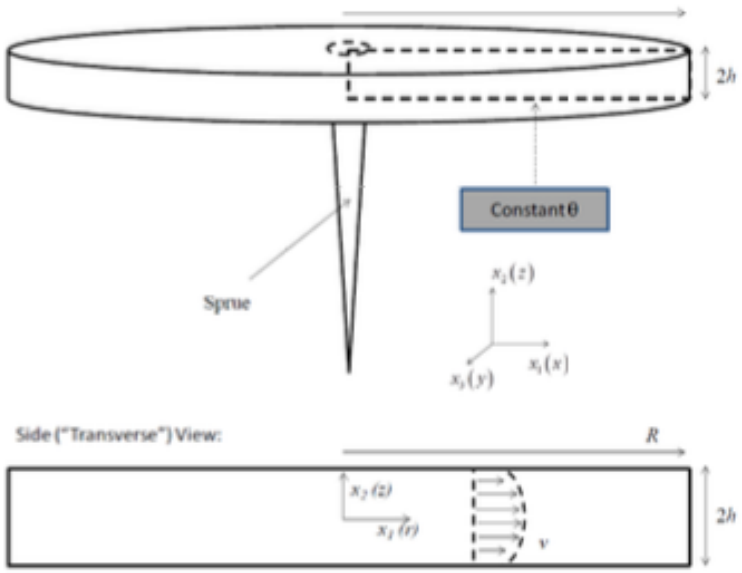

Figure 1.4: Center-gated disk geometry showing sprue and transverse view, includes coordinate system [18]. Reproduced with permission from Virginia Tech.

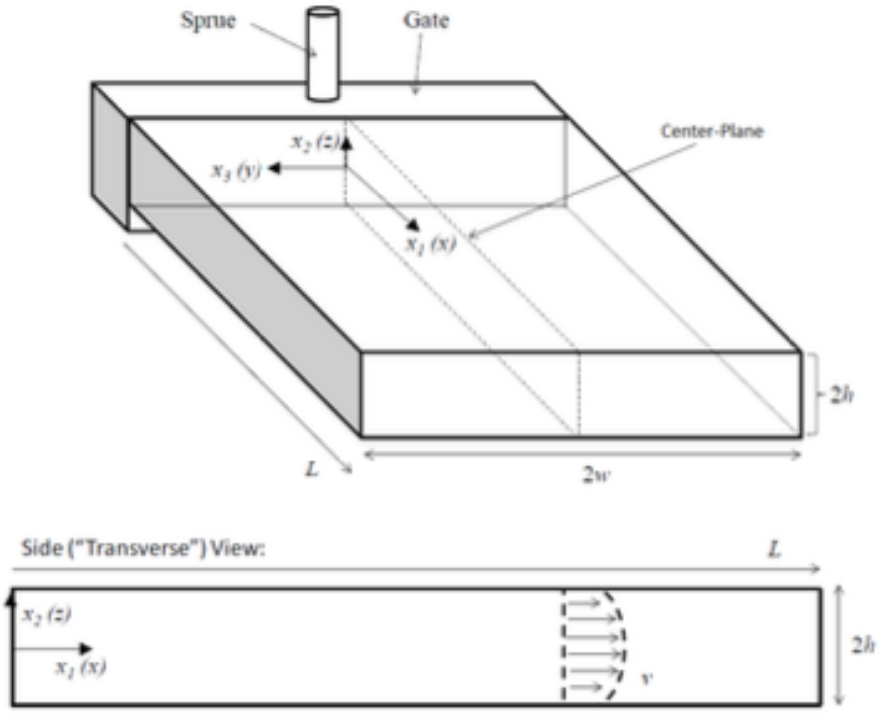

Figure 1.5: End-gated plaque geometry showing sprue and transverse view, includes coordinate system [18]. Reproduced with permission from Virginia Tech.

1.2 Research Objectives

1. Determine whether lab developed long fiber composite simulation and data collection methods for polypropylene reinforced with glass fiber will be able to evaluate the orientation of nylon 6,6 reinforced with carbon fiber.
2. Assess the viability of using non-lubricated squeeze flow testing developed for polypropylene and glass fiber to determine the empirical parameters in the orientation model for nylon 6,6 reinforced with carbon fiber.

Works Cited

1. Savage, G., *Composite Materials Technology in Formula 1 Motor Racing.* Honda Racing F1, 2008.
2. Jacky C. Prucz, S.N.S., Gergis W. William, Mark S. Shoukry, *LIGHTWEIGHT COMPOSITE MATERIALS FOR HEAVY DUTY VEHICLES*, O.o.E.E.a.R.E. US Department of Energy, National Energy Technology Laboratory, Editor. 2013: West Virginia University.
3. Bing Liu, A.X., Limin Bao, *Preparation of carbon fiber-reinforced thermoplastics with high fiber volume fraction and high heat-resistant properties.* Journal of Themoplastic Composite Materials, 2015.
4. Lee Harper, T.T., Nicholas Warrior, Christopher Rudd, *Automated Preform Manufacture for Affordable Lighweight Body Structures.* SAMPE Europe Conference and Exhibition, 2005. **26th**.
5. T A Turner, L.T.H., N A Warrior, C D Rudd *Low-cost carbon-fibre-based automotive body panel systems: a performance and manufacturing cost comparison.* J. Automobile Engineering, 2007. **222**.
6. Donald G. Baird, D.I.C., *Polymer Processing Principles and Design*. Second ed. 2014, New Jersey: John Wiley & Sons, Inc.
7. Lambert, G., *Using Non-Lubricated Squeeze Flow to Obtain Empirical Parameters for Modeling the Injection Molding of Long-Fiber Composites*, in *Chemical Engineering*. 2018, Virginia Polytechnic Instititue and State University.
8. Jay H. Phelps, A.I.A.E.-R., Vlastimil Kunc, Charles L. Tucker III, *A model for fiber length attrition in injection molded long-fiber composites.* Composites: Part A, 2013.
9. Huan-Chang Tseng, R.-Y.C., Chia-Hsiang Hsu, *Numerical prediction of fiber orientation and mechanical performance for short/long glass and carbon fiber-reinforced composites.* Composites Science and Technology, 2017. **144**.
10. Seyyedvahid Mortazavian, A.F., *Effects of fiber orientation and anisotropy on tensile strength and elastic modulus of short fiber reinforced polymer composites.* Composites: Part B, 2015. **72**: p. 116-129.
11. Hongyu Chen, D.G.B., *Prediction of Young's Modulus for Injection Molded Long Fiber Reinforced Thermoplastics.* Journal of Composite Sciences, 2018.
12. Harrington, K.D., *Factors Affecting Fiber Orientation and Properties in Semi-Flexible Fiber Composites: Including the Addition of Carbon Nanotubes*, in *Chemical Engineering*. 2015, Virginia Polytechnic Institute and State University.
13. Meyer, K.J., *Improved Prediction of Glass Fiber Orientation in Basic Injection Molding Geometries*, in *Chemical Engineering*. 2013, VIrginia Tech.
14. Ortman, K.C., *Assessing an Orientation Model and Stress Tensor for Semi-Flexible Glass Fibers in Polypropylene Using a Sliding Plate Rheometer: for the Use of Simulating Processes*, in *Chemical Engineering*. 2011, Virginia Polytechnic Institute and State University.
15. Velez-Garcia, G.M., *Experimental Evaluation and Simulations of Fiber Orientation in Injection Molding of Polymers Containing Short Glass Fibers*, in *Chemical Engineering*. 2012, Virginia Polytechnic Institute and State University.

16. Eberle, A.P.R., *The Dynamic Behavior of a Concentrated Composite Fluid Containing Non-Brownian Glass Fibers in Rheometrical Flows*, in *Chemical Engineering*. 2008, Virginia Polytechnic Institute and State University.
17. Cieslinski, M.J., *Using a Sliding Plate Rheometer to Obtain Material Parameters for Simulation Long Fiber Orientation in Injection Molded Composites*, in *Chemical Engineering*. 2015, Virginia Polytechnic Institute and State University.
18. Herrington, K.D., *Factors Affecting Fiber Orientation and Properties in Semi-Flexible Fiber Composites: Including the Addition of Carbon Nanotubes*, in *Chemical Engineering*. 2015, Virginia Polytechnic Institute and State University.
19. Hongyu Chen, P.W., Donald G. Baird, *Simulation of Long Semi-flexible Fiber Orientation during Injection Molding.* SPE ANTEC Indianapolis 2016, 2016.
20. Goddard, J.D., *TENSILE STRESS CONTRIBUTION OF FLOW-ORIENTED SLENDER PARTICLES IN NON-NEWTONIAN FLUIDS.* Journal of Non-Newtonian Fluid Mechanics, 1976. **1**.
21. Maw-Ling Wang, T.-C.C., *A constitutive approach for studying concentrated suspensions of rigid fibers in a non-Newtonian Ellis fluid.* Journal of the Chinese Institute of Engineers, 2011. **14**.
22. J. Thomasset, P.J.C., B. Sanschagrin, G. Ausias, *Rheological properties of long glass fiber filled polypropylene.* Journal of Non-Newtonian Fluid Mechanics, 2004. **125**.
23. kevin Ortman, d.B., Peter Wapperom, Abby Whittington, *Using startup of steady shear flow in a sliding plate rheometer to determine material parameters for the purpose of predicting long fiber orientation.* Journal of Rheology, 2012. **56**.
24. Aaron P. R. Eberle, D.G.B., Peter Wapperom, Gregorio M. Velez-Garcia, *Using transient shear rheology to determine material parameters in fiber suspension theory.* Journal of Rheology, 2009. **53**.
25. Mazahir, S.M., *Improvement in Orientation Predictions of High-Aspect Ratio Particles in Injection Mold Filling Simulations*, in *Chemical Engineering*. 2013, Virginia Polytechnic Institute and State University.

Chapter 3: Using Non-Lubricated Squeeze Flow to Determine Orientation Model Parameters for Injection Molded Long Carbon Fiber Reinforced Nylon 6,6

Kennedy R. Boyce[1,2], Peter Wapperom[3], and Donald G. Baird[1,2]
Virginia Polytechnic Institute and State University
Blacksburg, VA USA
1) *Department of Chemical Engineering*
2) *Macromolecules Innovation Institute*
3) *Department of Mathematics*

3.1 Abstract

Long fiber reinforced thermoplastic composites are used for creating lightweight, but mechanically sound, automotive components. Injection molding is a manufacturing technique commonly used for traditional thermoplastics due to its efficiency and ability to create complex geometries. Injection molding feedstock is often in the form of pellets. Fiber composites must be chopped for use, and fiber attrition occurs during processing. The combination of chopping the fibers into pellets and fiber breakage creates a distribution of mostly short fiber lengths, with some longer fibers remaining. The use of chopped discontinuous fibers requires a method to predict the orientation of the fibers in the final molded piece because mechanical properties are dependent on fiber length and orientation. This work evaluates the optimization of empirical parameters for the strain reduction factor (SRF) method of orientation prediction. The previous work was conducted to establish a method of using non-lubricated squeeze flow as an efficient way to determine the strain reduction factor, α, and Brownian motion like factor, C_I, parameters for short glass fiber polypropylene. The goal of this study is to test the use of the experimental procedures and the flow simulation with a long fiber composite with a different reinforcement and matrix. Discontinuous fiber reinforcements are classified as long for aspect ratios (length/diameter) greater than 100. For glass fibers, that distinction

occurs at 1 mm, and for carbon fibers 0.5 mm. Long carbon fiber (40 weight percent, weight averaged length of 1.242 mm) reinforced nylon 6,6 samples were compression molded and then underwent non-lubricated squeeze flow testing. The flow was simulated using finite element analysis to predict the fiber orientation using the SRF model. The empirical parameters were fit by comparing the simulated orientation to experimentally measured orientation. The simulation predicted a reasonable degree of accuracy for orientation but not to the same level of accuracy as the short glass fiber polypropylene material. This is a successful method for predicting orientation parameters that is significantly more efficient than optimizing the parameters based on fitting orientation generated in injection molded pieces.

3.2 Introduction

The goal of this research is to explore the use of non-lubricated squeeze flow (NLSF) to determine the empirical parameters used in models for orientation prediction of injection molded long fiber reinforced thermoplastic composites. The ever increasing demand for lighter more fuel efficient vehicles requires the use of a process named lightweighting, with the objective being to replace traditional metallic components with new lighter composite counterparts. A Department of Energy study conducted by researchers at West Virginia University in 2013 found that these substitution practices can reduce vehicle weight by up to 70%, and that a 10% decrease in vehicle weight corresponds to a nearly 7% increase in fuel efficiency [1].

Injection molding has been employed as a means to create composite parts with complex geometries in an efficient manner. However, injection molding of fiber

reinforced composites does introduce a certain set of challenges. Traditional manufacturing techniques use methods of laying the fibers in mats or other arrangements where the orientation is manipulable and the length is controlled, often extending the entire length of the part, known as continuous reinforcement. In order to injection mold these materials, the fiber and matrix is pultruded into a pellet and then chopped to a desired length. The fibers then undergo further breakage during the injection molding process, the majority of this breakage occurring in the screw [2]. The length of fibers in the final part is represented by a distribution that has a large peak in the short fiber region and tailing toward long fiber lengths (aspect ratio, a_r, greater than 100). This fiber length distribution (FLD) is represented by the mean and number average of which greater definition and derivations can be found in many sources, including the work of Nguyen et al. [3]. The FLD is important because mechanical properties, such as the strength, modulus, and impact resistance of the composite increase with the length of the reinforcement [4].

Not only must the fiber length be represented by a statistical distribution, but the orientation must also be tracked. The orientation of an injection molded composite may appear random, but it has a noticeable trend. The final part consists of five distinct layers through the thickness with a transition layer between each of the different zones. Upon examination of a cross section of the part, one would find an axis of symmetry along the center of the thickness direction (z). The center region is a core layer with the greatest fiber orientation aligned in the direction of flow. In the +z and -z directions (toward the top and bottom of the part) is a shell layer with cross-flow fiber orientation. Then on the very outer skin and in the transition zones between each layer are random

fiber orientation. (If unfamiliar with this pattern, the reader is directed to the work of Teuwsen et al. [5] for diagrams and greater explanation.)

3.2.1 Orientation Equations

In order to mathematically represent the orientation of these fibers, a system of equations has been derived. An individual fiber was first thought to be represented by a single vector, **p**, along the fibers' axis. Jeffery described the motion of this fiber in a dilute Newtonian fluid and through solving the equations of motion and continuity a vector form is developed for the motion of a single fiber [6]. Of course, tracking every single fiber in a commercially developed material would be cumbersome, if not impossible, so a probability distribution function $\psi(\mathbf{p})$ is used to represent the orientation state for a population of fibers in a suspension. Advani and Tucker [7] developed a set of orientation tensors by taking the dyadic products of **p** and integrating with $\psi(\mathbf{p})$ over all orientation directions. The second and fourth order tensors are used by Folgar and Tucker [8] in their model to predict the orientation distribution of rigid fibers in concentrated suspensions, as shown in Equation (3.1):

$$\frac{D\mathbf{A}}{Dt} = \mathbf{W}\cdot\mathbf{A} - \mathbf{A}\cdot\mathbf{W} + \xi(\mathbf{D}\cdot\mathbf{A} + \mathbf{A}\cdot\mathbf{D} + 2\mathbf{D}\colon\mathbf{A_4}) + 2C_I\dot{\gamma}(\mathbf{I} - 3\mathbf{A}) \qquad (3.1)$$

where **D** is the rate of deformation tensor ($\boldsymbol{D} = \frac{1}{2}[\boldsymbol{\nabla v} + (\boldsymbol{\nabla v})^t]$), **W** is the vorticity tensor ($\boldsymbol{W} = \frac{1}{2}[(\boldsymbol{\nabla v})^t - \boldsymbol{\nabla v}]$), C_I is a phenomenological constant and $\mathbf{I}$ is the unit tensor. C_I is a phenomenological constant that represents the fiber-fiber interactions. As the value of C_I increases the fiber-fiber interactions are greater and thus result in less fiber orientation along the flow direction. In the evaluation of this model it was found that the

predicted fiber orientation rate was much greater than what was experimentally observed [9].

The Strain Reduction Factor (SRF) model, shown in Equation (3.2), included a strain reduction factor, α, to correct the evolution rate [9]. The strain reduction factor, α, is a scalar with a value between 0 and 1.

$$\frac{D\mathbf{A}}{Dt} = \alpha[\mathbf{W}\cdot\mathbf{A} - \mathbf{A}\cdot\mathbf{W} + \xi(\mathbf{D}\cdot\mathbf{A} + \mathbf{A}\cdot\mathbf{D} + 2\mathbf{D}\colon\mathbf{A_4}) + 2C_I\dot{\gamma}(\mathbf{I} - 3\mathbf{A})] \qquad (3.2)$$

The addition of α improved the accuracy of the model, but resulted in a loss of material objectivity and a model where the coordinate system could not be changed, nor the frame rotated or translated [10].

As fiber length increases, the representation of the fiber as a rigid rod becomes increasingly less effective [11]. This work focuses on the extension of short fiber modeling into that of long fibers. Glass and carbon fibers cross the aspect ratio threshold into the long fiber region at lengths of 1.0 and 0.5 mm each, respectively. Fibers experience greater flexibility and bending in this long region. The bending is an effect of fiber-matrix and fiber-fiber interactions. In order to account for bending, a new method of vector representation was developed for the fiber. Detailed in the work of Strautins and Latz [12], the fiber is now considered to be a combination of 3 beads connected by 2 rods, called the bead-rod model. The 2 rods are named as two unit vectors **p** and **q**. A vector **r** is the end-to end vector and connects the ends of vectors **p** and **q.** It is used to define a dimensional end-to-end orientation tensor **R**. The two vectors result in three moments, **A**, **B**, and **C** which have been put in the same notation as the **A** tensor from the rigid rod models, Equations (3.3-3.5) [13].

$$\mathbf{A}(t) = \iint \mathbf{pp}\ \psi(\mathbf{p}, \mathbf{q}, t) d\mathbf{p} d\mathbf{q} \tag{3.3}$$

$$\mathbf{B}(t) = \iint \mathbf{pq}\ \psi(\mathbf{p}, \mathbf{q}, t) d\mathbf{p} d\mathbf{q} \tag{3.4}$$

$$\mathbf{C}(t) = \iint \mathbf{p}\ \psi(\mathbf{p}, \mathbf{q}, t) d\mathbf{p} d\mathbf{q} \tag{3.5}$$

Ortman et al. [13] extended the bead-rod model to non-dilute suspensions by the addition of the isotropic diffusion term. The following equations (3.6-3.9) show that the flexibility is induced by a combination of rotary and hydrodynamic effects:

$$\frac{D\mathbf{A}}{Dt} = \alpha((\mathbf{W}\cdot\mathbf{A} - \mathbf{A}\cdot\mathbf{W}) + (\mathbf{D}\cdot\mathbf{A} + \mathbf{A}\cdot\mathbf{D} - 2\mathbf{D}\colon\mathbf{A_4}) - 6C_I\dot{\gamma}\left(\mathbf{A} - \frac{1}{3}\mathbf{I}\right) + \frac{l_B}{2}[\mathbf{Cm} + \mathbf{mC} - 2(\mathbf{m}\cdot\mathbf{C})\,\mathbf{A}] - 2k[\mathbf{B} - \mathbf{A}\,tr(\mathbf{B})]) \tag{3.6}$$

$$\frac{D\mathbf{B}}{Dt} = \alpha((\mathbf{W}\cdot\mathbf{B} - \mathbf{B}\cdot\mathbf{W}) + (\mathbf{D}\cdot\mathbf{B} + \mathbf{B}\cdot\mathbf{D} - (2\mathbf{D}\colon\mathbf{A})\mathbf{B}) - 4C_I\dot{\gamma}\mathbf{B} + \frac{l_B}{2}[\mathbf{Cm} + \mathbf{mC} - 2(\mathbf{m}\cdot\mathbf{C})\,\mathbf{B}] - 2k[\mathbf{A} - \mathbf{B}\,tr(\mathbf{B})]) \tag{3.7}$$

$$\frac{D\boldsymbol{C}}{Dt} = \alpha\left(\nabla v^t\cdot\boldsymbol{C} - (\boldsymbol{A}\colon\nabla v^t)\boldsymbol{C} + \frac{l_B}{2}[\boldsymbol{m} - \boldsymbol{C}\,(\boldsymbol{m}\cdot\boldsymbol{C})] - k\boldsymbol{C}[1 - tr(\boldsymbol{B})] - 2C_I\dot{\gamma}\boldsymbol{C}\right) \tag{3.8}$$

$$\boldsymbol{m} = \sum_{i=1}^{3}\sum_{j=1}^{3}\sum_{k=1}^{3}\frac{\partial^2 v_i}{\partial x_j \partial x_k}A_{ijk}e_i \tag{3.9}$$

In these equations (3.6-3.9), k is the resistive bending potential. The **m** vector accounts for melt flow induced fiber bending.

An end-to-end vector, **r,** is drawn from each of the end beads and is used to define a dimensional end-to-end orientation tensor,

$$\boldsymbol{r} \equiv \iint l_B^2(\boldsymbol{p} - \boldsymbol{q})\psi(\boldsymbol{p}, \boldsymbol{q}, t)\, d\boldsymbol{p} d\boldsymbol{q} = 2l_B^2(\boldsymbol{A} - \boldsymbol{B}) \tag{3.10}$$

$$\mathbf{R} = \frac{\mathbf{r}}{\mathrm{tr}(\mathbf{r})} = \frac{\mathbf{A} - \mathbf{B}}{1 - \mathrm{tr}(\mathbf{B})} \tag{3.11}$$

in which l_B is the half fiber length. The degree of bending can then be defined as the reduction in this end- to- end distance. Use of the **R** tensor has been shown to better

predict the orientation evolution than the **A** tensor for some injection molded geometries using long glass fiber reinforced polypropylene [13].

3.2.2 Empirical Parameters

The SRF and bead-rod model both predict fiber orientation with the use of empirical parameters: C_I and α. These parameters must be determined experimentally. Commercially available prediction software uses optimally fit parameters that have been determined for the material without explaining the rationale for the chosen value [14]. Work by Tseng et al. [15] used Moldex3D and reported the same model parameters for both glass and carbon fiber suspensions. Most researchers make the parts and fit the parameters to the measured orientation [16]. Not only is this a tedious and time consuming task, but it traps the work into a loop of product manufacturing and design without a true ability to predict the outcome. Researchers at Virginia Tech [4, 10, 17-19] have aimed to provide a method of manipulating the rheological properties of materials to provide these empirical parameters. Past work led to the development of these empirical parameters by fitting to the fiber orientation evolution during simple shear flow in a cone- and-donut geometry [17]. Most recently, Lambert et al. [4] concluded that fiber orientation is significantly faster during planar extension than shear flow, which led to the development of a test that would combine both types of flow, and be able to induce fiber bending for expansion into long fiber composites.

3.2.3 Non-Lubricated Squeeze Flow

Non-lubricated squeeze flow (NLSF) was investigated as a method for obtaining empirical parameters by Lambert et al. [20]. The researchers used short glass fiber reinforced polypropylene that had been collected from the injection molder as nozzle

purge. The nozzle purge was then chopped and compression molded to make rectangular samples (88.9 mm long, 50.8 mm wide, and 8 mm thick) [20]. Tooling was developed in-house for testing on an Instron 5969. The device consisted of a rectangular channel on the bottom fixture with a plate on the upper fixture that fit into the channel. All of the tests were run at 200°C at a constant Hencky strain rate of -0.50 s^{-1} for 2 seconds to a strain of 1 [20]. Greater details about the experimental processes can be found in their work [20]. This process has not been previously tested for long fiber reinforced materials, nor other composites. The goal of this work was to expand and test this method for a long carbon fiber reinforced nylon 6,6 material.

The viscosity of the matrix is required for orientation prediction models. Commercial simulation packages utilize the viscosity of the composite, but previous work proved that it was more accurate to use the viscosity of the matrix and account for the fiber interactions with the parameters [11]. Using the viscosity of the composites produces too fast of an orientation evolution [11]. Previous NLSF simulations assumed a Newtonian viscosity for the polypropylene matrix [20]. This work represented the nylon 6,6 viscosity using the Carreau-Yasuda model, viscosity curves and Carreau-Yasuda fit data can be found in the work of Boyce [21].

3.3 Experimental Methods

The outline for these experiments consisted of four main components: sample preparation, sample testing, fiber orientation measurements, and modeling. The NLSF samples were prepared, and then a portion of samples were analyzed to determine the baseline for initial fiber orientation, the remaining samples then underwent testing, and

the orientation was taken of the final product. The before- and after-testing fiber orientation was used to calculate the empirical parameters.

3.3.1 Sample Preparation

In order to keep the fiber treatment similar to injection molding, the material was run through the injection molder and collected as purge material. The mold was removed, and the material was extruded from the nozzle in strands. These strands were then cut into pieces that were approximately 50 mm long. Due to the moisture properties of nylon 6,6 the material was dried in a vacuum oven prior to being injection molded for 4 hours at 85°C and then again prior to being compression molded to create the piece shown in Figure 3.1. The cut pieces were stacked into a mold that was 50.87 mm wide, 103.96 mm long, and 29.36 mm deep. A controlled initial orientation was used for this work. The pieces were aligned in the transverse direction, as shown in Figure 3.2.

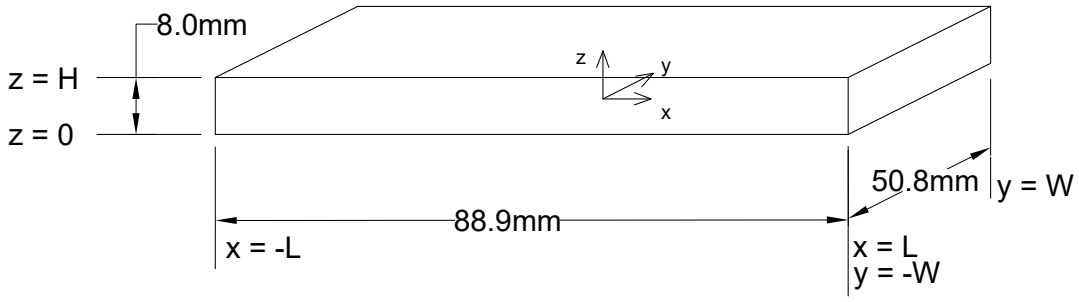

Figure 3.1: Diagram of compression molded part showing the origin in the center of the width and length and on the bottom xz plane. The sample is cut to be 88.9 mm long, 50.8 mm wide, and has a thickness of 8 mm.

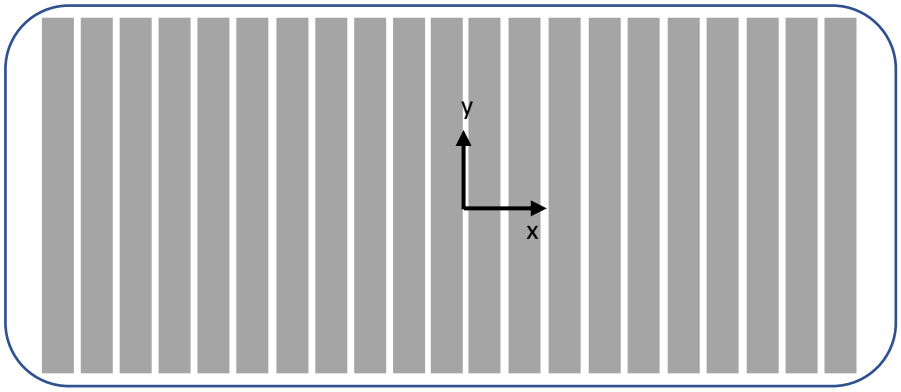

Figure 3.2: Diagram of mold filling with purge strands. The gray bars represent one layer of the strands. The pieces were aligned in the y direction and stacked to fill the mold.

The pieces were compression molded using a Carver lab press with two heated platens. The mold was heated to 300°C and pressed under 2 tons for 5 minutes to create the initial plies. The mold was subsequently moved to a cooling press for 20 minutes. Three to four plies, depending on the weight of each initial ply, were then stacked in the mold after being dried in a vacuum oven for 4 hours and pressed to 3 tons for 20 minutes, and then cooled for an additional 20 minutes. The final piece had a thickness of 8 mm, width of 50.8 mm, and was cut to be a length of 88.9 mm, as shown in Figure 3.1. The final piece was then dried under vacuum for 12 hours, due to the greater density of the part, before NLSF testing.

3.3.2 NLSF Testing

The custom device designed and built by Lambert et al. [20] for the NLSF work with glass fiber reinforced polypropylene was used for the testing of the carbon fiber reinforced nylon 6,6 along with their published experimental procedures. The device consists of an 88.9 mm rectangular channel mounted on a bottom fixture, and an upper fixture with an 88.9 mm by 50.8 mm compression head as shown in Figure 3.3. The fixtures were designed to be mounted onto an Instron 5969 tensile device with an

environmental chamber. All tests using the LCF/PA 6,6 material were run at 301°C at a constant Hencky strain rate of -0.50 s^{-1} (this value is negative because it is under compression) for 2 seconds to reach a strain of 1.0. Note that this work defines the Hencky strain rate as $\dot{\varepsilon} = \dot{H}/H$ and the strain as $\varepsilon = \dot{\varepsilon}t$, with H being the time dependent thickness of the sample and $\dot{H}$ is the closure rate of the fixtures, dH/dt [20].

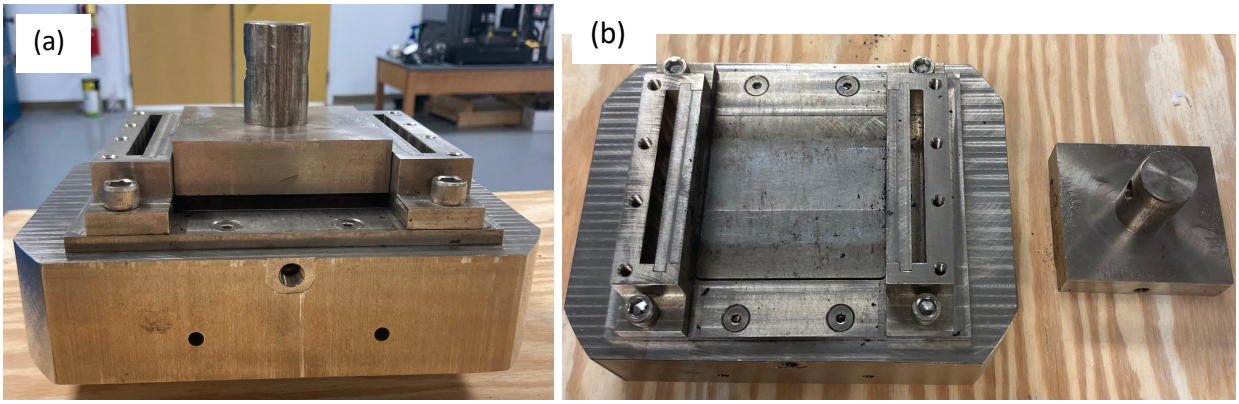

Figure 3.3: Photographs showing testing device. (a) NLSF testing device showing both the top and bottom fixtures as they fit together. The top fixture slides into a channel in the bottom. (b) This is a top down image showing both pieces separately, the top fixture is sitting to the right of the bottom. The top fixture lowers down into the channel shown in the bottom fixture.

3.3.3 Fiber Orientation Measurements

The fiber orientation is experimentally measured from the compression molded samples and then once again from the samples that underwent squeeze flow. The through thickness orientation was measured at the center point. The method of ellipses outlined in the work of Hoffman [22] and Velez-Garcia [23] was used. This method utilizes the elliptical footprint that a fiber intersecting the xz plane created and used the ellipses to calculate orientation. The samples were cut with a band saw, allowing for a 5 mm buffer zone to decrease the chance of damage to the fibers. The cut pieces were sanded to reach the plane of interest using progressively less coarse sandpapers (120, 220, 320 grit), and then were polished using alumina slurries that progressed from

particle diameter sizes of 5 μm, 1 μm, to 0.3 μm. The samples were then plasma etched for 30 minutes to get an unambiguous orientation. The plasma etches away a small amount of the matrix resulting in a shadow effect behind the fibers that allows for the three-dimensional orientation to be calculated. A greater explanation of this method can be found in the literature [22, 23] . Micrographs are then taken through the thickness of the sample at 20x magnification, and the region imaged is 1.16 mm wide. These micrographs were analyzed using a system of MATLAB files to calculate the orientation. A weighting function was used to account for bias for the fibers that were aligned in the two-dimensional plane [22, 23].

3.3.4 Simulation Efforts

Finite element analysis was used to simulate the orientation for the non-lubricated squeeze flow samples. The NLSF testing geometry is shown in Figure 3.4.

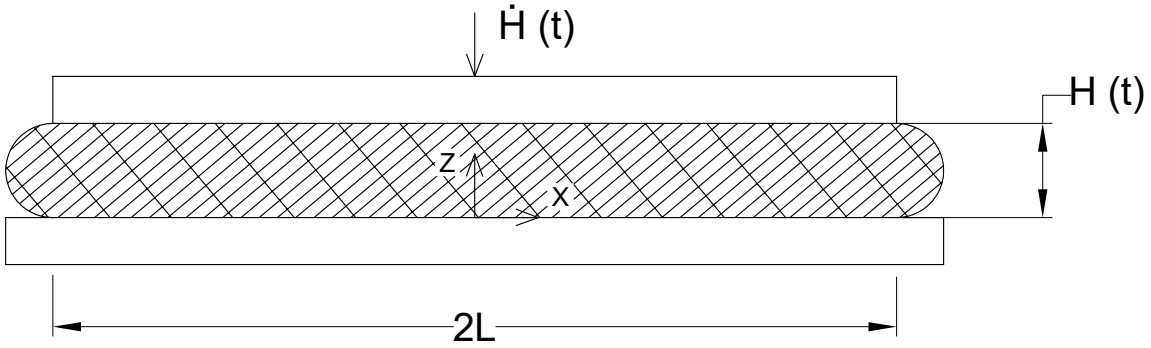

Figure 3.4: Non-lubricated squeeze flow test apparatus and geometry. The compression molded piece is loaded into the tool. The top platen at height H(t) is lowered at the rate Ḣ(t). The sample then squeezed out in the x direction.

A series of equations can be used to describe this geometry and the flow that occurs during testing. For $L \gg H$ the equations of motion reduce to Equations (3.12-14)

$$\frac{\partial p}{\partial x} = \eta \frac{\partial^2 u}{\partial z^2} \tag{3.12}$$

$$\frac{\partial p}{\partial z} = \eta \frac{\partial^2 w}{\partial z^2} \tag{3.13}$$

$$\frac{\partial u}{\partial x} + \frac{\partial w}{\partial z} = 0 \tag{3.14}$$

The solution for this system was in the form $u(x,z,t) = xf(z,t),\ w = w(z,t),\ \text{and}\ p = p_0(x,t) + p_1(z,t)$. The bottom and top walls had a non-slip boundary condition, Equations (3.15-17):

$$u(x,H,t) = u(x,0,t) = 0 \tag{3.15}$$

$$w(H,t) = \dot{H}\ ;\ w(0,t) = 0 \tag{3.16}$$

$$p(L,t) = 0 \tag{3.17}$$

The equations of motion and continuity were solved independent of fiber orientation to determine the pressure and velocity fields, this method was validated by Lambert et al. [20]. The resulting velocity and pressure are Equations (3.18-20):

$$u(x,z,t) = -6\frac{\dot{H}}{H^3}x(zH - z^2) \tag{3.18}$$

$$w(z,t) = \frac{\dot{H}}{H^3}3z^2H - 2z^3) \tag{3.19}$$

$$p(x,z,t) = 6\eta\frac{\dot{H}}{H^3}(x^2 - L^2) + 6\eta\frac{\dot{H}}{H^3}(6Hz - 6z^2) \tag{3.20}$$

The empirical parameters were fit by simulating the NLSF orientation with the SRF model using values for α ranging from 0-1.0 at 0.1 increments, and C_I from 0.0005-0.3 at increments of 0.0005. The orientation results were compared to experimental orientation. Best fit equations were set to the experimental data and the error was calculated for each simulation result. The test with the lowest sum error for the A_{xx} and A_{yy} components of the orientation tensor was considered the best set of parameters. The A_{zz} component was considered negligible due to the low number of fibers oriented out of the plane.

3.4 Results and Discussion

The initial fiber orientation for the compression molded samples had a large number of fibers oriented in the y direction, negligible alignment in the z direction, and low alignment in the x direction as shown in Figure 3.5. After the NLSF test, the fibers were more greatly aligned in the y direction than the x, and there was still negligible alignment in the z direction, shown in Figure 3.6. Previous work by Lambert et al. [20] used a short glass fiber reinforced polypropylene (SGF/PP) material with a random initial orientation, but they recommended future studies with a controlled transverse initial orientation. The fibers experienced significant movement as they underwent the squeezing force, as evidenced by the dramatic orientation shift between Figures 3.5 and 3.6. NLSF is a combination of shear and extensional flows. The higher A_{xx} value and lower A_{yy} value in the center of the sample signifies that the flow through the center of the sample was dominated by extension, which is in agreement with what was found in the previous work [20]. Approaching the top and bottom surfaces (z=0 and z=h), the flow is shear dominated which is represented by the lower A_{xx} value and higher A_{yy} values. This bell shaped curve is analogous to the results for the glass reinforced polypropylene material [20].

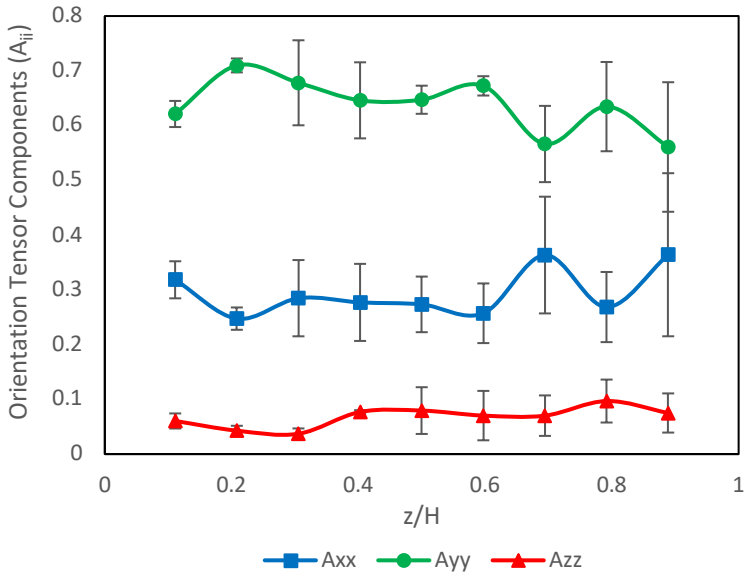

Figure 3.5: Initial through-thickness experimental data for compression molded parts. One millimeter wide samples were taken from the center of the part for analysis. Orientation is represented using the tensor components A_{xx}, A_{yy}, and A_{zz}. Error bars represent a 95% confidence interval.

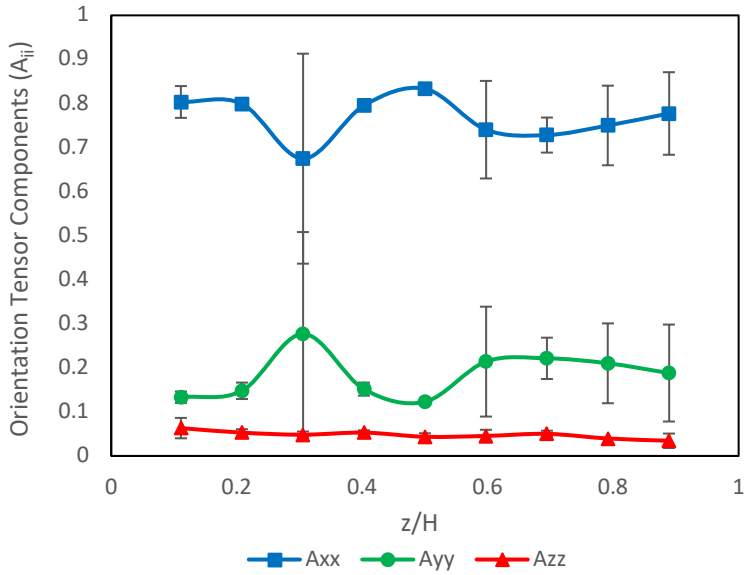

Figure 3.6: Experimental orientation data, represented by the tensor components A_{xx}, A_{yy}, and A_{zz} for samples after undergoing NLSF testing. The tested samples were analyzed at the center of the original as-molded shape. A 1 mm region was analyzed for orientation. Error bars represent a 95% confidence interval.

The experimental orientation data for the samples after testing was represented by Equation (3.21) with a series of constants in order to fit the simulation data. Two set of constants were used for each parameter, A_{zz} was considered insignificant for fitting purposes, one for the top half of the sample (z/h=0.5-1.0) and one for the bottom

(z/h=0-0.5). The constants are listed in Table 3.1. The R^2 value was significantly greater for the top of the sample because of the large error for the parameter values at z/h =0.31 as shown by the error bars in Figure 3.6. The parameter set with the least sum error based on these equations was determined to be α=0.7 and C_I=0.0005, as is shown in Figure 3.7.

$$A_{ii} = C_1(z/h)^4 + C_2(z/h)^3 + C_3(z/h)^2 + C_4(z/h) + C_5 \quad (3.21)$$

Table 3.1: Equation constants that were fit to the post-testing experimental orientation data. The constants are shown in correlation to the range of the sample that they fit, along with their respective R^2 values.

A_{ii}	Thickness Range	C_1	C_2	C_3	C_4	C_5	R^2
A_{xx}	$0 \leq z/h \geq 0.5$	-36.336	42.030	-13.934	1.012	0.834	0.61
A_{xx}	$0.5 \leq z/h \geq 1.0$	8.487	-30.412	40.519	-23.533	5.741	1
A_{yy}	$0 \leq z/h \geq 0.5$	48.592	-55.198	18.543	-1.556	0.123	0.62
A_{yy}	$0.5 \leq z/h \geq 1.0$	-26.626	80.564	-91.535	46.162	-8.480	1

The simulation results shown in Figure 3.7 has an opposite shape to the curves for the two parameters than what was evident in the experimental data and the work for the SGF/PP material. The simulated A_{xx} should demonstrate a peak in the center shear dominated region, and the A_{yy} data should have been lower in this same region instead of the peak that is shown. The Axx parameter is predicted lower through the entire thickness of the sample than what was experimentally measured, and the Ayy parameter is predicted to be higher than experimental values. The prediction is closer to a random orientation (both parameters being 0.5) than what was observed. The long fibers had greater alignment in the flow direction than the short fibers that were used for the development of the initial simulation.

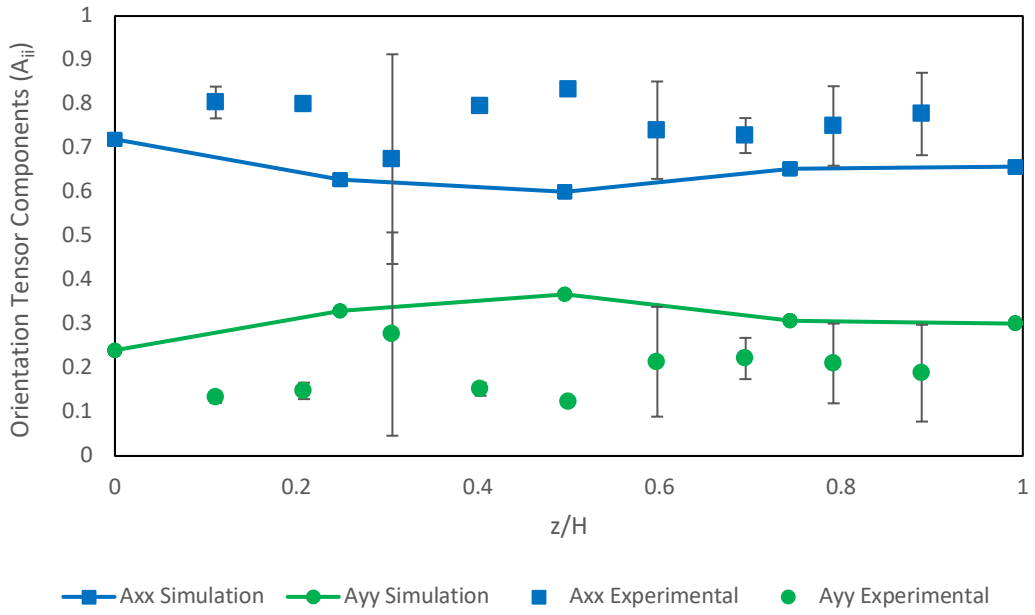

Figure 3.7: Non-lubricated squeeze flow simulation results using the SRF model with the optimized parameters, α=0.7, C_I=0.0005, compared to experimental data. The error bars represent a 95% confidence interval.

Figure 3.8 shows a zoomed in view of the SRF predicted parameters. Holding α=0.7 constant, three C_I values are shown, C_I=0.0005, 0.01, and 0.02. The shape of the curve did not change when the parameter values were changed. The A_{xx} values increased and A_{yy} values decreased slightly with decreasing C_I values for this range. Figure 3.9 shows a comparison for multiple α values. C_I=0.0005 is held constant and α values of 0.1, 0.5, and 0.9 are shown. Once again, changing the parameter value did not change the shape of the curve. Increasing α values led to a decrease in the minimum A_{xx} value and an increase in the shear dominated region which is opposite to what was expected, due to the opposite shape of the curve. Changing the parameter values did not result in a meaningful difference in the predicted orientation.

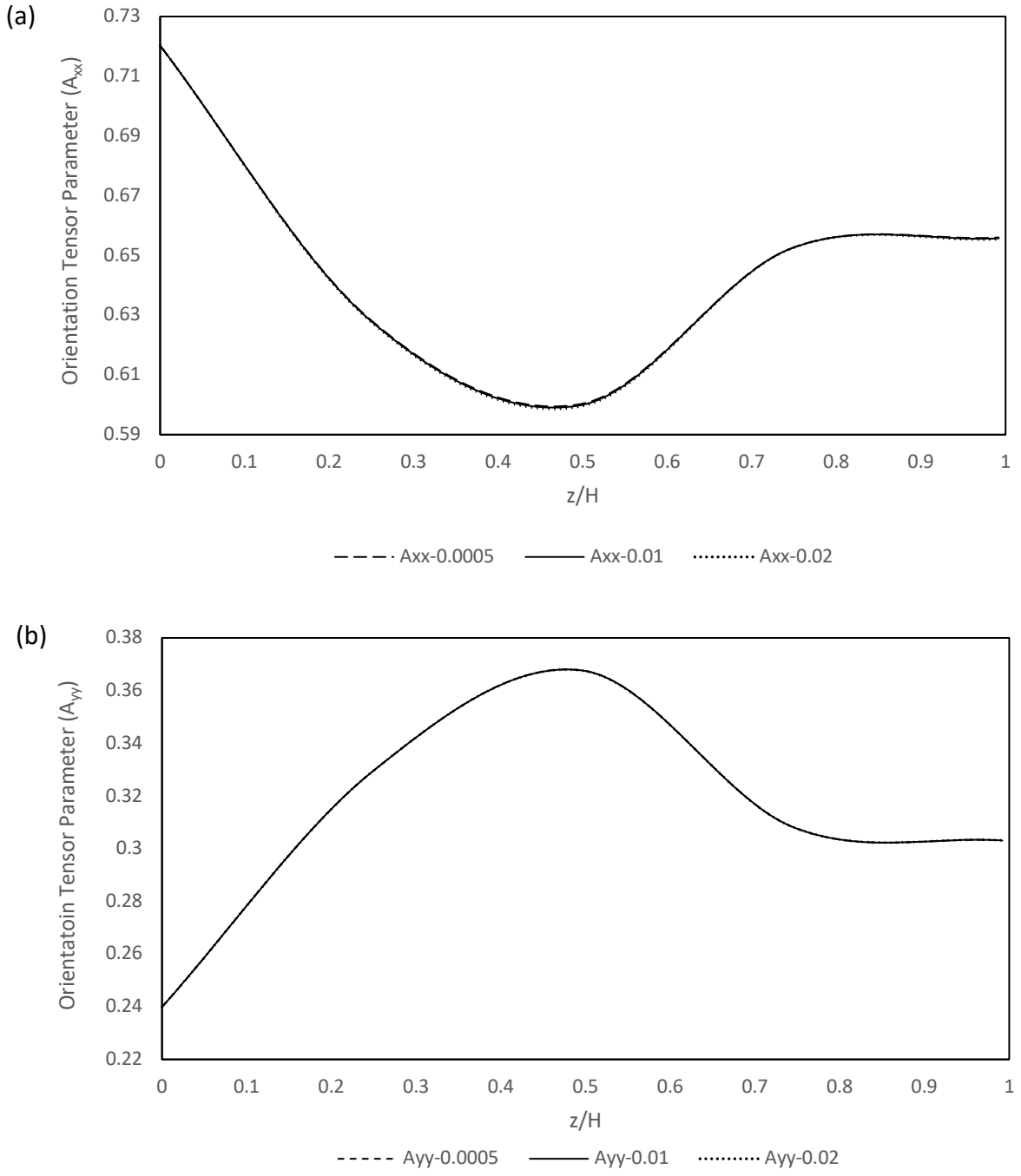

Figure 3.8: Comparison of SRF simulation results for three values of C_I while maintaining a constant α value of 0.7. (a) A_{xx} and (b) A_{yy} are shown comparing the modeled orientation results for C_I values of 0.0005, 0.01, and 0.02.

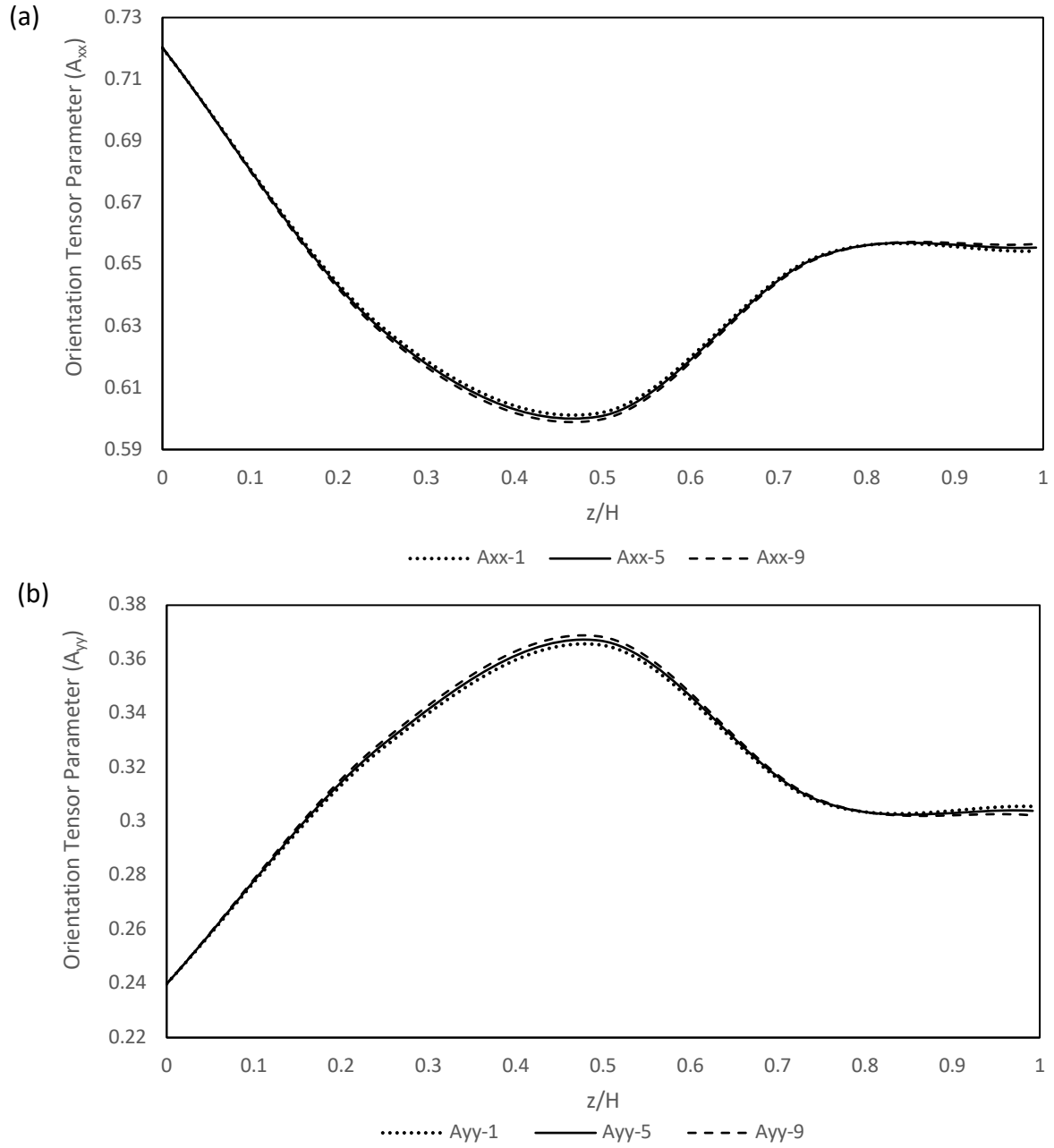

Figure 3.9: Comparison of SRF simulation results for three values of α while maintaining a constant C_I value of 0.0005. (a) A_{xx} and (b) A_{yy} are shown comparing the modeled orientation results for α values of 0.1, 0.5, and 0.9.

The optimal parameters calculated for simulations of the LCF reinforced PA 6,6 are significantly different than those chosen by Lambert et al. [20] for the SGF/PP material. The C_I value is the same as that chosen by Tseng et al. [24] for a 50 wt% LCF/PP material. The consistency in findings validates this research because both are

LCF materials and C_I is a fiber-fiber interaction parameter. The alpha value is different, accounting for the rheology of the different matrices. These parameters are listed in Table 3.2 for comparison.

Table 3.2: Comparison of SRF model parameters from literature (Lambert et al. [20] and Tseng et al. [24]) and this work for fiber reinforced thermoplastics.

Parameter	40 wt% SGF/PP [20]	50 wt% LCF/PA6,6 [24]	40 wt% LCF/PA 6,6
C_I	0.020	0.0005	0.0005
α	1.00	0.1	0.7

The simulated values for A_{yy} are more representative of the trend of experimental A_{xx} values, and simulated A_{xx} values are more representative of the trend of experimental A_{yy} values. The modeled results were switched to account for this change in axis. The results of both were then in the wrong order of magnitude. In order to correctly model the experimental data, the axis were switched, and the A_{xx} data was decreased by a scalar value of 0.47 and the A_{yy} data was increased by a scalar value of 0.47. These adjustments, shown in Figures 3.10 and 3.11, caused a significant increase in fit to the experimental data within a 95% confidence interval.

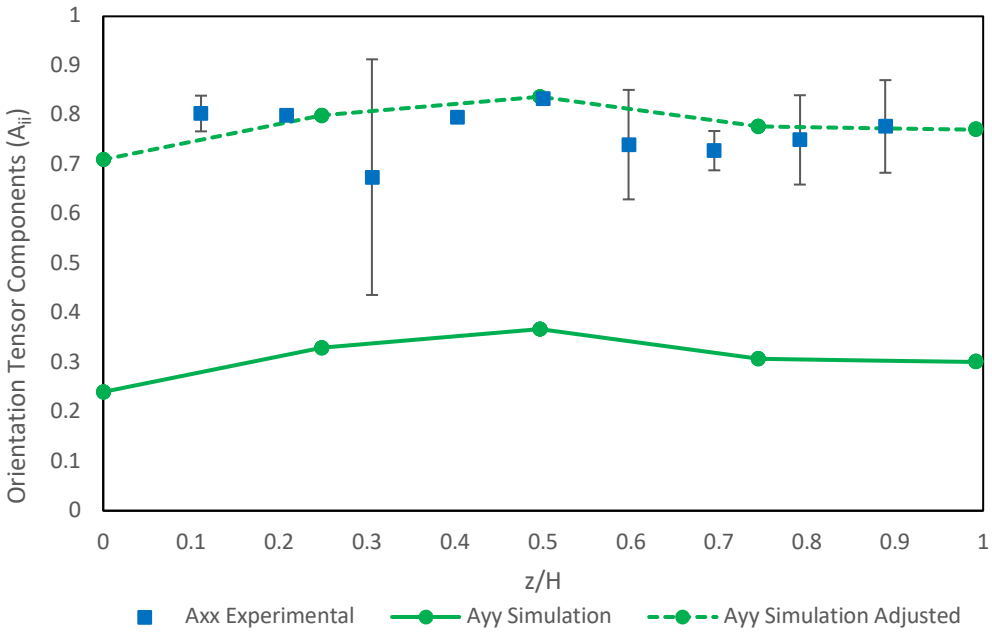

Figure 3.10: SRF simulation results adjusted for experimental A_{xx} data. The modeled A_{yy} orientation tensor values were increased by 0.47. The error bars for the experimental data represent a 95% confidence interval.

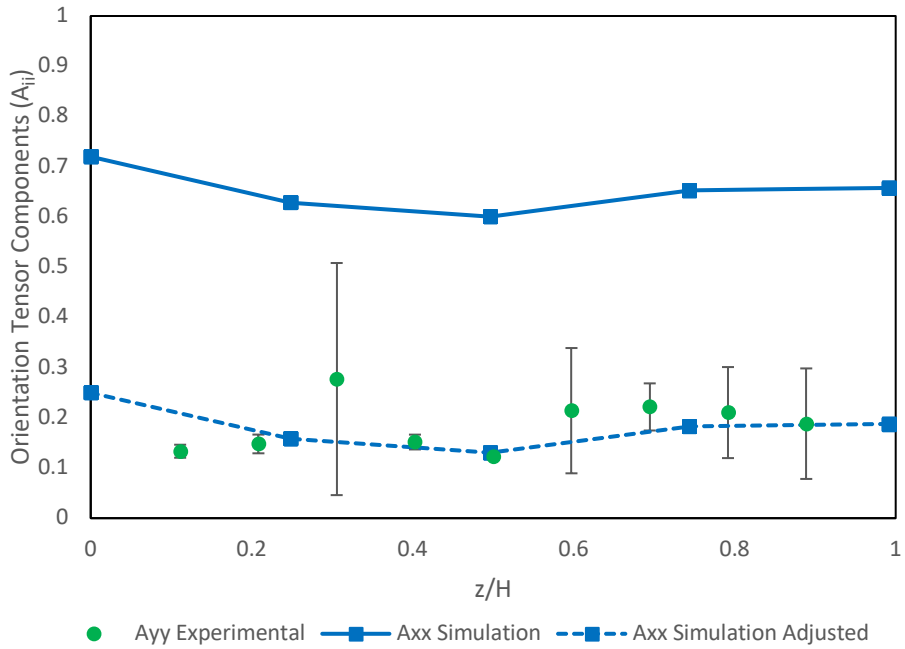

Figure 3.11: SRF simulation results adjusted for experimental A_{yy} data. The modeled A_{xx} orientation tensor values were decreased by 0.47. The error bars for the experimental data represent a 95% confidence interval.

3.5 Conclusions and Recommendations for Future Work

Empirical parameters for orientation simulations of the long carbon fiber reinforced nylon 6,6 material can be predicted using non-lubricated squeeze flow. The methodology and simulation techniques developed for short glass fiber reinforced polypropylene can be used for this new material. The SRF model simulations were not as accurate for the long fiber material as they were for the short fiber material. Future work should include the development of a simulation using the bead-rod model to account for the bending that occurs in long fibers. The SRF model which was developed for short fibers did not accurately account for the greater alignment of long fibers in the flow direction. This was the first test of using NLSF to predict orientation model parameters using long fibers, and the longer lengths account for greater alignment in the x direction. This alignment was not well represented by the SRF model.

The simulated orientation also did not follow the expected curve shapes for Axx and Ayy. Once the x and y axis were switched in the simulation the results followed the expected pattern but were off by a scalar factor of almost 0.5. The predicted orientation tensor values were shifted up by 0.47 for Axx and down by 0.47 for Ayy. The adjusted simulation values resulted in a valid prediction of the experimental orientation within a 95% confidence interval. These findings can be used to provide direction for how to adjust the simulation to increase the accuracy of the model predictions.

Despite the differences in predicted and experimental orientation, the SRF model parameters that were determined correspond with those found in literature (Lambert et al. [20] and Tseng et al. [24]). The parameters were optimized before the adjustments to the simulation results were made. The adjustments used the optimized parameter values

of α=0.7 and C_I=0.0005. These parameters were used in injection molding predictions using the SRF model for the PA 6,6/LCF material with success [21].

3.6 Acknowledgements

The authors thank Michael Vaught and the Virginia Tech Chemical Engineering machine shop for assisting with the adaptation of the non-lubricated squeeze flow fixture, and machinist Rodger Twigg for his assistance with manufacturing the mold tooling. The authors also thank Samuel Hicks for assisting with the image analysis. This work was partially funded by Ford Motor Company.

Works Cited

1. Jacky C. Prucz, S.N.S., Gergis W. William, Mark S. Shoukry, *LIGHTWEIGHT COMPOSITE MATERIALS FOR HEAVY DUTY VEHICLES*, O.o.E.E.a.R.E. US Department of Energy, National Energy Technology Laboratory, Editor. 2013: West Virginia University.
2. R. Bailey, H.K., *A Study of Fibre Attrition in the Processing of Long Fibre Reinforced Thermoplastics.* International Polymer Processing, 1987. **2**: p. 94-101.
3. Ba Nghiep Nguyen, S.K.B., James D. Holbery, Mark T. Smith, Vlastimil Kunc, Barbara J. Frame, Jay H. Phelps, Charles L. Tucker III, *Fiber Length and Orientation in Long-Fiber Injection-Molded Thermoplastics- Part I: Modeling of Microstructure and Elastic Properties.* Composite Materials, 2008. **42**: p. 1003-1029.
4. Lambert, G., *Using Non-Lubricated Squeeze Flow to Obtain Empirical Parameters for Modeling the Injection Molding of Long-Fiber Composites*, in *Chemical Engineering*. 2018, Virginia Polytechnic Instititue and State University.
5. Jan Teuwsen, S.G., Tim A. Osswald, *IMPACT OF THE PROCESS-INDUCED MICROSTRUCTURE ON THE MECHANICAL PERFORMANCE OF INJECTION MOLDED LONG GLASS FIBER REINFORCED POLYPROPYLENE.* SPE ANTEC, 2017.
6. Paal Skjetne, R.F.R., Daniel J. Klingenberg, *Simulation of single fiber dynamics.* Journal of Chem. Phys., 1997. **107**.
7. Suresh G. Advani, C.L.T.I., *The Use of Tensors to Describe and Predict Fiber Orientation in Short Fiber Composites.* Journal of Rheology, 1987. **31**.
8. Fransisco Folgar, C.L.T.I., *Orientation Behavior of Fibers in Concentrated Suspensions.* Reinforced Plastics and Composites, 1984. **3**: p. 98-119.
9. Huynh, H.M., *Improved fiber orientation predictions for injection-molded composites*. 2001, University of Illinois at Urbana-Champaign.

10. Meyer, K.J., *Improved Prediction of Glass Fiber Orientation in Basic Injection Molding Geometries*, in *Chemical Engineering*. 2013, VIrginia Tech.
11. Hongyu Chen, D.G.B., *Experimental Evaluation of Fiber Length Distribution and Modeling of Fiber Orientation and Elastic Properties for Long Glass Fiber Reinforced Thermoplastics*, in *Chemical Engineering*. 2017, Virginia Polytechnic Institute and State University.
12. Uldis Strautins, A.L., *Flow-driven orientation dynamics of semiflexible fiber systems.* Rheol Acta, 2007. **46**: p. 1057-1064.
13. Kevin Ortman, D.B., Peter Wapperom, Alex Aning *Prediction of Fiber Orientation in the Injection Molding of Long Fiber Suspensions.* Polymer Composites, 2012: p. 1360-1367.
14. Peter H. Foss, H.-C.T., John Snawerdt, Yuan-Jung Chang, Wen-Hsien Yang, Chia-Hsiang Hsu, *Prediction of Fiber Orientation Distribution in Injection Molded Parts Using Moldex3D Simulation.* Polymer Composites, 2013.
15. Huan-Chang Tseng, R.-Y.C., Chia-Hsiang Hsu, *Numerical prediction of fiber orientation and mechanical performance for short/long glass and carbon fiber-reinforced composites.* Composites Science and Technology, 2017. **144**.
16. Jay H. Phelps, C.L.T.I., *An anisotropic rotary diffusion model for fiber orientation in short- and long-fiber thermoplastics.* Journal of Non-Newtonian Fluid Mechanics, 2008. **156**.
17. Eberle, A.P.R., *The Dynamic Behavior of a Concentrated Composite Fluid Containing Non-Brownian Glass Fibers in Rheometrical Flows*, in *Chemical Engineering*. 2008, Virginia Polytechnic Institute and State University.
18. Ortman, K.C., *Assessing an Orientation Model and Stress Tensor for Semi-Flexible Glass Fibers in Polypropylene Using a Sliding Plate Rheometer: for the Use of Simulating Processes*, in *Chemical Engineering*. 2011, Virginia Polytechnic Institute and State University.
19. Cieslinski, M.J., *Using a Sliding Plate Rheometer to Obtain Material Parameters for Simulation Long Fiber Orientation in Injection Molded Composites*, in *Chemical Engineering*. 2015, Virginia Polytechnic Institute and State University.
20. Gregory Lambert, P.W., Donald G. Baird, *Obtaining short-fiber orientation model parameters using non-lubricated squeeze flow.* Physics of Fluids, 2017. **29**.
21. Boyce, K., *Modeling Fiber Orientation using Empirical Parameters Obtained from Non-Lubricated Squeeze Flow for Injection Molded Long Carbon Fiber Reinforced Nylon 6,6* in *Chemical Engineering*. 2021, Virginia Polytechnic Institute and State University.
22. Hofmann, J.T., *Extension of the Method of Ellipses to Determining the Orientation of Long, Semi-flexible Fibers in Model 2- and 3-dimensional Geometries*, in *Macromolecular Science and Engineering*. 2013, Virginia Polytechnic Institute and State University.
23. Velez-Garcia, G.M., *Experimental Evaluation and Simulations of Fiber Orientation in Injection Molding of Polymers Containing Short Glass Fibers*, in *Chemical Engineering*. 2012, Virginia Polytechnic Institute and State University.
24. Huan-Chang Tseng, R.-Y.C., Chia-Hsiang Hsu, *Numerical Predictions of Fiber Orientation and Mechanical Properties for Injection Molded Long-Carbon-Fiber Thermoplastic Composites.* Polymer Composites, 2018.

Chapter 2: Literature Review

The overall goal of this research is to accurately model the orientation and stiffness of a discontinuous long carbon fiber reinforced nylon 6,6 polymer in two and three dimensions. A thorough understanding of the existing literature must be achieved for clarity of the background and theories involved. This literature review will be divided into three sections, one for each of the three types of information required as input for the simulation: fiber length, orientation, and empirical parameters.

2.1 Fiber Breakage Mechanisms and Length Distribution Models

In order to injection mold fiber reinforced thermoplastic composites (LFTs), the material must be drawn and cut into pellets. Traditional materials are reinforced with glass or carbon fibers and are cut into 10-13 mm long pellets. (The initial length of the pellets does not determine final average lengths for glass or carbon fibers [1].) Long fiber materials are pultruded so the fibers are continuous throughout the pellet resulting in an initial fiber length of 10-13 mm, as opposed to short fibers that are randomly oriented in the pellet and are 0.2-0.4 mm long [2]. Some sources refer to discontinuous or chopped fibers as “short” and continuous fibers as “long”, but within the discontinuous fiber literature “short” refers to fibers that are less than 1 mm in length (usually around 0.2-0.4 mm), and “long” refers to fibers that are 1 mm or longer [3]. This 1 mm cutoff was determined based on the mechanical behavior of glass fibers. Figure 2.1 is a popular graph used to show the dependence of many material properties on fiber length using glass fibers. The graph demonstrates how the modulus begins to

plateau at 1 mm while the strength and impact resistance continue to increase with increasing fiber length.

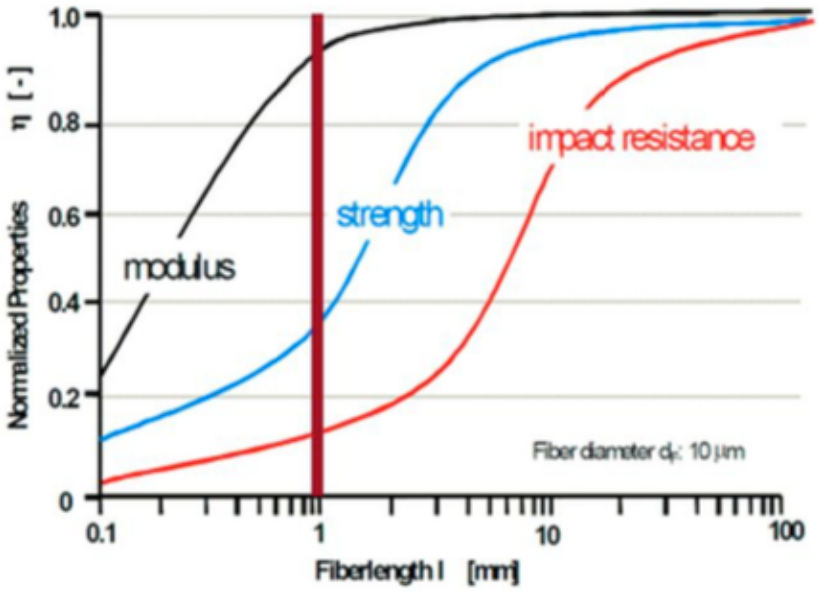

Figure 2.1: Mechanical properties of wet-laid glass reinforced composites dependent on fiber length [4]. Reproduced with permission from author and Virginia Tech.

A more universal method of classification would be to use the fibers' aspect ratio. The aspect ratio is the comparison of the fiber's length to the diameter. Figure 2.2 illustrates the relationship between a composite's modulus and the aspect ratio of the fiber reinforcement [5]. The plateau that was discussed for Figure 2.2 is shown at the aspect ratio of 100. The diameter of carbon fibers ranges from 5-10 microns, nearly half that of glass fibers. Young's modulus of LFTs. The aspect ratio of carbon fibers is approximately twice that of glass fibers at the same length, so this modulus plateau happens at a lower length. For example, the plateau begins at the 1 mm mark for glass fibers and that corresponds to an aspect ratio of 100, so the length of carbon fiber at the

same aspect ratio would be 0.5 mm. This means that for stiffness, carbon fibers exhibit long fiber properties beginning at 0.5 mm.

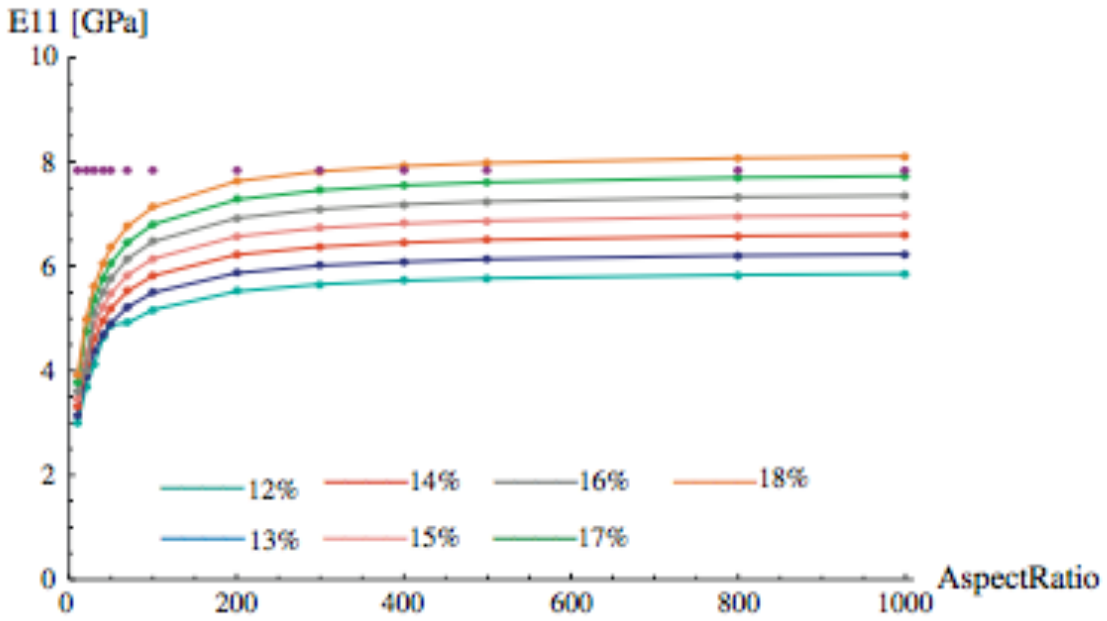

Figure 2.2: Young's modulus as a function of aspect ratio for different fiber volume fractions [5]. Reproduced with permission from Journal of Composites Science and Technology.

Composite failure strain will decrease with an increase of fiber content (if the aspect ratio of the reinforcement is constant), because under tensile loading cracks in the matrix start at fiber ends and propagate along the interfaces between fibers and the matrix or cross through the matrix until total failure occurs [6]. With shorter fiber reinforcement, there are naturally more fiber ends, leading to concentrations in the stress and weaker composites. Fiber-matrix adhesion can be improved based on the sizing used in carbon fiber production [7]. Due to all of the material used in this research having the same treatment, sizing selection will not be discussed further in this review.

As pellets undergo processing, the fibers experience a significant amount of breakage. This breakage has many causes: fiber-polymer, fiber-fiber, and fiber-machine interactions[6]. Due to the large number of fibers, tracking and measuring an individual fiber's length would be computationally expensive and unrealistic. Instead, a fiber length distribution is determined. A normalized probability density function $f(l)$ is used, where $f(l)dl$ is the probability of a fiber's length being between l and $l + dl$ [8].

$$\int_0^\infty f(l)dl = 1 \tag{2-1}$$

The normalized function is used to calculate the number and weight averages, L_n and L_w [8].

$$L_n = \int_0^\infty f(l)ldl \tag{2-2}$$

$$L_w = \frac{\int_0^\infty f(l)l^2dl}{\int_0^\infty f(l)ldl} \tag{2-3}$$

Approximations are used to estimate the average values, resulting in a summation that is easier for calculations. Details about the derivation can be found in a paper by Nguyen, et al. [8].

$$L_n = \sum_i \overline{f_i} l_i \Delta l = \frac{\sum_i N_i l_i}{\sum_i N_i} \tag{2-4}$$

$$L_w = \frac{\sum N_i l_i^2}{\sum N_i l_i} \tag{2-5}$$

When the fibers all have the same length L_w=L_n - for all other systems, L_w>L_n [2]. For modeling, it is also helpful to track total fiber length, because fibers must be conserved in the closed system. The total fiber length as defined by Phelps et al. [2] is:

$$L_t = \sum N_i l_i \tag{2-6}$$

Fiber breakage typically produces a distribution with a long tail trailing toward the initial fiber length, an example of this distribution is shown in Figure 2.3, the difference in weight- and length-averages is also shown [2, 8] [9] [4].

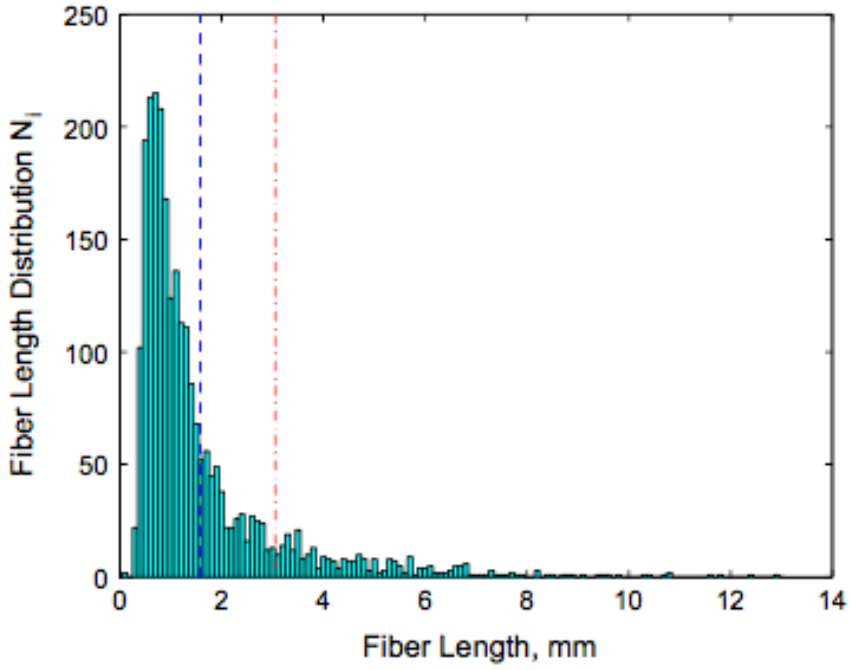

Figure 2.3: Experimental fiber length from an example of an injection molded long fiber thermoplastic material, the initial fiber length was 12 mm. Vertical lines indicate the values for number-average and weight-average fiber lengths [2]. Reproduced with permission from Journal of Composites: Part A.

In the injection molding process, fibers will experience high levels of stress and strain. In moderate stress regions, it has been observed that fiber breakage typically depends on total strain; however, fiber length can be preserved if stress levels are significantly reduced [2]. Work by Shon et al. [2] indicates that the fibers will degrade

during compounding until they reach an average equilibrium length (L_∞), the rate at which the average fiber length L approaches equilibrium is modeled as:

$$\frac{dL}{dT} = -k_f(L - L_\infty) \tag{2-7}$$

The method for determining average length was not explained, nor were the details for the kinetic constant k_f, which is used as a fitting parameter.

Fiber-matrix breakage typically happens as a function of buckling. Salinas and Pittman [10] report that breakage is low in purely extensional flow because the fibers align and are in tension, but that fibers rotate and bend across stream lines in shear flow causing significant breakage. Injection molding is a combination of shear and extensional flows making the mathematical analysis of fiber attrition difficult [10]. These researchers also observed that as fiber flexibility increased and/or as shear stress increased the minimum radius of curvature decreased [10]. Fiber breakage models and observations are highly dependent on the stiffness of the fibers in the composite. Switzer and Klingenberg [11] developed an equation for an effective stiffness:

$$S^{eff} = E_Y \pi D^4 / 64 \eta_m \dot{\gamma} L^4 \tag{2-8}$$

E_Y is the Young's modulus for the fiber, D is the fiber's length, η_m is the viscosity of the matrix, $\dot{\gamma}$ is the shear rate, and L is the fiber's length [12]. As this dimensionless quantity approaches 0 the fibers resemble completely flexible threads, and as the quantity approaches infinity the fibers are rigid retaining their original shape despite flow interferences [12]. Many attempts have been made to model the effects of hydrodynamic forces on the fiber. This work began with Forgac and Mason's [13] explanation that rigid fibers have a tendency to rotate and buckle in simple shear flow, and primarily focused on the bulk stress and suspension viscosity [2]. Phelps and

Tucker [9, 14, 15] expanded that idea, using Dinh and Armstrong's [9, 14, 15] slender body analysis, to examine the force at local points along the length of the fiber $f(s)$, where s is a local coordinate along the fiber axis [9, 14, 15]. The overall force on a fiber in a dilute suspension was modeled by Burgers as a function of the fiber's orientation and the shear rate [9]:

$$F = -\int_{L/2}^{0} f(s)ds = \frac{M\pi\eta_m\dot{\gamma}L^2}{ln2a_r - 1.75} \tag{2-9}$$

In this equation, $\dot{\gamma}$ is the shear rate, M is the orientation factor for a single fiber ($M = sin^2\theta\ sin\phi\ cos\phi$), and the sign of F, determines whether it is under compression or tension, depends on the fibers orientation relative to the flow field.

A method of modeling the fiber attrition has been developed using a constitutive equation that uses flow conditions and fiber properties to determine a breakage rate, assuming a dilute-suspension and that the majority of breakage comes from flow-induced buckling [2]. The research clarifies that a rigid fiber will undergo a Jeffrey orbit because flow induces a rotational pattern in the fibers [2]. Thus, the fiber rotates through an orientation space where the fiber is in compression even though the bulk material is loaded in tension [2]. When the individual fibers are in compression the stress exerted on the surface of the fiber reaches the tensile strength of the fiber causing buckling and eventually breakage. Nominally the original fiber is referred to as the parent fiber, and the fibers that result from the break are the child fibers. It is important to note that the total fiber length must be conserved [2]. The conservation equation is given as:

$$\frac{dN_i}{dt} = -P_iN_i + \sum_k R_{ik}N_{ik} \tag{2-10}$$

where P_i is the breakage rate, N_i, is the local fiber length, or the expected number of fibers of length l_i, and R_{ik} is the child generation rate [2]. This equation can be used to create a rate of change for total length, L_t, and if total fiber length is conserved, $dL_t/dt=0$ [2]. The magnitude of the compressive force in the center of the fiber is a function of the fiber's orientation vector **p:**

$$F_i(\boldsymbol{p}) = \frac{\zeta \eta_m l_i^2}{8}(-\boldsymbol{D}:\boldsymbol{pp}) \tag{2-11}$$

where ζ is a dimensionless drag coefficient, η_m is the matrix viscosity, and **D** is the rate of deformation tensor [2]**.**

The critical buckling force can then be calculated as:

$$F_{crit} = \frac{\pi^3 E_f d_f^4}{64\ l_i^2} \tag{2-12}$$

where E_f is the elastic modulus of the fiber and d_f is the fiber diameter [2].

Buckling occurs when $F_i > F_{crit}$. This analysis continues to yield the critical shear rate, and the length when fibers are too short to break from buckling [2]. The buckling parameter (B) can be used for modeling and it is defined as:

$$B_i = \frac{4\zeta \eta_m \dot{\gamma} l_i^4}{\pi^3 E_f d_f^4} \tag{2-13}$$

here $\dot{\gamma}$ is added as the scalar magnitude of the rate of deformation tensor [2]. The breakage probability is then modeled for fibers of length, l_i, using a breakage coefficient, C_B, this model gives a reasonably accurate representation of fiber length for center-gated disks molded with polypropylene that is reinforced with 40 weight percent glass fiber [2].

$$P_i = \begin{cases} 0, & B_i < 1 \\ C_B\dot{\gamma}(1 - \exp(1 - B_i), & B_i \geq 1 \end{cases} \quad (2\text{-}14)$$

The conclusions of this study give some overall insight into the behavior of fiber attrition. Phelps, et al. [2] discovered that fiber length is severely degraded in this particular center-gated disk mold, the average fiber length was longer at the gate than in the advancing front region. The researchers also verified their prediction that shorter fiber lengths are found closer to the mold walls, due to the higher shear stresses in this region, and that longer fiber lengths lie along the midplane and very close to the mold walls because the material travels along the midplane and then is pushed to the wall and freezes before breakage can occur [2]. The average fiber length also initially decreases in the radial direction with the weight average decreasing more quickly than the number average, but then closer to the end of the disk both averages increase due to fountain effects [2]. Weight-average length drops from approximately 3 mm to just under 2.5 mm, and number-average length drops from approximately 1.5 mm to just under 1.5 mm [2]. This data shows that the majority of fiber breakage occurs before the material reaches the mold. This model is very similar to that derived of Durin et al. [9, 15] and Phelps and Tucker [9, 15]; it represents what Moldflow uses for simulations.

The viscosity also affects the breakage of fibers, other researchers used the breakage model developed by Phelps and Tucker [9] to show that the lower the power law index, the lower the average fiber breakage. As the power law index increases, the material is more shear thinning, and there is a smaller region dominated by high shear rates [9].

Fiber breakage models, such as those proposed by Phelps and Tucker [2, 9, 15], Phelps, et al. [2, 9, 15], Frederick et al. [2, 9, 15], and others only account for the fiber-

matrix interactions, and only study the axial properties of the fibers. Research by Vu-Khanh et al. [16] shows that most of the fiber length attrition occurs in the beginning of the injection molding process, not in the mold itself. These researchers found that glass fibers with an average length of 10 mm in a polypropylene matrix reduced to mean fiber lengths of 1.6 mm or less at the entrance of the mold, however fiber lengths were 2-3 times less in a polyamide matrix [2]. Fiber breakage in the injection molding process is affected by many processing variables, including the screw back pressure (residence time), screw geometry, injection speed, gate size, and nozzle design [1, 2]. These variables control the fiber-fiber, fiber-polymer, and fiber-machine interactions.

The buckling work was expanded and evaluated in the extrusion process by Mittal et al. [17]. A single fiber's rotation and orientation in the suspension was restricted by one end being affixed to the solid bed; the fixed fiber will then experience normal forces perpendicular to its axis, breaking it off from the solid bend [17]. The broken fiber is then free to move about the matrix and may experience further attrition due to buckling deformations [17]. This work still ignores the fiber-fiber interactions. Fiber-fiber interactions may also increase fiber breakage, but it may also decrease the breakage by allowing the fibers to bundle together, thus lowering the aspect ratio and decreasing the effects of the fiber flexibility [2, 15].

In suspensions where fibers not only undergo hydrodynamic forces, but also physically contact one another, normal stress differences are present. The primary normal force difference (N_1) is linearly proportional to shear rate, and the secondary normal forces are significantly less and can be neglected [12]. Keshtkar et al. [12] showed that in semi-dilute and semi-concentrated regime fiber concentration increases

result in an increase in N_1 as well. The assumption that fiber-fiber collisions are the major cause for normal forces in steady flow leads to the following equation for N_1 [12]:

$$N_1 = K\eta_m\dot{\gamma}\frac{\phi r^{1.5}}{\ln 2r - 1.8} \tag{2-15}$$

Goto et al. [12] expressed N_1 as a power law expression:

$$N_1 = m\dot{\gamma}^n \tag{2-16}$$

H. J. Wolf [18] developed a technique for evaluating the breakage at different positions within a single screw extruder. He focuses on screw plasticating because it has been expressed as the location of greatest length reduction [18]. He extruded the material continuously through a circular die and then stopped the process and cooled the material rapidly, the screw was removed and the hardened polymer composite, which had formed a helix, was removed [18]. He then examined the fiber length at multiple locations by burning off the matrix [18]. Wolf [18] separates the breakage into 6 discreet mechanisms that happen along the screw. Figure 2.4 (a) illustrates these mechanisms in an unwound representation of the screw channel; Figure 2.4 (b) shows a cut out of what is happening in the channel to better demonstrate mechanisms 3-6 [18]. Mechanism 1 occurs when granules enter the screw and breakage begins [18]. Depending on the size of the granules and the channel depth in the feed zone, some granules are squeezed between the edge of the intake and the screw flight [18]. Mechanism 2 describes granule-granule interactions that start as the granules continue into the feed zone [18]. In the melting zone, both solid and melted polymers exist [18]. The material touching the heated barrel walls is melted and then scraped forward by the screw in a circular pattern [18]. Fibers that become wedged between the barrel wall and the flight are severed or damaged by shear and frictional forces, this is mechanism 3

[18]. A model similar to that suggested by Mittal et al. [17, 18] is used for mechanism 4, where fiber breakage is induced by melt flow at the barrel surface [17, 18]. Mechanism 5 considers the breakage from the movement of the solid bed at the screw core [18]. Both mechanisms 4 and 5 are due to the interference of solid and melted polymer layers, however at the screw core (M5) the velocity field has no cross-sectional component [18]. Fibers will begin to circulate along with the melt flow as illustrated in Figure 2.4, and the degree of breakage due to this circular motion, mechanism 6, depends on the length, number, and flexibility of the fibers [18]. The most important factor for length conservation is the residence time, because greater residence times lead to more time in this circular flow [18]. Wolf [18] draws the conclusion that processing parameters must be optimized. While more gentle processing conditions (lower residence times and screw speeds) will lead to longer residual fibers, it will be at the sacrifice of inferior mixing and more bundles [18]. Chen et al. [1] also show that larger machines with greater barrel diameters lead to longer mean fiber lengths (a barrel diameter 1.66 times larger had an L_n that was 61% longer).

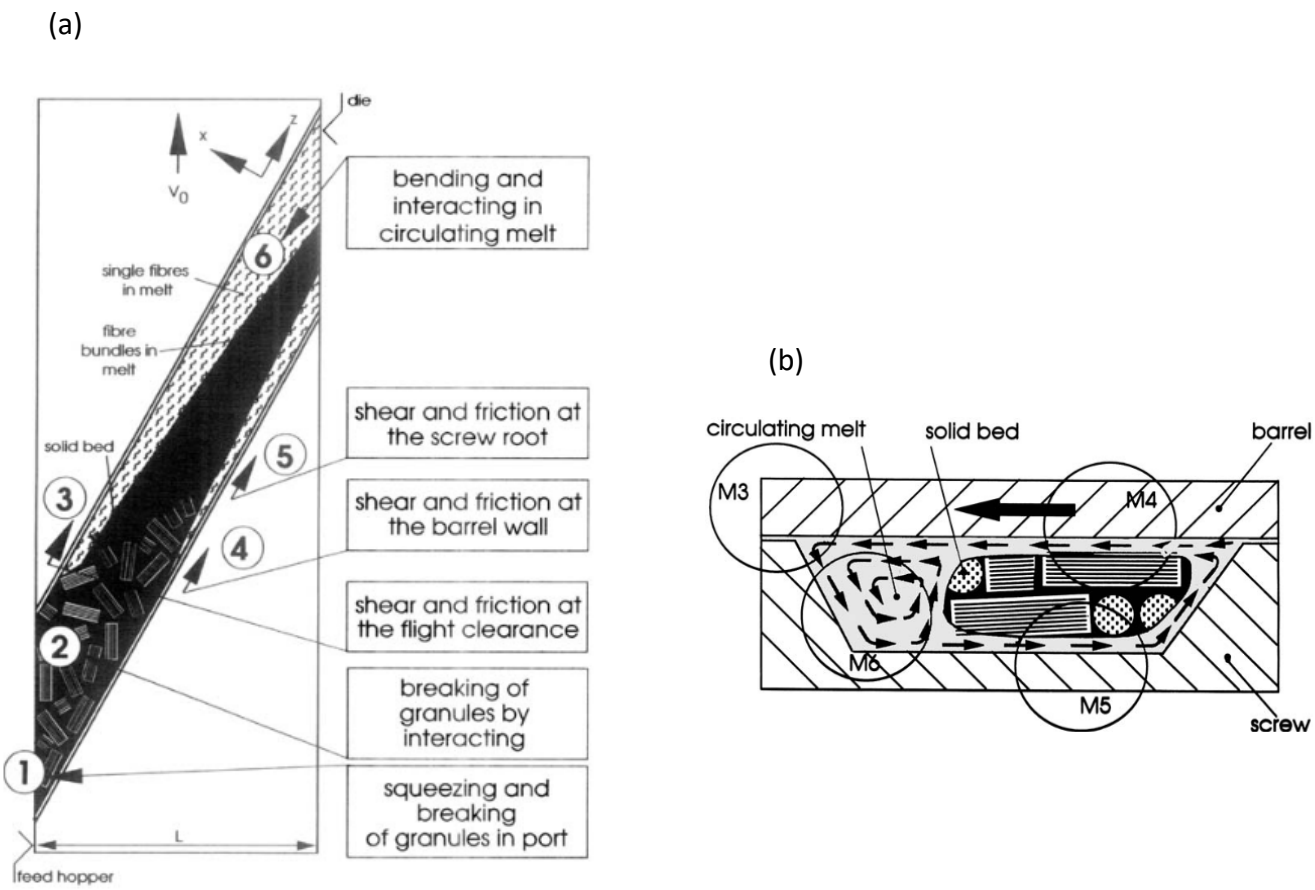

Figure 2.4: (a) Fiber breakage mechanisms (M1-M6) in an unwound representation of a screw channel. (b) Fiber breakage mechanisms in a cross section of a screw channel [18]. Reproduced with permission from Journal of Polymer Composites.

The ability of Baird and coworkers to model fiber breakage has been tested for both glass and carbon long fibers in a polypropylene matrix. The model demonstrated that glass and carbon fibers have a similar trend and that carbon fibers experience greater attrition, which agrees with literature. The predicted number average length values are in reasonable agreement with experimental values for two screw sizes [1]. The greatest amount of breakage occurs in the screw and experimental length values measured in the sprue match those measured from the part.

2.2 Orientation Models

With the intention to efficiently injection mold LFT parts for industrial use, it is imperative to be able to understand the orientation evolution of the fiber reinforcement. Mechanical performance is dependent on fiber orientation. Being able to model and predict the fiber orientation during mold flow and in the final part provides engineers with the ability to tailor mold the design for preferred orientations and therefore mechanical properties.

2.2.1 Fiber Orientation Models

This discussion on orientation models will be divided into four sections. It will begin by discussing the evolution of equations for rigid fibers and then expand into the ways that researchers are accounting for fiber length. Many of the models that will be investigated use a fourth order tensor; Section 3 will describe the closure approximations used to define a fourth order tensor in terms of lesser second order tensors. Finally, in the fourth section, the challenges associated with modeling a carbon fiber reinforced nylon 6,6 composite will be addressed.

The development of fiber orientation models exposes that the evolution of fibers is dependent of the concentration of fibers in the matrix. It is important to define the classifications of fiber concentrations that will be used in the following discussion. The classifications established by Doi and Edwards [19] are explained in Table 2.1. These definitions are commonly used in the polymer dynamics field.

Table 2.1: Concentration regime definitions and bounds [19].

	Definition	Fiber Volume Fraction Bounds	Fiber- Fiber Interactions
Dilute Suspension	Fibers are at least 1 fiber length away from the closest neighboring fiber.	$\varphi < a_r^{-2}$	Fibers rotate freely without contacting other fibers, and all disturbances made to the flow field of the matrix dissipate before reaching other fibers.
Semi-Concentrated Suspension	Fibers are between 1 fiber length and (on average) 1 fiber diameter from the closest neighboring fiber.	Parallel Systems: $\varphi < \frac{\pi}{4}$	Fibers do not physically contact other fibers, but the disturbances to the flow field made by a fiber can be felt by those around it.
		Isotropic Systems: $\varphi < a_r^{-1}$	
Concentrated	Fibers are closer than 1 fiber diameter to the nearest fiber.		Fibers physically encounter other fibers, and feel the hydrodynamic effects induced by other fibers.
$*$ φ is the fiber volume fraction and a_r is the fiber's aspect ratio L/D			

2.2.1.1 Rigid Fiber Models

The work of Jeffery [20] in 1922 to describe ellipsoidal particle motion in a moving Newtonian fluid serves as the origin of the fiber orientation models. Figure 2.5 reveals the evolution of the models for rigid fibers starting with Jeffery's work and finishing with the work of Tseng, et al. [21] for the commercial simulation package, Moldex3D. Figure 2.5 is provided as a reference that gives brief explanations of each of the models and shows the progression of their development.

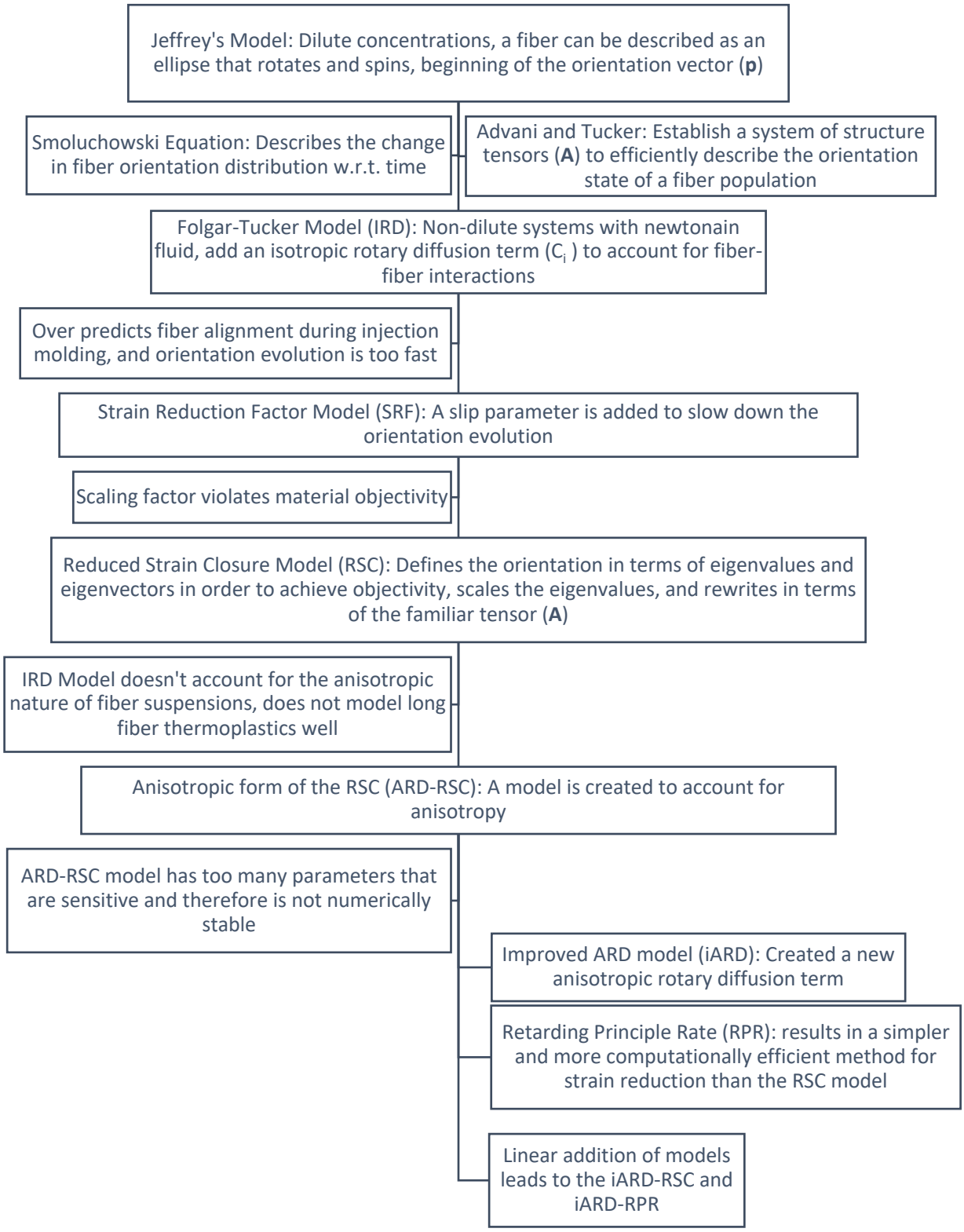

Figure 2.5: Evolution of fiber orientation evolution models.

Jeffery describes the motion of a fiber in a dilute Newtonian fluid [22]. He claims that in simple shear flow ($v_1 = \dot{\gamma} y, v_2 = v_3 = 0$) the fiber center moves at the same velocity as the fluid in that point [22]. The fiber is represented as an ellipsoid with the following angular evolution, where $\xi = \frac{a_r^2 - 1}{a_r + 1}$ defines the shape of the ellipsoid and a_r =l/d is the aspect ratio, shown in Figure 2.6 [23]:

$$\frac{\partial \theta}{\partial t} = \xi \frac{\dot{\gamma}}{4} \sin 2\theta \ \sin 2\phi \tag{2-17}$$

$$\frac{\partial}{\partial t} = \frac{\dot{\gamma}}{a_r^2 + 1}(a_r^2 cos^2\phi + sin^2\phi) \tag{2-18}$$

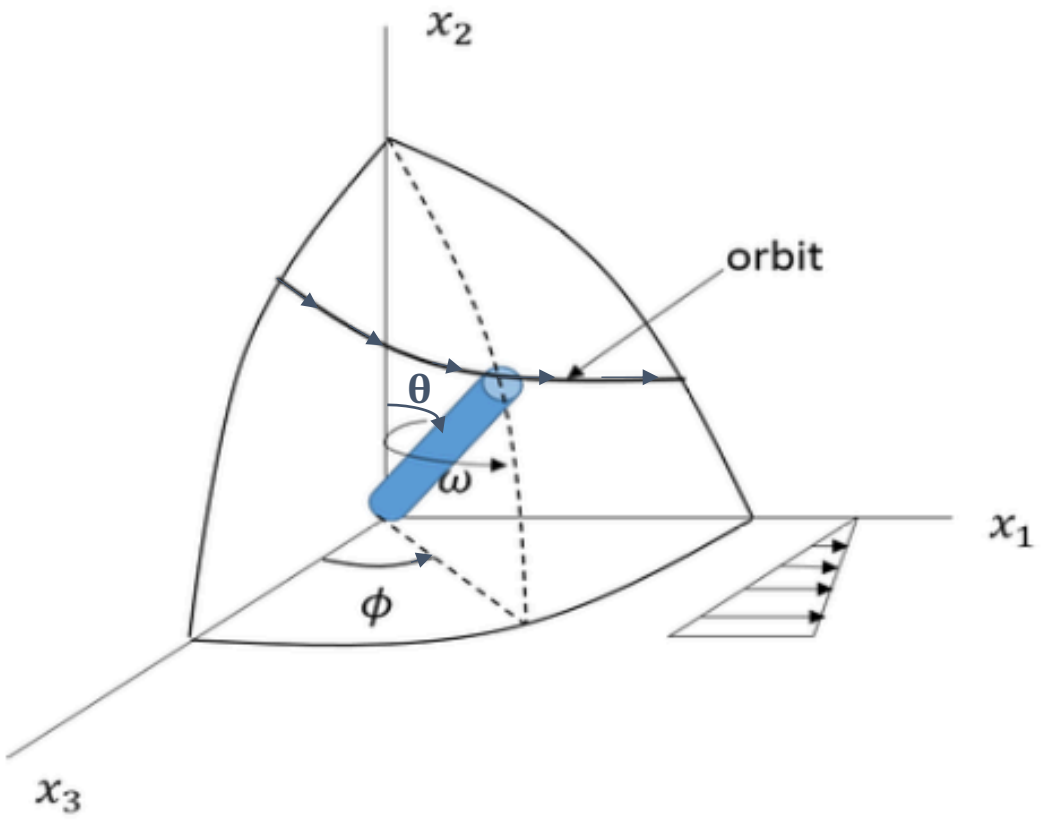

Figure 2.6: The Jeffrey's orbit of a fiber in simple shear flow and the angular motion [24]. Reproduced with permission from the Journal of Physical Chemistry A.

The periodic motion that the particle undergoes has been called a Jeffery orbit [2]. By defining a vector **p** along the fiber's axis and solving the equations of motion and continuity, the following vector form results for the motion of a single fiber [9]:

$$\frac{\partial \boldsymbol{p}}{\partial t} + \boldsymbol{v} \cdot \boldsymbol{\nabla p} = \boldsymbol{W} \cdot \boldsymbol{p} + \xi[\boldsymbol{D} \cdot \boldsymbol{p} - (\boldsymbol{p} \cdot \boldsymbol{D} \cdot \boldsymbol{p})\boldsymbol{p}] \tag{2-19}$$

Inspection of this model indicates that the fiber will rotate in simple shear flow, and align in the direction of extension for simple extensional flow [25].

In commercial LFTs the fiber count is too high to track every fiber's evolution, so a probability distribution function $\psi(\boldsymbol{p})$ is a statistical representation of the orientation state for a population of particles or fibers in a suspension, ψ (the probability of a fiber being oriented between **p** and **p**+d**p** [26]. The orientation of a particle is the same for **p** and –**p**, therefore $\psi(\boldsymbol{p}) = \psi(-\boldsymbol{p})$. The function must also meet a normalization condition so that the probability equals unity when summed over all orientation states [9]. The Smoluchowski equation is used to describe the change in orientation distribution over time at a specific location in the fluid [27]:

$$\frac{D\psi(\boldsymbol{p})}{Dt} = -\frac{\partial}{\partial \boldsymbol{p}} \cdot (\psi(\boldsymbol{p})\dot{\boldsymbol{p}}) \tag{2-20}$$

This orientation distribution is a complete and unambiguous description of the orientation state that can be calculated from processing conditions. The downside is that it is cumbersome to track, due to its dependence on both the orientation angles of **p** and position [27], which results in too much information for a numerical simulation [27]. Advani and Tucker [27] developed a set of orientation tensors by taking the dyadic products of the vector **p** and integrating with $\psi(\boldsymbol{p})$ over all orientation directions. The

distribution is even, so odd integrals are negated and therefore only the even-order tensors are left [27]. The second and fourth order tensors are [8]:

$$A_{ij} = \langle p_i p_j \rangle = \int \psi(\boldsymbol{p}) p_i p_j d\boldsymbol{p} \tag{2-21}$$

$$A_{ijkl} = \langle p_i p_j p_k p_l \rangle = \int \psi(\boldsymbol{p}) p_i p_j p_k p_l d\boldsymbol{p} \tag{2-22}$$

The higher the order of the tensor the more accurately the orientation state is represented [28] [27]. These tensors are symmetric, and their trace equals unity [28] [27]. Closure approximations are used to find values for the fourth-order tensor.

The tensors developed by Advani and Tucker [27] can be used to create a continuum form of Jeffrey's equation given as [9]:

$$\frac{D\mathbf{A}}{Dt} = \frac{\partial \mathbf{A}}{\partial t} + \mathbf{v} \cdot \nabla \mathbf{A} = \mathbf{W} \cdot \mathbf{A} - \mathbf{A} \cdot \mathbf{W} + \xi(\mathbf{D} \cdot \mathbf{A} + \mathbf{A} \cdot \mathbf{D} + 2\mathbf{D}\colon \mathbf{A_4}) \tag{2-23}$$

where **D** is the rate of deformation tensor ($\boldsymbol{D} = \frac{1}{2}[\boldsymbol{\nabla v} + (\boldsymbol{\nabla v})^t]$) and **W** is the vorticity tensor ($\boldsymbol{W} = \frac{1}{2}[(\boldsymbol{\nabla v})^t - \boldsymbol{\nabla v}]$). Jeffery's model is only valid for dilute suspensions in creeping Newtonian fluids [25]. Hydrodynamic forces greatly influence fiber motion and keep fibers from aligning as predicted by the Jeffery's model [4].

Folgar and Tucker [25] developed a mathematic model to predict the orientation distribution function of rigid fibers in concentrated suspensions by adding an isotropic rotary diffusion term to Jeffery's model in which C_I is a phenomenological constant and $\mathbf{I}$ is the unit tensor .

$$\frac{D\mathbf{A}}{Dt} = \mathbf{W} \cdot \mathbf{A} - \mathbf{A} \cdot \mathbf{W} + \xi(\mathbf{D} \cdot \mathbf{A} + \mathbf{A} \cdot \mathbf{D} + 2\mathbf{D}\colon \mathbf{A_4}) + 2C_I\dot{\gamma}(\mathbf{I} - 3\mathbf{A}) \tag{2-24}$$

Their model makes some assumptions about the fibers, the matrix, and the suspension. The fibers are represented by rigid cylinders (uniform in length and diameter). They are large enough that Brownian motion is negligible, and their centers of mass are randomly distributed [25]. The matrix is sufficiently viscous so that particle inertia and particle buoyancy can be ignored [25]. Finally, the suspension is incompressible, and there are no external forces or torques acting on it [25]. The authors found that the motion for an individual fiber in a concentrated suspension is dependent on its current angle, the flow field, the ability to reorient when interacting with other fibers, and their behavior, which is contingent on angle and flow field, until they interact with another fiber [25]. The first two causes are the same for a dilute fiber, and, hence, the similarities between equations (2-23) and (2-24) [25]. The interaction between two fibers causes an orientation change for both fibers [25]. The orientation changes may have a directional bias, but this is neglected, and the interactions result in orientation changes that are considered to be independent, identically distributed random variables with zero mean, similar to Brownian motion [25]. The isotropic rotary diffusion term C_I must be determined experimentally. Several attempts have been made to model this coefficient, but none have been successful at this time [9]. Steady flow creates a steady state distribution for orientation, and the breadth of this distribution is dependent on C_I [25]. As C_I increases, the steady state orientation is more disperse [25]. C_I increases with fiber length, because higher fiber length leads to more dispersion. Yamane [9] also suggested that C_I increases with an increase in fiber concentration. All of the empirical attempts to model C_I denote the term as a function of fiber size and concentration [9]. Bay et al. [28] state that other C_I models assume that fiber length and diameter were

constant throughout the suspension and proposed that a fiber length distribution would increase the accuracy of modeling C_I trends [28]. Note that if C_I is set to zero, the Folgar-Tucker model reverts back to the Jeffery's model.

Stress growth experiments in the startup of simple shear flow, using glass fiber reinforced polypropylene, demonstrate that orientation kinetics in reality are slower than predicted [29]. A scaling factor, α, is a slip parameter with a value between 0-1 [29]. The right side of Equation 2-24 is multiplied by this factor resulting in the Strain Reduction Factor (SRF) model [29]. The addition of this strain reduction term improves the accuracy of the model, but results in a loss of material objectivity, meaning that the coordinate system cannot be changed, nor the frame rotated, or translated [29]. Note that if α is set to unity then the Folgar-Tucker model is maintained.

Wang et al. [9] developed a method to correct the material objectivity by redefining the **A** tensor in terms of its eigenvectors and eigenvalues. The rotation rate of the eigenvectors ($\boldsymbol{e_i}$) remains the same, but the eigenvalues (λ_i) are scaled by an empirical value κ that ranges from 0-1. After the equations are reconfigured in terms of the **A** tensor the Reduced Strain Closure (RSC) model was developed [30]:

$$\frac{D\mathbf{A}}{Dt} = \mathbf{W}\cdot\mathbf{A} - \mathbf{A}\cdot\mathbf{W} + \xi\{\mathbf{D}\cdot\mathbf{A} + \mathbf{A}\cdot\mathbf{D} + 2[\mathbf{A_4} + (1-\kappa)(\mathbf{L}_4 - \mathbf{M}_4 : \mathbf{A}_4)] : \mathbf{D}\} + 2C_I\dot{\gamma}(\mathbf{I} - 3\mathbf{A}) \tag{2-25}$$

$$\mathbf{L}_4 = \sum_{i=1}^{3} \lambda_i(\boldsymbol{e_i e_i}\, \boldsymbol{e_i e_i}) \tag{2-26}$$

$$\mathbf{M}_4 = \sum_{i=1}^{3} \lambda_i(\boldsymbol{e_i e_i}\, \boldsymbol{e_i e_i}) \tag{2-27}$$

Values of κ are found to have a corresponding relationship with fiber length and fiber concentration, yet an inverse relationship with matrix viscosity and fiber elastic modulus [9]. Note that if κ is set to unity, the SRF model is recovered.

Nguyen and collaborators [8] highlight the need for better model accuracy for LFTs. The next phase in the evolution of the models is to correct the isotropic rotary diffusion term to further reflect the anisotropy in the materials [8]. The single, scalar IRD term was only able to predict one of the orientation components in LFT moldings [8]. Other researchers proposed ways to adjust for anisotropy, but had no measurable success [9]. Phelps and Tucker [26] built off of these theories to develop the Anisotropic Rotary Diffusion (ARD) term:

$$\boldsymbol{C} = b_1\mathbf{I} + b_2\mathbf{A} + b_3\mathbf{A^2} + \frac{b_4}{\dot{\gamma}}\mathbf{D} + \frac{b_5}{\dot{\gamma}^2}\mathbf{D^2}, \tag{2-28}$$

where the b_i's are material parameters. Further derivations can be found in their paper [26]. This ARD term is combined with the RSC model to form the ARD-RSC model [26]:

$$\begin{aligned}\dot{\mathbf{A}}^{ARD,RSC} = {} & (\mathbf{W}\cdot\mathbf{A} - \mathbf{A}\cdot\mathbf{W}) + \xi\{\mathbf{D}\cdot\mathbf{A} + \mathbf{A}\cdot\mathbf{D} - 2[\mathrm{A} + (1-\kappa)(\mathrm{L} - \mathrm{M}\colon \mathrm{A})]\colon \mathbf{D} \\ & + \dot{\gamma}\{2[\boldsymbol{C} - (1-\kappa)M\colon \boldsymbol{C}] - 2\kappa\,(tr\boldsymbol{C})\boldsymbol{A} - 5(\boldsymbol{C}\cdot\boldsymbol{A} + \boldsymbol{A}\cdot\boldsymbol{C}) \\ & + 10[A + (1-\kappa)(L - M\colon A)]\colon \boldsymbol{C}\}a\end{aligned} \tag{2-29}$$

Three of the parameters, b_1, b_2, and b_4 are determined by matching experimental tensor data, and the other two, b_3 and b_5 are for stable convergence in numerical computation [26]. Note that setting κ=1 reduces the model to the ARD model [26]. These criteria lack a physical meaning and are sensitive, which leads to instability in numerical results. These shortcomings lead Tseng et al. [21] to propose an improved ARD model (iARD) with less parameters making the model more stable [9]. Their new iARD term is:

$$\dot{\mathbf{A}}^{iARD} = 2C_I\dot{\gamma}(\mathbf{I} - 3\mathbf{A}) + 2\dot{\gamma}C_IC_M\left\{(\mathbf{A} - \tilde{\mathbf{L}}) + 5\left[\frac{1}{2}\mathbf{A}\cdot\tilde{\mathbf{L}} + \frac{1}{2}(\mathbf{A}\cdot\tilde{\mathbf{L}})^T - \mathbf{A_4}\!:\tilde{\mathbf{L}}\right]\right\} \quad (2\text{-}30)$$

$$\tilde{\mathbf{L}} = \frac{\mathbf{L}^T\cdot\mathbf{L}}{\mathbf{L}^T\!:\mathbf{L}} \quad (2\text{-}31)$$

The new term accounts for both fiber-fiber, C_I, and fiber-matrix, C_M, interactions. C_M is referred to as the fiber-rotary-resistance (FRR) [9]. $\bar{\bar{\boldsymbol{L}}}$ is a second-order symmetric tensor that is non-objective, and **L** is the velocity gradient tensor [9]. This new iARD can be added linearly to the SRF model [9]. Tseng et al. [21] also contributed work on the improvement of strain reduction by developing the Retarding Principle Rate (RPR) as a correction to the isotropic model, but it can be combined with the iARD model to yield the following equations [4]:

$$\frac{D}{Dt}\boldsymbol{A}^{iARD-RPR} = \frac{D}{Dt}\boldsymbol{A}^{\boldsymbol{HD}} + \frac{D}{Dt}\boldsymbol{A}^{\boldsymbol{iARD}}(C_I, C_M) + \frac{D}{Dt}\boldsymbol{A}^{\boldsymbol{RPR}}(\alpha,\beta) \quad (2\text{-}32)$$

$$\frac{D}{Dt}\boldsymbol{A}^{\boldsymbol{HD}} = (\boldsymbol{W}\cdot\boldsymbol{A} - \boldsymbol{A}\cdot\boldsymbol{W}) + \boldsymbol{\xi}(\boldsymbol{D}\cdot\boldsymbol{A} + \boldsymbol{A}\cdot\boldsymbol{D} - 2\boldsymbol{A_4}\!:\boldsymbol{D}) \quad (2\text{-}33)$$

$$\frac{D}{Dt}\boldsymbol{A}^{\boldsymbol{iARD}} = 2\dot{\gamma}C_I(\boldsymbol{I} - 3\boldsymbol{A}) + 2\dot{\gamma}C_IC_M\left\{\left(\boldsymbol{A} - \tilde{\boldsymbol{L}}\right) + 5\left[\left(A\cdot\tilde{L}\right)_{symm} - (\boldsymbol{A_4}\!:\tilde{\boldsymbol{L}})\right]\right\} \quad (2\text{-}34)$$

$$(\boldsymbol{A}\cdot\tilde{\boldsymbol{L}})_{symm} = \frac{1}{2}\left[\left(\boldsymbol{A}\cdot\tilde{\boldsymbol{L}}\right) + (\boldsymbol{A}\cdot\tilde{\boldsymbol{L}})^T\right] \quad (2\text{-}35)$$

$$\frac{D}{Dt}\boldsymbol{A}^{\boldsymbol{RPR}} = -\boldsymbol{R}\cdot\frac{D}{Dt}\boldsymbol{\Lambda}^{\boldsymbol{IOK}}\cdot\boldsymbol{R}^T \quad (2\text{-}36)$$

$$\frac{D}{Dt}\Lambda_{ii}^{IOK} = \frac{D}{Dt}\lambda_i^{IOK} = \alpha\left[\frac{D\lambda_i}{Dt} - \beta\left(\left(\frac{D\lambda_i}{Dt}\right)^2 + \frac{D\lambda_j}{Dt}\frac{D\lambda_k}{Dt}\right)\right];\ i,j,k = 1,2,3 \quad (2\text{-}37)$$

Note that setting C_M=0, α=1-κ, β=0 reverts the equations to the ARD-RSC model.

2.2.1.2 Flexible Fiber Models

As discussed previously in this literature review, fibers will rotate, bend, and break in the processing of LFTs and the configurations of the fibers have a direct relationship to the mechanical properties of the final parts. The longer the reinforcing fibers, the greater the mechanical properties because the discontinuous fibers approach the properties of continuous fibers (Section 2.1). However, longer fibers come with more challenges, due to their flexibility, for modeling and predicting orientation [31]. Consequently, suspensions of flexible fibers are rarely discussed in literature [32]. Multiple researchers have attempted to represent the flexural behavior of these long fibers. Yamamoto et al. [31] regarded a fiber as a group of beads that are lined up and bonded together, a bead chain, where the flexibility of fibers varied with the strengths associated with the stretch, bend, or twist of the chain. Tang and Advani [33] modeled a fiber as a chain of spheres connected by massless rods with ball-socket joints to allow free rotation. The interactions between the fiber and the suspending fluid is through the spheres. There are reports of two types of forces acting on the spheres: external-viscous drag and short rang lubrication forces from close spheres, and internal forces between neighboring spheres and along the connective rods [33]. Wang et al. [31] modeled the flexible fibers in a similar manner, using a chain of several rigid rods where each rod is assumed to be a chain of beads. These models are computationally expensive. Wang et al. [32, 33] attempted to optimize the length of rods necessary for accurate simulation while maintaining computation efficiency, and others tried to create models using only a small number of fibers in a solvent [32, 33]. But, similar to the

Folgar-Tucker style models, the effects of Non-Newtonian matrices are still ignored [4, 31-33].

Strautins and Latz [34] modified the Folgar-Tucker equations to account for semi-flexible fibers. They concentrated on the effect of local flexibility on the orientation of the long fibers [34]. The long fiber is represented by three beads connected by ball and socket joints with two rigid rods, and, hence, it has been aptly named the bead-rod Model (shown in Figure 2.7) [34]. There are two unit vectors **p** and **q** that point from the central bead out to the other two beads.

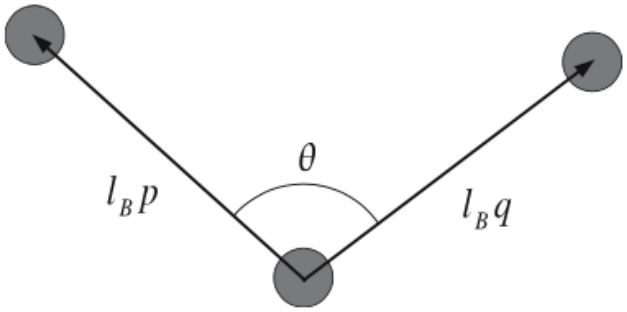

Figure 2.7: A two rod and three bead model of an elastic fiber. The two rods are represented by vectors **p** and **q** [34]. Reproduced with permission from the Rheologica Acta journal.

The two rods have a resistance to bending, and their discussion is restricted to fibers with limited bending [34]. The bending potential of the chain includes a bending potential constant, $\tilde{k}$, and is defined as [34]:

$$U(\mathbf{p}, \mathbf{q}) = \tilde{k}(\mathbf{p} \cdot \mathbf{q} + 1) \tag{2-38}$$

The state of equilibrium is achieved when the beads are aligned, i.e. **p**=-**q**. The effects of diffusivity were neglected in the investigation so that flexibility could be isolated [34]. The velocity field of the fluid around the fibers is represented through an expanded Taylor series and incorporates second order terms [34]. Strautins and Latz [34] solved a force and torque balance on each bead that results in linear and angular velocities for

each, which could be used to derive the orientation distribution function. The orientation was put in the familiar Folgar-Tucker notation, but the two vectors resulted in three moments, A, B, and C as defined [35]:

$$\mathbf{A}(t) = \iint \mathbf{pp}\ \psi(\mathbf{p}, \mathbf{q}, t) d\mathbf{p} d\mathbf{q} \tag{2-39}$$

$$\mathbf{B}(t) = \iint \mathbf{pq}\ \psi(\mathbf{p}, \mathbf{q}, t) d\mathbf{p} d\mathbf{q} \tag{2-40}$$

$$\mathbf{C}(t) = \iint \mathbf{p}\ \psi(\mathbf{p}, \mathbf{q}, t) d\mathbf{p} d\mathbf{q} \tag{2-41}$$

A full derivation and description can be found in the work by Strautins and Latz [34]. The **A** tensor is the second moment of any one of the rods with respect to the orientation tensor. The **B** tensor is a mixed second moment of the orientation tensor, and the trace of **B** describes the bending. The **C** tensor is the first moment of the orientation distribution function using either rod's orientation. The bead-rod model was extended to non-dilute suspensions by Ortman et al. [35] by the addition of the isotropic diffusion term. The resulting equations show that the flexibility is induced by a combination of rotary diffusion and hydrodynamic effects [35]:

$$\frac{D\mathbf{A}}{Dt} = \alpha((\mathbf{W}\cdot\mathbf{A} - \mathbf{A}\cdot\mathbf{W}) + (\mathbf{D}\cdot\mathbf{A} + \mathbf{A}\cdot\mathbf{D} - 2\mathbf{D}\colon\mathbf{A_4}) - 6C_I\dot{\gamma}\left(\mathbf{A} - \frac{1}{3}\mathbf{I}\right) + \frac{l_B}{2}[\mathbf{Cm} + \mathbf{mC} - 2(\mathbf{m}\cdot\mathbf{C})\,\mathbf{A}] - 2k[\mathbf{B} - \mathbf{A}\,tr(\mathbf{B})]) \tag{2-42}$$

$$\frac{D\mathbf{B}}{Dt} = \alpha((\mathbf{W}\cdot\mathbf{B} - \mathbf{B}\cdot\mathbf{W}) + (\mathbf{D}\cdot\mathbf{B} + \mathbf{B}\cdot\mathbf{D} - (2\mathbf{D}\colon\mathbf{A})\mathbf{B}) - 4C_I\dot{\gamma}\mathbf{B} + \frac{l_B}{2}[\mathbf{Cm} + \mathbf{mC} - 2(\mathbf{m}\cdot\mathbf{C})\,\mathbf{B}] - 2k[\mathbf{A} - \mathbf{B}\,tr(\mathbf{B})]) \tag{2-43}$$

$$\frac{D\boldsymbol{C}}{Dt} = \alpha\left(\nabla v^t\cdot\boldsymbol{C} - (\boldsymbol{A}\colon\nabla v^t)\boldsymbol{C} + \frac{l_B}{2}[\boldsymbol{m} - \boldsymbol{C}\,(\boldsymbol{m}\cdot\boldsymbol{C})] - k\boldsymbol{C}[1 - tr(\boldsymbol{B})] - 2C_I\dot{\gamma}\boldsymbol{C}\right) \tag{2-44}$$

$$\boldsymbol{m} = \sum_{i=1}^{3}\sum_{j=1}^{3}\sum_{k=1}^{3} \frac{\partial^2 v_i}{\partial x_j \partial x_k} A_{ijk} e_i \tag{2-45}$$

In these equations, k is the resistive bending potential. The **m** vector accounts for melt flow induced fiber bending [35]. However, the value for **m** is zero in simple shear flow resulting in a bending potential due only to the fiber-fiber interactions [35]. Note also that the fourth order tensor needs a closure approximation.

An end-to-end vector, **r,** is drawn from each of the end beads and is used to define a dimensional end-to-end orientation tensor:

$$\boldsymbol{r} \equiv \iint l_B^2(\boldsymbol{p}-\boldsymbol{q})\psi(\boldsymbol{p},\boldsymbol{q},t)\, d\boldsymbol{p}d\boldsymbol{q} = 2l_B^2(\boldsymbol{A}-\boldsymbol{B}) \tag{2-46}$$

$$\mathbf{R} = \frac{\mathbf{r}}{\mathrm{tr}(\mathbf{r})} = \frac{\mathbf{A}-\mathbf{B}}{1-\mathrm{tr}(\mathbf{B})} \tag{2-47}$$

in which l_B is the half fiber length. The degree of bending can then be defined as the reduction in this end- to- end distance. The **R** tensor is shown to predict the orientation evolution for a center-gated disk molded from glass fiber reinforced polypropylene with more accuracy than the basic Folgar-Tucker model [35].

2.2.1.3 Closure Approximations

The evolution equations for the second moments in the orientation models discussed in Sections 2.2.1.1 - 2 contain the fourth order moments as well. In order to evaluate these higher order moments, a closure approximation is used to reframe the fourth order moment into terms from the second order moment [9]. The development of nine closure approximations will be discussed and their accuracy compared. The accuracy of the orientation predictions are heavily dependent on the ability of the chosen approximation to represent the higher order moment [9]. Advani and Tucker [27]

established a set of guidelines to aid in the construction of these closure approximations:

1. The approximation must be constructed only from the lower order orientation tensors and the unit tensor;
2. The approximation must satisfy normalization conditions ($\sum_k \mathbf{A}_{ijkk} = 1$);
3. The approximation should maintain the symmetries of the orientation tensors ($\mathbf{A}_{ijkl} = \mathbf{A}_{jikl} = \mathbf{A}_{kijl}$, etc.);

Hand [36] established the first closure approximation in 1961 by using all of the products of $\mathbf{A}$ and δ (unit tensor) to determine all 15 independent terms of $\mathbf{A}_4$.

$$A_{ijkl} \approx -\frac{1}{35}\left(\delta_{ij}\delta_{kl} + \delta_{ik}\delta_{jl} + \delta_{il}\delta_{jk}\right) + \frac{1}{7}\left(A_{ij}\delta_{kl} + A_{ik}\delta_{jl} + A_{il}\delta_{jk} + A_{kl}\delta_{ij} + A_{jl}\delta_{ik} + A_{jk}\delta_{il}\right) \tag{2-48}$$

For an isotropic orientation, this linear approximation exactly calculates $\mathbf{A}_4$ [4, 9]. It also meets the 3 requirements established by Advani and Tucker [27]. Later research found that this approximation has non-physical stabilities [4, 9]. A quadratic approximation is exact for an aligned orientation [4, 9]. This style of approximation multiples the lower order tensors [4, 9]:

$$A_{ijkl} \approx A_{ij}A_{kl} \tag{2-49}$$

Quadratic approximations give poor results for random fiber orientations, and do not possess the full symmetries of the fourth order tensor [4, 9]. When these two approximations are combined the following hybrid closure approximation results [4, 9]:

$$A_{ijkl} \approx (1-f)A_{ijkl(linear)} + fA_{ijkl(quadratic)} \tag{2-50}$$

When fibers are isotropic the value of $f = 0$, and when perfectly aligned $f = 1$ [37]. This additive method is useful for a range of orientations, but it is not accurate and because the quadratic does not meet the symmetric requirement, neither does this approximation [4, 9].

The next generation of closure approximations aim to give results for several flow types by calculating $\mathbf{A}_4$ in terms of polynomial expressions of the components of $\mathbf{A}$ [4, 9]. A group of orthotropic fitted closure approximations (ORF) ensure that the principle axes of the $\mathbf{A_4}$ tensor match the principle axes of the $\mathbf{A}$ tensor [4, 9]. This increased the accuracy of this approximation, however orientation simulations yielded non-physical oscillations in simple shear flow [4, 9]. Two more models were proposed by expanding the polynomials of the two largest eigenvalues of $\mathbf{A}$, the ORW is a second order expansion and the ORW3 is a third order expansion [4, 9].

Further attempts reduced the computational effort by using the invariants of $\mathbf{A}$ in their natural closure approximation (NAT) [4, 9]. This method was accurate enough, but singularities were introduced for some flow types. These singularities were addressed in the invariant-based optimal fitting closure approximation (IBOF) [4, 9]:

$$A_{ijkl} \approx \beta_1 S(\delta_{ij}\delta_{kl}) + \beta_2 S(\delta_{ij}A_{kl}) + \beta_3 S(A_{ij}A_{kl}) + \beta_4 S(\delta_{ij}A_{km}A_{ml}) + \beta_5 S(A_{ij}A_{km}A_{ml}) + \beta_6 S(A_{im}A_{mj}A_{kn}A_{nl}) \tag{2-51}$$

$$S(T_{ijkl}) \approx \frac{1}{24}(T_{ijkl} + T_{jikl} + T_{jkli} + \cdots 24 \text{ terms}) \tag{2-52}$$

The accuracy of the IBOF is comparable to that of the eigenvalue-based closure approximations, but more computationally efficient [4, 9]. The coefficients in this model, and the others listed, are obtained by a least squares fitting technique [4, 9]. The kinematics are established for a set of simple, homogenous flow fields and then plugged

into the Smoluchowski equation. This allows for the determination of the ODF which yields the calculation of $\mathbf{A_4}$ [4, 9]**.**

2.2.2 Theory of Orientation Measurements- Method of Ellipses (MOE)

Experimental orientation measurements are needed to verify predictive models. There are several methods of calculating orientation: scanning acoustic microscopy, irradiation, micro-CT imaging, electromagnetic, and optical imaging [38, 39]. The most commonly used method is an optical microscopy approach to looking at a cross-sectional through thickness sample, known as the method of ellipses (MOE) [40]. The orientation of a fiber is defined in terms of its orientation vector **p**, further explanation can be found in Section 2.1. The in-plane angle ϕ and out-of-plane angle θ associated with this orientation vector are demonstrated in Figure 2.8 [41].

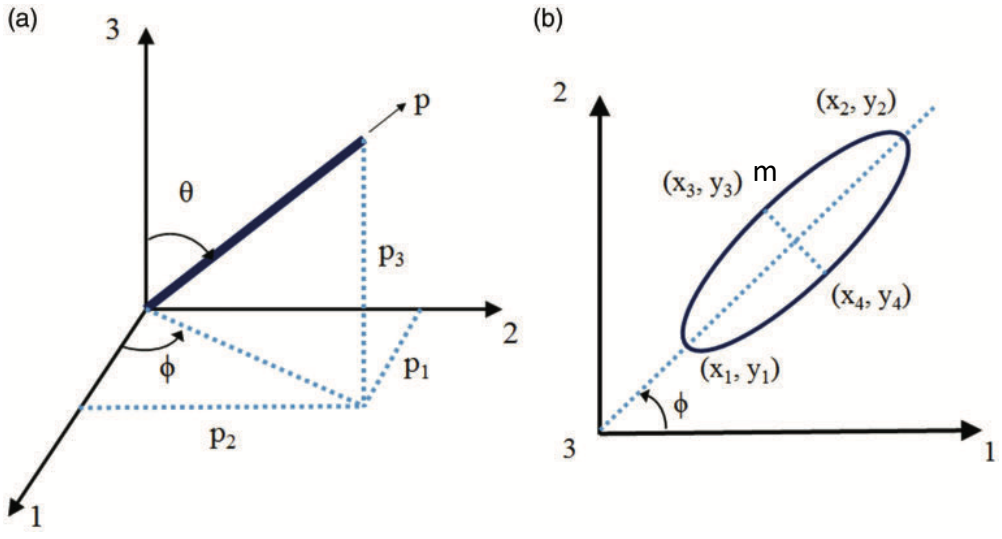

Figure 2.8: Definition of the fiber orientation vector **p** (a), the coordinate system (a), and the major (M) and minor (m) axis on the elliptical cross section of the fiber (b) [39]. Reproduced with permission from the Journal of Composite Materials.

The components of the second-order orientation tensor for a group of fibers are [39] :

$$A_{ij} = \langle p_i p_j \rangle = \begin{bmatrix} \langle sin^2\theta cos^2\phi \rangle & \langle sin^2\theta cos\phi sin\phi \rangle & \langle sin\theta cos\theta cos\phi \rangle \\ \langle sin^2\theta cos\phi sin\phi \rangle & \langle sin^2\theta sin^2\phi \rangle & \langle sin\theta cos\theta sin\phi \rangle \\ \langle sin\theta cos\theta cos\phi \rangle & \langle sin\theta cos\theta sin\phi \rangle & \langle cos^2\theta \rangle \end{bmatrix} \quad (2\text{-}53)$$

Samples are cut from locations along the flow direction of an injection molded part using a band saw. The locations of interest are often directly at the bottom of the sprue, the Hele-Shaw region, and near the end of the piece as shown in Figure 2.9 [42]. The samples are then cut with a 10 mm buffer region on each side of the plane of interest, Figure 2.9 shows the cutting pattern [43]. The buffer region aids in protecting the fibers from being pulled out or fractured by the aggressive motion of cutting with a band saw [43]. Tridimensional markers, shown in Figure 2.9, are made out of colored squares of PET and glued to the samples as a guide to the desired location, one end is used to indicate the plane of interest, and the other indicates the location of interest for image acquisition [43].

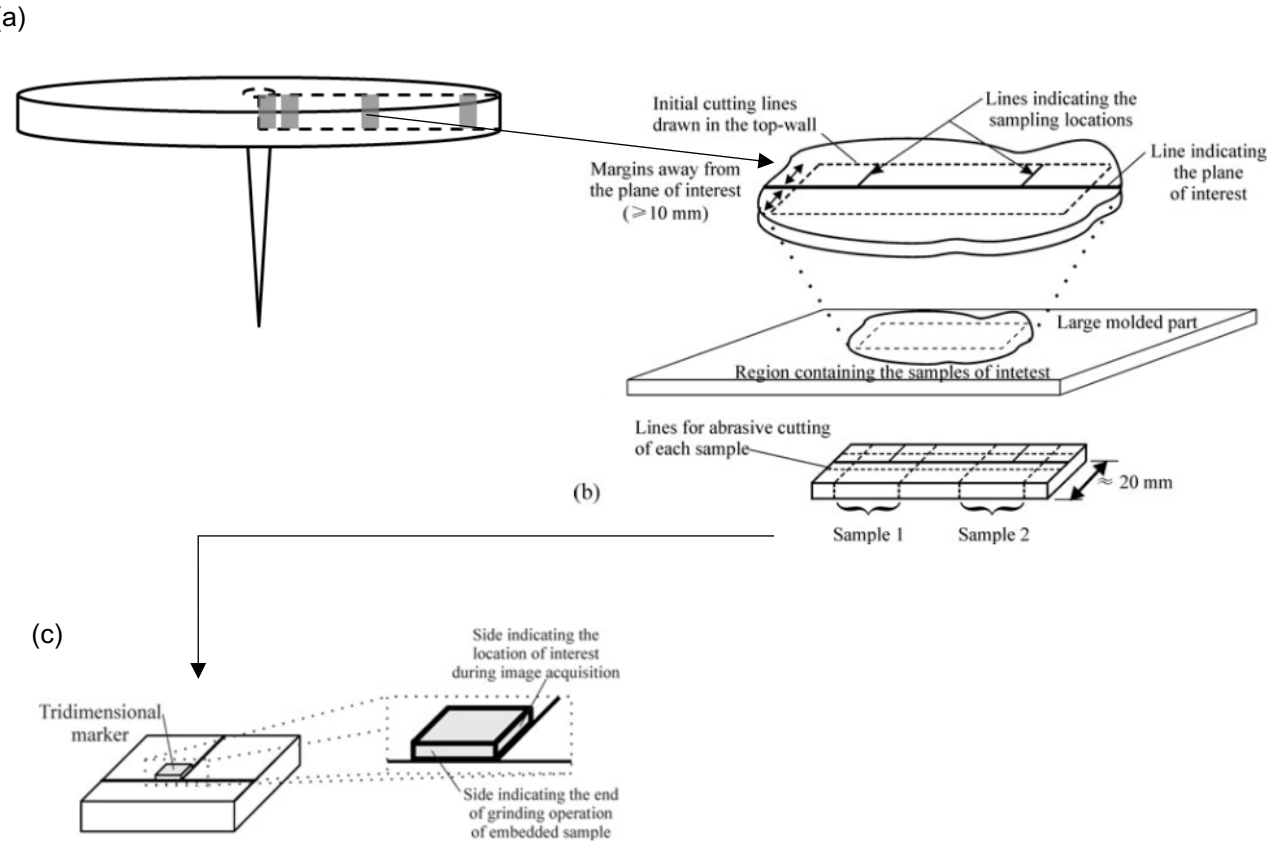

Figure 2.9: (a) Location of sampling regions within a CGD geometry, (b) an up-close look at an example of a sampling region showing cutting lines and the plane of interest, and (c) an even closer view of the sample region after cutting and with the addition of a tridimensional marker [42, 43]. Produced from reproductions that were used with permission from the Polymer Composites journal and Journal of Composites: Part A.

The samples are secured in a thermoplastic resin resulting in a puck that can be used for metallurgic sanding to remove the buffer region below the plane of interest, and for polishing to achieve a smooth plane for imaging and smooth edges on the elliptical footprint of the fiber [42].

Traditionally, images of this polished surface would be taken using an optical microscope. However, there is an inherent limitation in this method, because the ambiguity in the A_{12} and A_{23} components of the orientation tensor shown in Figure 2.10 [39]. In other words, it is not possible to differentiate between a fiber at (ϕ_1, θ_1) and

$(\phi_1 + \pi, \theta_1)$ [28]. There have been several attempts to determine the unambiguous full orientation. Sharma et al. [39] suggested taking an initial image and then removing more of the puck and taking an image at a slightly lower plane, giving two locations on the same fiber. Bay and Tucker [28] make a similar proposal, using 3 perpendicular sections at different location along the fiber. There have also been researchers who have made different averages, or who have determined the upper and lower bounds for the value [28, 39]. Previous research by the Baird group, introduces a novel solution. Using an oxygen plasma etcher, the polymer matrix is uniformly excavated and roughed, creating a shadow-like area around the fiber [38]. The direction of the shadow shows the full unambiguous orientation of the fiber [38]. After plasma etching, an optical microscope is used to take images of the surface. Multiple images are taken at 20x magnification and stitched together by computer software to create a total scan of the area [41]. Figure 2.11 shows images taken for polypropylene matrix and nylon-6 matrix, showing that this procedure works adequately for both [38].

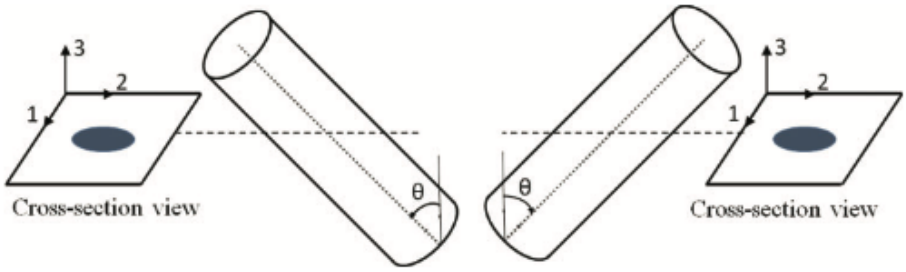

Figure 2.10: *Demonstration of the ambiguity in the determination of the 3D orientation of the fiber [39].* Reproduced with permission from the Journal of Composite Materials.

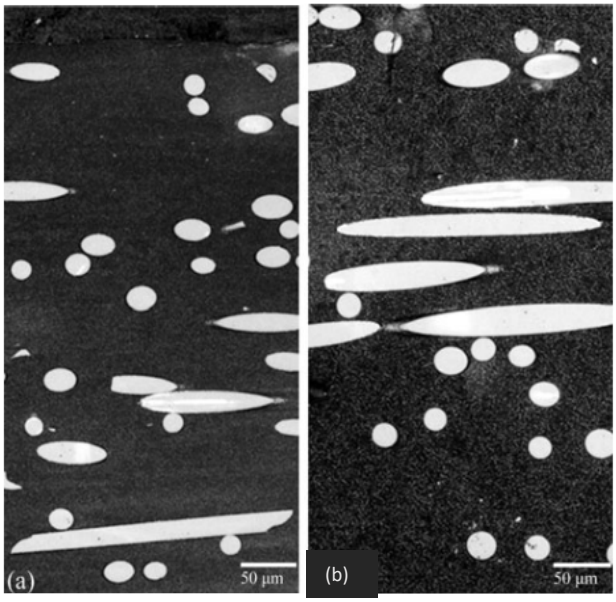

Figure 2.11: Examples of microscope in-focus images (objective 20x) for glass fiber with (a) PP and (b) PA matrices [38]. Reproduced with permission from the journal of Composites: Part A.

The elliptical footprint is analyzed to determine the orientation of the fiber. Figure 2.8 shows the major and minor axes of the ellipse. The components of the A tensor can be calculated as a discretization as opposed to an average as [28]:

$$A_{ij}^{t} = \frac{\sum (p_i p_j)_k L_k^t F_k}{\sum L_k^t F_k} \tag{2-54}$$

L_k is the length of the k^{th} fiber and F_k is a weighting factor. A bias is introduced because the fibers that are parallel to the plane of interest are less likely to be detected than those that are perpendicular [28, 39, 42]. Some research has been introduced to cut the sample at an angle to the cross section as opposed to perfectly perpendicular, but then more corrections are needed [44]. The weighting function gives a higher value to the fibers that are parallel to the cross-sectional surface [42]:

$$F_n = \begin{cases} \dfrac{1}{L_n \cos(\theta_f)_n + d_n \sin(\theta_f)_n}, & \theta_f < \theta_c \\ \dfrac{1}{d_n}, & \theta_f > \theta_c \end{cases} \quad (2\text{-}55)$$

Where θ_f is the out-of-plane angle and θ_c is the critical fiber angle defined as $\cos^{-1}(d/L)$, with d and L being fiber diameter and length respectively [28, 42]. The average fiber length is used because one cannot measure the length of every fiber [4]. Hofman established that an image width of 5.5 mm was the optimized combination of accurate reproducible results with minimum computational effort [42]. Bay and Tucker [28] propose that the flexibility of longer fibers will not impact the accuracy of MOE orientation data as long as the length of the fiber is much longer than the fiber's radius of curvature, ($L/2r_c << 1$). Work by Sharma et al. [28, 39] and Bay and Tucker [28, 39] verifies that the MOE is valid for carbon fibers as well as glass fiber.

2.2.3 Modeling Efforts

Material properties of an injection molded LFT part depend on the microstructures within the part. Therefore, it is important to be able to model and predict the orientation throughout a final product. Industry currently utilizes two commercially available software packages, Moldex and Moldflow. The Baird research group [45] has developed a system of equations that can predict orientation of injection molded glass fiber reinforced polypropylene center-gated disks with greater accuracy than the models used by the commercially available software. In order to verify the adaptability of the simulation efforts, the current researcher will be applying the model to a new composite and a new geometry. Section 2.2.3.1 will focus on the background literature addressing the Hele-Shaw assumption, decoupled simplifications, and the progress made with the

semi-flexible model. Section 2.2.3.2 will then address the current literature associated with modeling PA-6,6 and carbon fiber, and Section 2.2.3.3 will examine modeling success using different geometries.

Fibers are oriented in the mold filling stage of injection molding by three main flow mechanisms, shown in Figure 2.12 [46]:

1. Radial diverging flow near the inlet gates.
2. Shearing flow near the mold wall in the Hele-Shaw region.
3. Fountain flow at the advancing front (free surface) region.

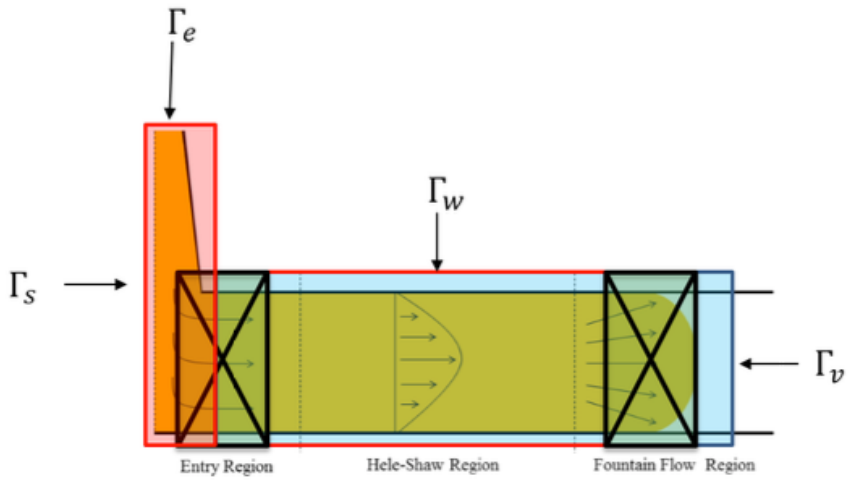

Figure 2.12: Illustration of the Hele-Shaw approximation showing the different regions in an injection filled mold [9]. Reproduced with permission from the author and Virginia Tech.

These three flow mechanisms create a shell and core layered structure within the part. Figure 2.13 shows an example microstructure containing seven layers [47]. The skin layer consists of fibers that have frozen to the mold walls before being aligned. The shell layers are highly aligned in the flow direction by the high shear forces along the walls. The core layers have a cross flow orientation due to extensional flow. This particular model contains a transition layer between the core and shell layers [47].

Some models are denoted as five layers. These do not separate out the transition layers. Teuwsen et al. [47] established a range of values for A_{11} to indicate the different orientation states found in the layers:

$A_{11} < 0.35$ cross-flow orientation (core layer)

$0.35 < A_{11} < 0.7$ random orientation (skin and transition layers)

$0.70 < A_{11}$ in-flow orientation (shell layers)

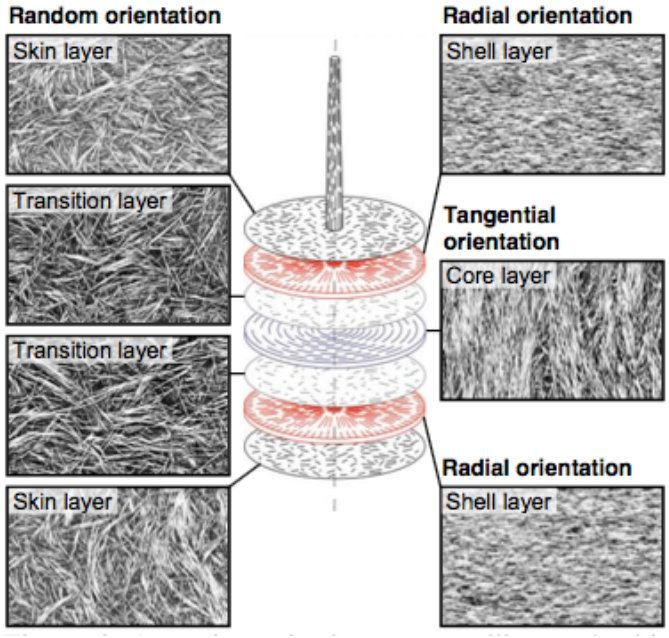

Figure 2.13: Seven-layer shell and core orientation shown with μCT images of a 60 wt% LGF/ PP center-gated sample [47].

Understanding the fluid dynamics is essential for determining the movement of fibers, due to the coupled relationship between flow and orientation. Just as in any fluid problem, the equations of motion and continuity are used to define the situation [48]:

$$\frac{\partial \rho}{\partial t} + \boldsymbol{\nabla} \cdot \rho \boldsymbol{v} = 0 \tag{2-56}$$

$$\frac{\partial}{\partial t}(\rho \boldsymbol{v}) + \boldsymbol{\nabla} \cdot (\rho \boldsymbol{v}\boldsymbol{v} - \sigma) = \rho g \tag{2-57}$$

where ρ is the density, t is time, $\boldsymbol{v}$ is the velocity, σ is the total stress tensor, and g is the gravitational acceleration. The energy equation is also needed if the problem is non-isothermal [9]:

$$\rho c_p \frac{DT}{Dt} = \boldsymbol{\sigma} : \boldsymbol{D} + k\nabla^2 T \tag{2-58}$$

The assumption of isothermal conditions is valid when the filling phase is rapid, which is the case for most industrial injection molding setups, because the mold experiences a negligible change in temperature [49]. Although, more recent work suggests that it is important to include the thermal effects to fully model the orientation evolution toward the free surface edge of the mold [50].

2.2.3.1 Approximations and Simplifications

Pressure driven flow in a thin gap between parallel plates is a common fluid dynamics problem [51]. The Hele-Shaw region is an application of the lubrication approach that is similar to this flow where the velocity field consists of x and y components that are dependent only on the z direction [51]. There are three important assumptions for modeling filling using this approximation [9]:

1. the cavity is much thinner than it is long (h/L <<1, where h is the gap height, and L is the length along flow direction);
2. fluid is moving at a low Reynolds number, i.e. creep flow [48];
3. the flow dynamics in the entry and advancing front regions are ignored.

In order to implement the Hele-Shaw approximation, a velocity profile and initial fiber orientation need to be specified, and the accuracy of those initial conditions determine the quality of the orientation predictions [52].

Ranganathan et al. [53] showed that an orientation simulation of a semi-concentrated fiber solution had very different predictions using a random initial condition compared to a perfectly aligned initial condition. VerWeyst and Tucker [54, 55] started their CGD simulation at the top of the sprue and generated more realistic orientation states, as did Chung and Kwon [54, 55] in a similar simulation. The addition of the entry region increases the accuracy of the Hele-Shaw approximation.

Rose [56] introduced fountain flow in 1961 to describe the fluid/air interface in channel flow. The fluid advances at a constant velocity, and the fluid near the wall moves slower than the fluid in the core, causing the fluid to “spill over” toward the wall region being vacated by the advancing region and thus creating a fountain effect as can be seen in Figure 2.14 [56] .

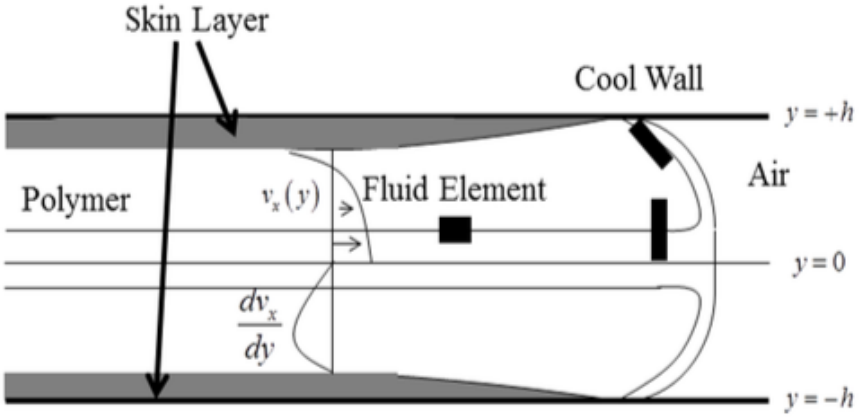

Figure 2.14: Flow between two parallel plates, shows the fountain flow effects and fiber movements near the advancing front [9]. Reproduced with permission from the author and Virginia Tech.

As one can imagine, this fountain effect has a large impact on fiber orientation in the advancing front region of the part. Although it has been generally accepted that Hele-Shaw flow provides an accuracy that is satisfactory for the prediction of fiber orientation for most parts, Figure 2.15 shows the improvement to the orientation predictions when the advancing front is included [57, 58].

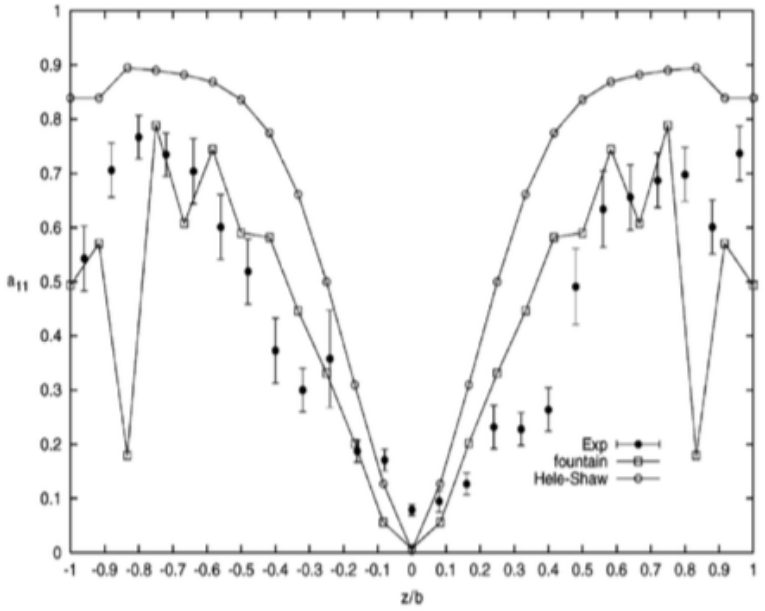

Figure 2.15: Comparison of A_{11} predictions using the Hele-Shaw approximation and including fountain effects versus the experimental orientation [9]. Reproduced with permission from the author and Virginia Tech.

Fiber orientation is highly coupled to the flow equations, and so another simplification that is made to approach the modeling of orientation, is to decouple the flow and orientation equations. The introduction of fibers will influence the viscosity and the velocity profile of a polymer, and the viscosity and the flow determine the orientation of the fibers [46]. A stress equation is used in the coupled approach to represent the relationship between orientation and flow [59]. A study of a Newtonian fluid with rigid fibers shows that if the channel were long enough, despite the addition of the short

fibers the fluid would regain its Newtonian parabolic velocity profile [46]. But in realistic applications the mold is not long enough and the velocity profile of suspensions is more plug like [46]. Tucker [59] established four flow regimes for fiber suspensions in narrow planar gaps, as shown in Figure 2.16. The fibers were assumed to have negligible out-of-plane orientation and the rotary diffusion term was ignored [59]. Regime I maintains the parabolic velocity profile, and, therefore, decoupled simulations are valid in this regime.

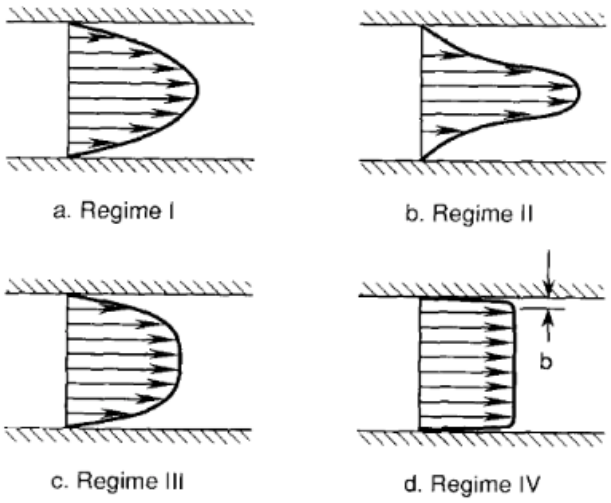

Figure 2.16: General gapwise velocity profiles for different flow regimes of fiber suspensions [59]. Reproduced with permission from the Journal of Non-Newtonian Fluid Mechanics.

In a decoupled model the fluid flow is simulated as if there were no fibers present, and then the flow kinematics are used to calculate the fiber orientation; there is significant research to suggest that this is a valid simplification [54]. VerWeyst and Tucker [54] suggest that this is only true in the portions of the mold that have thin gaps and simple geometries, and that it does not hold in regions such as the gate. They perform an isothermal steady state simulation of a concentrated suspension in a center-gated disk (including the sprue), and found that the addition of fibers caused a pointed

velocity profile [54]. The change in predicted results for the coupled and decoupled solutions are modest near the center of the disk and decrease rapidly in the radial direction [54]. They conclude that decoupled models will give accurate and useful predictions of fiber orientation in CGDs [54].

In contrast, Ranganathan and Advani [50] claim that the presence of the fibers, even at moderate volume fractions, cause significant effects on the velocity field [53]. The biggest difference is that the center-line velocity has an overshoot [54]. This overshoot has a direct effect on the solution of the orientation field, and, therefore, coupling is necessary to make accurate predictions of fiber orientation [54].

The aforementioned simulations were for rigid short fibers and did not include bending. More recently, Meyer et al. [45] conducted a test to investigate the effects of initial conditions on the orientation predictions of a long glass fiber reinforced center-gated disk. The study included the advancing front, was isothermal, and used a decoupled flow approach [45]. The authors also addressed the addition of fiber flexibility by comparing the results from the bead-rod model to the Folgar-Tucker model with RSC [45]. The results show that the prediction accuracy is increased when the simulation starts at the sprue instead of dictating random initial fiber orientation at the entry of the disk [45]. This agrees with the results from previous literature [54, 55]. The initial conditions at the beginning of the sprue were washed out by 80% of the sprue length and, therefore, not affecting the flow in the mold cavity [45]. The authors also found that the initial conditions for orientation in the disk are neither random nor planar random, they are a function of the thickness [45]. The comparison of orientation data for the bead-rod model significantly over performed compared to the rigid rod, leading a reader

to infer that fiber length and flexibility are significant in modeling fiber orientation [45]. A study conducted by Chen et al. for PP/LGF center-gated disks also confirms the assessment of the bead-rod model's increased performance when compared to the rigid-rod model [60]. This study also looks at the effects of fiber length on the bead-rod model. As the average fiber length increases, the fibers are longer and thus more flexible, the core regions become wider and the flow direction orientation is less aligned near the walls [60].

2.2.3.2 Comparisons of Polypropylene/Long Glass Fiber and Nylon/Long Carbon Fiber

The majority of the literature for orientation simulations are done with glass reinforced polypropylene (PP) composites. The purpose of this research is to investigate the ability to predict orientation and properties of a nylon 6,6 (PA 6,6) carbon fiber suspension. There are several differences between the two matrix materials. The two have comparable flow and melt properties, such that hybrid polymers have been investigated, PA6,6 proves to be an effective copolymer to increase the mechanical properties of PP [61]. The chemical structure of PA contains nitrogen and is, therefore, moisture sensitive and requires drying and processing in an inert environment to prevent degradation [62]. PP is a non-polar polymer, and PA is a polar one [61]. Figure 2.17 shows the results of a study that compared PP to PA6 and used glass fiber reinforcement. It is clear that the two matrices have very different stress-strain responses when they are reinforced and unreinforced [62].

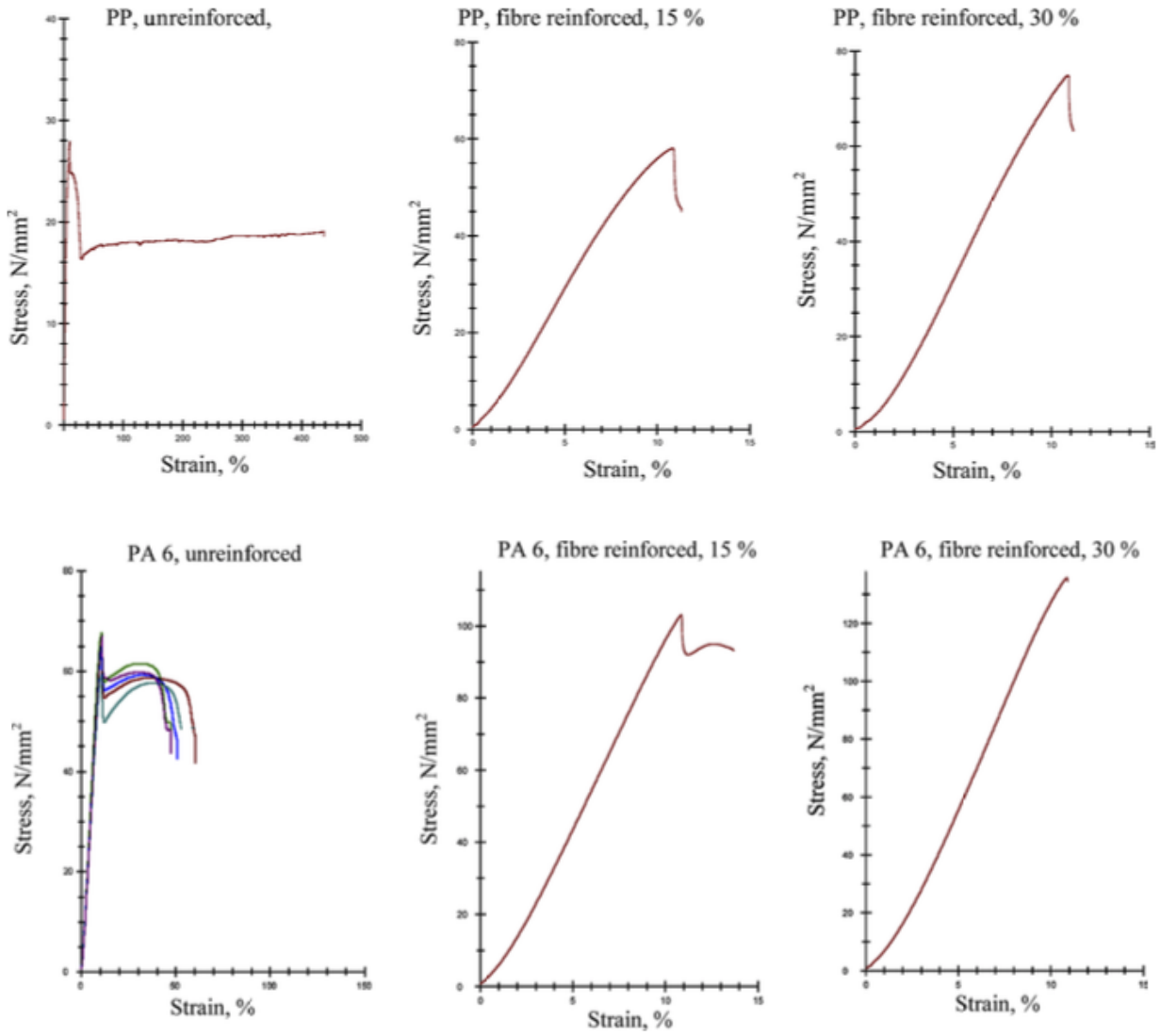

Figure 2.17: Stress vs. strain curves for unreinforced PP and PA 6, and PP and PA6 reinforced with 15 wt% and 30 wt% glass fibers [62]. Reproduced with permission from Materials and Design.

Polypropylene used in this study had a relatively lower viscosity and, therefore, had longer average fiber lengths, while the PA6 also required a higher pressure for injection molding which may have affected fiber breakage [62]. PA6 had better tensile properties before and after reinforcement, but the PP was reported to have a higher percent increase in tensile strength [62]. In contrast, a study by Tseng et al. [21] reported glass fiber reinforced PA 6,6 to have a better overall modulus when compared

to PP, but that the addition of LGF to the PA 6,6 was more efficient and had a higher change in the results than PP. The stress vs. strain response for the LGF/PP suspension was more linear than that for the LGF/PA 6,6 for the stress range reported [21].

Tseng et al. [21] tested the orientation predictions for a center-gated plaque using Moldex3D which used the iARD-RPR model. They used a PA 6,6 and a PP matrix both reinforced with 40 wt% LGF [21]. They also reported that the weight average length was longer in the PP matrix [21]. The injection molding temperature was higher for the PA 6,6 matrix [21]. The shear viscosity of the two suspensions was compared at 300°C, and the PP/LGF suspension shear thinned more than the PA 6,6/LGF [21]. The orientation curves in Figure 2.18 show the ability of the model to predict the orientation in the two matrices, and that the orientation evolution was similar despite the differences in matrix [21].

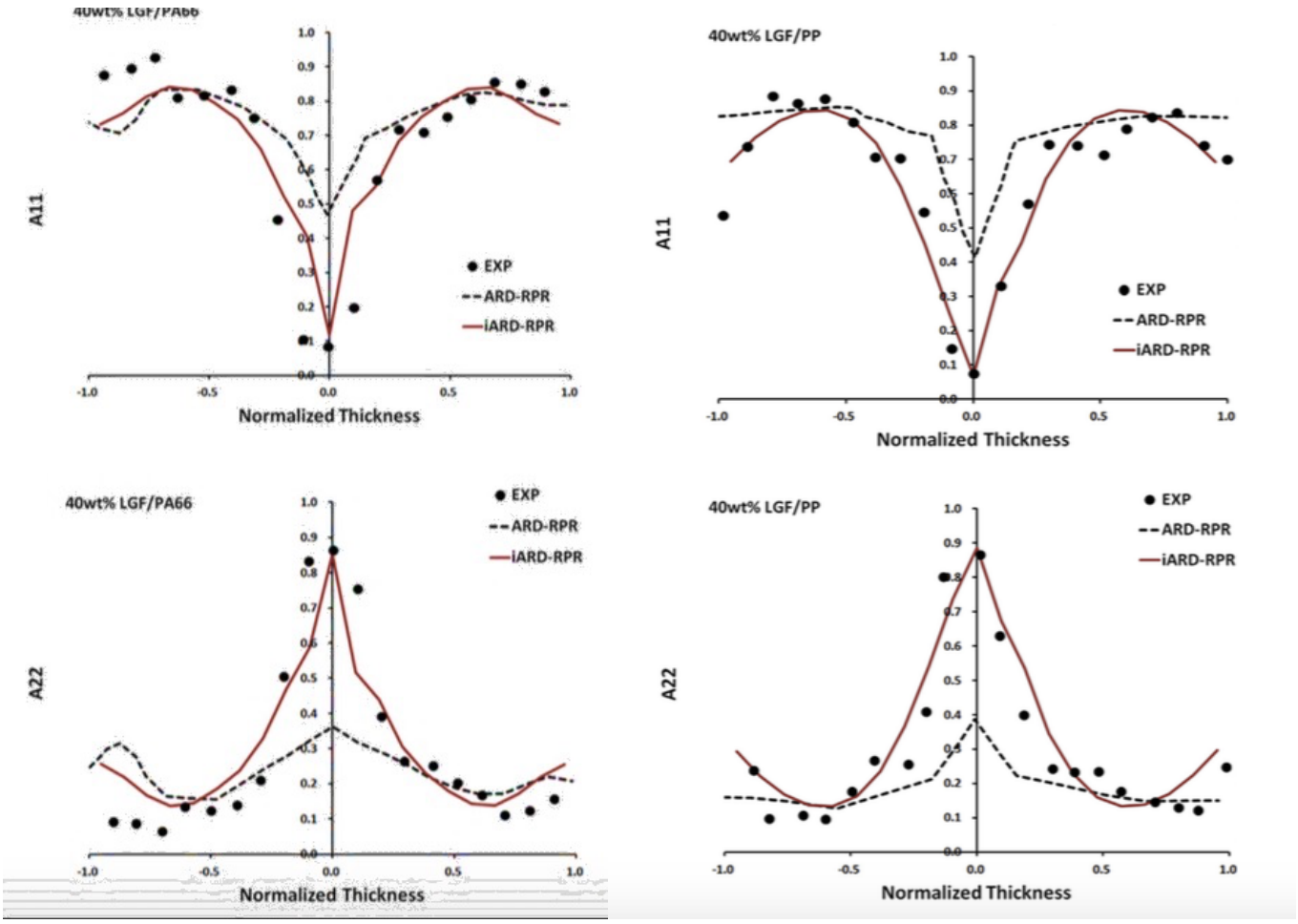

Figure 2.18: Orientation prediction results for the ARD-RPR and iARD-RPR with experimental results for PA 6,6 and PP with 40 wt% LGF reinforcement [21]. Reproduced with permission from Composites Science and Technology journal.

Another study by Tseng et al. [63] compares PP and PA 6,6 matrices reinforced with 50 wt% LGF in an injection molded EGP. The PA 6,6 is somewhat sensitive to shear rate and temperature, and the PP is very sensitive to temperature and contains a strong shear thinning slope [63]. The yield stress of the two suspensions overlap though [63]. The core width for the PP composite is thicker than that of the PA 6,6 due to the differences in their viscosities [63]. The iARD-RSC model is shown to adequately predict the orientation for both composites [63].

Nylon 6,6 with carbon fiber is a semi-crystalline thermoplastic composite that exhibits transcrystalline layers because the carbon fibers act as nucleation sites [64]. Thick and uniform transcrystalline layers grow directly on the fiber's surface [64]. The tensile modulus in the transcrystalline layer is higher than the crystalline matrix, adding to the improved modulus for the composite [64]. Klein et al. [64] show that most of the polymer chains for the crystallites are grown perpendicular to the fiber's axis thus affecting the fiber orientation distribution, the distance between fibers, and the appearance of the bulk crystallinity in the matrix.

Researchers with the commercially available Moldex software, Tseng et al. [3], conducted a study with plaques of PA 6,6 reinforced with LGF and LCF. The average fiber lengths of the carbon fibers, whose diameter was half that of the glass fibers, were preserved to be twice as long as the glass [3]. It is important to note that the plaques of the different material were produced on different machines and by different companies [3]. The iARD-RPR model was used to predict the orientation for both materials [3]. The wall orientation matched for A_{11}, but the core was wider for the LCF material [3]. The predictions for the LGF were closer to experimental than those for LCF [3]. It can be hypothesized that the LGF predictions were closer because the model used was for rigid rod fibers and the a_r of the carbon fibers was much higher than that for the glass fibers. The authors also note that adding a large number of carbon fibers is more effective in increasing mechanical properties than adding a large number of glass fibers [3]. A study conducted at South Dakota State University [65] showed the ability of the ARD-RSC model to predict the orientation of carbon fibers in injection molded thermoplastics when used for the design of spur gears.

2.2.3.3 Center Gated Disk Compared to End Gated Plaque and Challenges Associated with End Gated Plaque Geometry

Orientation modeling is often started with a center-gated disk (CGD) due to its radial symmetry and two-dimensional geometry. The end-gated plaque (EGP) is used to test orientation predictions in a three-dimensional flow. Tseng et al. [3,61] reported modeling success using two forms of the iARD model along the centerline of the EGP [3, 63]. Foss et al. used a 30 wt% GF reinforced thermoplastic to compare modeling efforts in a CGD and EGP [66]. The iARD-RPR model over predicted the orientation for all geometries, and the accuracies of the predictions was proposed to be independent of mold geometry and injection molding process parameters [66].

Wang et al. also investigated the differences in the EGP and CGP (center-gated plaque) geometries [67]. They used a PP/LCF composite and the ARD-RSC model [67]. The experimental orientation data demonstrate a wider core for the CGP than the EGP [67]. The EGP flow front is flat and the flow is unidirectional and dominated by simple shear in most of the cavity [67]. The radial flow pattern in the CGP causes a combination of shear and elongational flow leading to the wider core [67]. The flow length in the CGP is also half the length of the EGP, and, thus, the shell layers are thinner because the fibers have less time to align [67]. The orientation predictions were in agreement with these differences, and predicted both geometries with similar accuracy [67]. Wang et al. [68] in a different study using GF reinforced PA6,6 found good simulation verification for two different plaques and a disk geometry. Kunc et al. [69] also had success modeling the orientation and mechanical properties of a glass fiber reinforced PA6,6 plaque geometry.

Many EGP simulations only attempt to model the orientation along the center of the plaque, including those previously listed. Meyer et al. [29] analyzed EGPs injection molded from short and long glass fiber reinforced PP. For short fibers, the non-objective SRF and objective RSC models were tested [70]. A decoupled approach was used that included the gate and the advancing front [70]. At 50% of the mold width, the shell core was lost to a broad, flat orientation profile, similar to that found in other sources. Along the centerline, the SRF model predicted the orientation within a reasonable accuracy at all locations of interest, and anisotropic models were found to be even more accurate [70] [67]. The SRF model did an encouraging job predicting orientation away from the centerline, thus it proved that the model could predict orientation in a 3D molding geometry [70]. The non-objective and objective models appeared to exhibit similar trends suggesting that objectivity was not important in the prediction of fiber orientation, even in the 3-D test geometry [70]. The model parameters (discussed in greater detail in Section 2.3) that were obtained by fitting orientation to transient stress overshoots in shear flow over predicted the degree of orientation through the cavity thickness, resulted in a stronger shell-core region than was actually present [70]. These parameters worked for CGD prediction, but could not be used for the EGP [70].

In the EGP prediction of LGF reinforced PP, a non-isothermal decoupled approach was used to determine the accuracy of the rigid and semi-flexible models [29]. Once again, parameters determined from simple shear rheology that had been tested for CGD could not be used for sufficient prediction of EGP orientation evolution [29]. The rigid and semi-flexible models both predicted qualitatively similar orientations along the centerline, but the semi-flexible (bead-rod) model was better which corresponds well

with results from long fiber CGD tests [45, 60] [29]. Away from the centerline, the semi-flexible model more closely predicts the experimentally observed orientation at every location [29].

2.3 Stress Models and Rheological Methods for Empirical Model Parameters

Composite stress models link the fiber microstructure to the total composite stress. Having a model to couple flow and orientation can also be used in conjunction with rheological data to obtain orientation model parameters [4]. Non-lubricated squeeze flow is then discussed in the second section in order to lead into rheological methods for determining the orientation model parameters in the third section.

2.3.1 Stress Models

Orientation equations are based on Jeffery's modeling of a dilute system of ellipsoids and the stress tensor use the same starting point. The models progressed from dilute to concentrated suspensions in a Newtonian fluid, and then the Newtonian models are adapted with viscosity models to represent Non-Newtonian suspensions. Most recently, the flexibility of long fibers has been accounted for. The Newtonian models are the most frequently used, and their use is justified because the Folgar-Tucker style models are Newtonian [4].

Hand [36] proposed a stress tensor that is a function of the rate of deformation tensor and a symmetric tensor that describes the microscopic structure of the fluid from Jeffery [4, 36]. The volumetric average is taken of the stress acting on the individual ellipsoid, and this fiber stress is added to the fluid stress [4, 36]:

$$\sigma = -P\boldsymbol{I} + 2\eta_0\boldsymbol{D} + \varphi_0 \sum \boldsymbol{\sigma}_p \tag{2-59}$$

Most anisotropic theories of the time did not satisfy invariance conditions, and so Ericksen [4, 71] proposed a transversely isotropic fluid (TIF) described by isotropic tensors [4, 71]. The stress of the particle in time is dependent on its direction **p** [71]. The following equations describe the particle motion and the corresponding stress [4]:

$$\frac{D\boldsymbol{p}}{Dt} = \boldsymbol{W}\cdot\boldsymbol{p} + \xi(\boldsymbol{D}\cdot\boldsymbol{p} - \boldsymbol{D}:\boldsymbol{ppp}) \tag{2-60}$$

$$\sigma_{TIF} = -P_0\boldsymbol{I} + 2\mu_0\boldsymbol{D} + (\mu_1 + \mu_2\boldsymbol{D}:\boldsymbol{pp})\boldsymbol{pp} + 2\mu_3(\boldsymbol{D}\cdot\boldsymbol{pp} + \boldsymbol{pp}\cdot\boldsymbol{D}) \tag{2-61}$$

The material constants are used to couple the orientation state with the composite stress [4]. According to Lipscomb et al. [72], this work proves that the TIF stress from continuum theories is equal to the stress of a single ellipsoid from Hand's work.

Lipscomb et al. [72] extended the work from particles and ellipsoids to discontinuous glass fibers. The authors described the development of a stress equation based on the work of Batchelor [72, 73]. They used a coordinate system that coincided with the fiber's axis and equated the TIF stress to the particle stress contribution to derive material constants that have asymptotic values at really long fiber lengths [4, 72]. The following material constants were used for long fibers [4, 72]:

$$\mu_0 = 2\eta_0 \tag{2-62}$$

$$\mu_1 = \mu_3 = 0 \tag{2-63}$$

$$\mu_2 = \left(\frac{a_r^2}{\ln a_r}\right)\eta_0 \tag{2-64}$$

$$\xi = 1 \tag{2-65}$$

The TIF stress can then be written as [4, 72]:

$$\sigma_{TIF} = -P_0\boldsymbol{I} + 2\eta_0\boldsymbol{D} + \left(\frac{a_r^2}{\ln a_r}\right)\eta_0\boldsymbol{D}:\boldsymbol{pppp} \tag{2-66}$$

When the TIF stress is set equal to the particle stress, the bulk stress can be written as [4, 72]:

$$\sigma = -(P + \varphi P_0)\boldsymbol{I} + 2(1 + 2\varphi)\eta_0 \boldsymbol{D} + \varphi\left(\frac{a_r^2}{\ln a_r}\right)\eta_0 \boldsymbol{D}\colon \boldsymbol{A_4} \tag{2-67}$$

The evolution of the orientation tensor is the basic Jeffery's equation for infinitely long fibers [4, 72]:

$$\frac{D\boldsymbol{A}}{Dt} = \boldsymbol{W}\cdot\boldsymbol{A} - \boldsymbol{A}\cdot\boldsymbol{W} + \boldsymbol{D}\cdot\boldsymbol{A} + \boldsymbol{A}\cdot\boldsymbol{D} - 2\boldsymbol{D}\colon\boldsymbol{A_4} \tag{2-68}$$

Batchelor [73] developed an equation for particle suspensions that incorporated the hydrodynamic effects of neighboring particles. The velocities near a particle for a dilute and semi-dilute concentration were found to have similar forms, and the changes contributed to the neighboring particle were determined by replacing the nearby particles with an equivalent cylindrical boundary. This is known as the "cell model" [73]. Dinh and Armstrong [14] then built on Batchelor's findings to create a stress tensor equation and orientation evolution for a Newtonian, semi-concentrated suspension of rigid fibers. The equation gave the stress in terms of an integral over a function of the Cauchy strain tensor and the orientation vector [14]. They develop a model for the drag exerted on a single fiber by a neighboring fiber using the cell model, and then create an explicit stress equation based on those discoveries [14]. The equations differed for aligned and random fiber orientations [14]. The drag coefficients and stress equations are listed as follows [4]:

	Aligned	Random	
Slip Coefficient	$\zeta_p = \frac{4\pi L}{\ln(\pi/\varphi)}\eta_0$	$\zeta_p = \frac{2\pi L}{\ln(\pi/(2\varphi a_r))}\eta_0$	(2-69)
Stress Equation	$\sigma = -P\boldsymbol{I} + 2\eta_0\boldsymbol{D} + \left[\frac{4}{3}\frac{\varphi}{\ln(\pi/\varphi)}a_r^2\right]\eta_0\boldsymbol{D}:\boldsymbol{A_4}$	$\sigma = -P\boldsymbol{I} + 2\eta_0\boldsymbol{D} + \left[\frac{2}{3}\frac{\varphi}{\ln(\pi D/2\varphi a_r)}a_r^2\right]\eta_0\boldsymbol{D}:\boldsymbol{A_4}$	(2-70)

These models neglected the thickness of the particle, slender-body analysis, and, therefore, three of the material constants are zero (μ_0, μ_1, μ_3) [4]. Shaqfeh and Frederickson [4] reported a stress tensor of the same form developed on multiple scattering that had the ability to treat hydrodynamic effects more rigorously, it used the following form of μ_2:

$$\mu_2 = \frac{2a_r^2}{3(\ln(1/\varphi) + \ln(\ln(1/\varphi)) + C')} \tag{2-71}$$

Aligned rods: C'=0.1585; Random rods: C'=-0.6634

The same stress tensor equation can also be used for concentrated regime, but $\mu_2$is used as a fitting parameter [4].

The Lipscomb [72] and Dinh-Armstrong [14] models have been modified for non-Newtonian suspensions. Researchers have tried using the **D:A**$_4$ coefficient as a fitting parameter for both models. However, the normal stresses have a strong effect on the orientation evolution, and these models are unable to represent this non-Newtonian behavior [4].

Basing his research on the work of Batchelor, Goddard [74] subjected a suspension of highly aligned fibers in a power-law fluid to simple extension. He proposed that the effects of adding fibers on the stress is smaller than that in a

Newtonian fluid due to the fibers causing the matrix to shear thin [74]. Wang et al. [75] adapted Dinh and Armstrong's work to include the Ellis model, and the stress tensor maintains the same form, with a different slip equation to include the Ellis model parameters. The slip parameter is, therefore, a function of the applied shear rate and captures the shear-thinning behavior explained by Goddard [75]. In their work, the fibers are aligned in the maximum principle direction of the imposed flow [75]. The shear rates were limited, and so Thomasset et al. [76] extended the work of the Lipscomb model to include the Carreau model for viscosity over an increased range of shear rates using a long glass fiber-filled polypropylene. They propose a simple model that includes a yield stress and can be used for simple shear and extensional flows [4, 76]:

$$\sigma_Y = GC\gamma \tag{2-72}$$

$$\sigma = GC\gamma_s + \eta_0\left(1 + \frac{\lambda^2}{2}\dot{\gamma}\right)^{\frac{n-1}{2}}\left[(1+2\varphi)\dot{\gamma} + 15\mu_f \boldsymbol{A_4}\!:\dot{\boldsymbol{\gamma}}\right] \tag{2-73}$$

$$C = \frac{27}{6}(1 - 3\boldsymbol{A}\!:\boldsymbol{A} + 2\boldsymbol{A}\cdot\boldsymbol{A}\cdot\boldsymbol{A}) \tag{2-74}$$

Here, G is the proportionality constant; C is a constant for the interpolation of the hybrid closure approximation for $\mathbf{A_4}$, and is a function of the orientation state; γ is the strain (γ_s is the strain value at yield stress); η_0, λ, and n are the Carreau constants; and μ_f is the coefficient coupling orientation and stress. Eberle et al. [77] used the following form for high aspect ratio non-Brownian particles derived from the work of Hand [36] and Lipscomb [72] with limited success. Ortman et al. [78] extended this work to be better equipped for concentrated long fiber suspensions by making the coefficients functions of the invariants of **A** (Equations 2-75 to 2-81):

$$\sigma_{mod} = -P\boldsymbol{I} + \eta_m(\boldsymbol{D} + f_1\varphi\boldsymbol{D} + f_2\boldsymbol{A_4}\!:\boldsymbol{D}) \tag{2-75}$$

$$f_1 = \frac{c_1}{\dot{\gamma}_{min}^{b}} \quad \dot{\gamma} \leq \dot{\gamma}_{min} \tag{2-76}$$

$$f_1 = \frac{c_1}{\dot{\gamma}^{b}} \quad \dot{\gamma} > \dot{\gamma}_{min} \tag{2-77}$$

$$f_2 = c_2 I_A II_A III_A \tag{2-78}$$

where

$$I_A = tr(\boldsymbol{A}) \tag{2-79}$$

$$II_A = \frac{1}{2}[tr(\boldsymbol{A})^2 - tr(\boldsymbol{A}\cdot\boldsymbol{A})] \tag{2-80}$$

$$III_A = \det(\boldsymbol{A}) \tag{2-81}$$

Ortman et al. [78] also added a term to account for the flexibility of long fibers based on the bead-rod model:

$$\sigma_{bending} = \frac{3}{4}k\varphi a_r \frac{tr(\boldsymbol{r})}{l_B^2}(\boldsymbol{A} - \boldsymbol{R}) \tag{2-82}$$

$$r = l_B^2 \int\int (\boldsymbol{p} - \boldsymbol{q})\,(\boldsymbol{p} - \boldsymbol{q})\psi(\boldsymbol{p}, \boldsymbol{q}, t)d\boldsymbol{p}d\boldsymbol{q} \tag{2-83}$$

$$\boldsymbol{R} = \frac{\boldsymbol{r}}{tr(\boldsymbol{r})} \tag{2-84}$$

in which k is the fiber flexibility parameter, estimated as $(E_Y/64\eta_m)(d/l_B)^3$. This model relied on transient stress curves to fit the five empirical parameters, and the f parameters lack physical meaning. Despite the limitations of this model, it is the only theory that accounts for the additional stress from fiber bending [9].

2.3.2 Non-Lubricated Squeeze Flow

Non-lubricated squeeze flow (NLSF) contains both shear and extensional flow, similar to injection molding, and aids in understanding the dynamics of combination flows, including the influence of fiber flexing. Despite the widespread use of LFTs, the

effects of fiber flexing on stress tensor models is still not well defined [4]. Many different attempts using different flows and configurations have been proposed [4]. Forgacs and Mason [13] were able to observe fiber flexibility in Newtonian fluids during simple shear flow, but long glass fibers do not flex in polymer matrices under simple flows. The origin of the fiber flexibility lies in the second-gradient influences in the velocity field near the fiber's surface, therefore the flow field must be at least twice differentiable [4].

Ericsson et al. [4] defined the divergence-free parabolic velocity field in biaxial compression as:

$$u = \dot{\gamma}_{11}^{0}\left(1 - 4\left(\frac{x_3}{h}\right)^2\right)x_1 \tag{2-85}$$

$$v = \dot{\gamma}_{22}^{0}\left(1 - 4\left(\frac{x_3}{h}\right)^2\right)x_2 \tag{2-85}$$

$$w = -(\dot{\gamma}_{11}^{0} + \dot{\gamma}_{22}^{0})\left(1 - 4\left(\frac{x_3}{h}\right)^2\right)x_2 \tag{2-86}$$

Subscripts 1 and 2 denote the in-plane directions, and 3 the thickness direction with u,v,w referring to the velocity components in the 1,2,3 directions respectively. This flow field is coupled with the Lipscomb style stress tensor to predict anisotropic flow behavior, but fail to reorient fibers [4]. Kotsikos et al. [4] employed a different flow field approach and a pseudo-power law stress model to achieve the following radial and thickness components for velocity:

$$u_r = \left(\frac{2n'+1}{n'+1}\right)\left(\frac{r}{2}\right)\bar{\dot{\varepsilon}}\left[1 - \left(4\frac{z^2}{h^2}\right)^{\frac{n'+1}{2n'}}\right] \tag{2-87}$$

$$u_z = \left(\frac{2n'+1}{n'+1}\right)\bar{\dot{\varepsilon}}\left[\frac{z}{h} - \left(\frac{n'}{n'+1}\right)\left(\frac{z}{h/2}\right)^{\frac{2n'+1}{n'}}\right] \tag{2-88}$$

The r and z subscripts denote the radial and thickness directions, u is the velocity in the respective directions, h is the thickness of the sample, $\dot{\bar{\varepsilon}}$ is the rate of compression, and n' is the value of the power law exponent that minimizes the dissipation of energy. The researchers are able to derive a closure force model that can be fit to experimental forces. Once again, the non-lubricated biaxial compression failed to reorient the fibers [4]. However, NLSF is more complex than biaxial compression because of the side walls [4].

Cieslinski [30] used glass fibers in a polypropylene matrix and noticed fibers flexed when extruded into a slit die. A slit die has similar geometric properties as rectangular squeeze flow, and both are pressure driven. The closure forces discussed in Section 2.3.1 do not account for fiber reorientation in flow, and Ortman et al. [78] only accounted for small amounts of fiber bending. Lambert et al. [79] reported that NLSF provided a better test of fiber flexibility than rheological flows. The force required to close the platens could be measured and used to validate a stress model with limited success [79]. In previous cases, the stress models were fit to viscosity or normal stress differences, in NLSF pressure contributed to the closure stress [79]. The pressure gradients were dependent on the fiber orientation which add a layer of coupling for closure force fitting [79]. The closure force growth had two distinct periods. It initially increased very quickly and then at a much lower rate [79]. The following Lipscomb stress model was tuned to the correct magnitude by changing the value of N_p [79]:

$$\sigma = P\boldsymbol{I} + 2\eta\boldsymbol{D} + 2\eta N_P A_4 : \boldsymbol{D} \tag{2-89}$$

The magnitude could be matched, but the stress model was unable to represent the two distinct growth rates [79]. The authors proposed that the lack of a fiber-fiber interaction

leaves the model inadequate for this level of complex flow [79]. In conclusion, NLSF provides a complex enough flow field to induce fiber bending, and further development is needed to be able to use the closure force to improve stress models and predict fiber orientation [79].

2.3.3 Rheologically Determined Model Parameters

Current prediction software uses optimally fit parameters that have been determined for the chosen material, and the rationale is not described [66]. Work by Tseng et al. [3] with Moldex3D reported the same iARD-RSC model parameters used for both carbon fiber and glass fiber suspensions. The work done by the Baird Polymer Research group has been influential on the development of rheologically determined orientation parameters. Due to the connection of fiber orientation and flow patterns, research has been done to derive the empirical orientation model parameters from rheological flows. The following graphic Figure 2.19 describes the process used to determine these parameters [80].

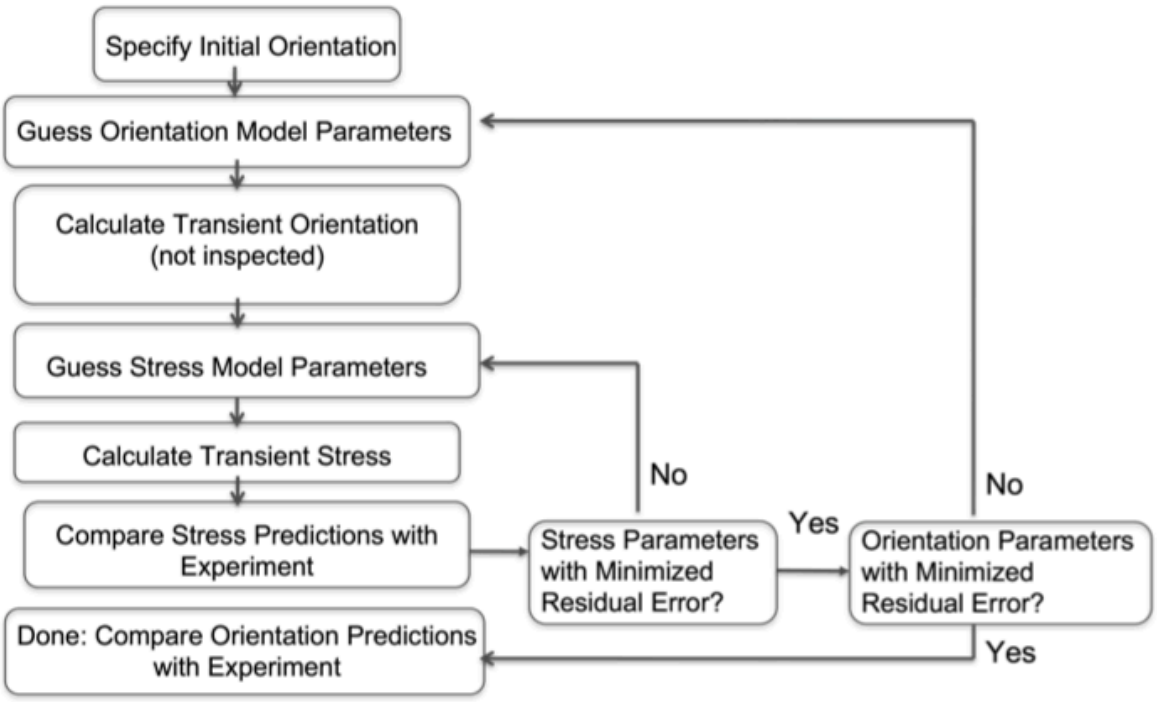

Figure 2.19: Process map for determining empirical parameters from rheology [80]. Reproduced with permission from Virginia Tech.

The work began with an attempt to understand the rheological behavior of concentrated suspensions. Eberle [77] developed a novel method for collecting and analyzing the transient rheology. Using donut shaped samples, he was able to use startup of shear flow to make connections between the stress and orientation [77]. Using the Folgar-Tucker model with a slip parameter and the Lipscomb stress model the author was able to determine model parameters that allowed for reasonable predictions of the transient stresses [77]. Velez-Garcia [50, 81] and Mazahir [50, 81] ran simulations using the Folgar-Tucker model with slip correction and the parameters determined from shear behavior by Eberle [77] to determine orientation that was in good agreement with the experimental data for a CGD. Meyer [29] confirmed reports that the rheologically determined parameters worked well for short and long glass fibers in CGD geometries,

but that they did not yield valid predictions for EGP geometries. The degree of orientation through the cavity thickness was over predicted, yielding a stronger shell-core-shell region than observed [29].

Ortman [80] explored using simple shear flows to determine the stress tensor and orientation model parameters for a suspension of long glass fibers in polypropylene. A sliding plate rheometer was used to determine the transient stress growth behavior of the long fiber systems as a function of shear rate [80]. Short fiber systems, analyzed using the donut style sample, were found to have a single overshoot peak followed by a steady state, the viscosity of LFTs often passed through multiple transient regions and was found to be highly dependent on the fiber orientation [80]. The authors continued to show that an understanding of the stress growth behavior could be used to derive a stress tensor that accounts for the semi-flexibility of the fibers [80]. The sliding plate rheometer was then used to calculate model parameters for the Folgar-Tucker and the bead-rod models [80]. The parameters worked encouragingly well for the CGD geometry but not for the EGP due to the differences in flow [80]. Cieslinski [30] made further improvements on the process of getting repeatable, valid material parameters for long fiber suspensions using the sliding plate rheometer.

Lambert [4] compared the orientation evolution in the startup of shear and planar extension, revealing that the fiber orientation is significantly faster during planar extension. This discovery contradicts the long-held assumption that dynamics were independent of flow, and motivates the use of NLSF to induce a mixed flow [4, 66]. He then fit an existing fiber orientation model to the gap-wise orientation profile to obtain orientation parameters [4]. Chen [9] extended the work of Lambert to show that the

scalar factor, α, used in many orientation models was more accurately represented as a function of the flow type. He used a flow-type parameter to locally describe the flow as shearing or extension [9]. Applying the improved parameter increased the accuracy of predicted orientation due to its ability to reflect the different rates at which fibers orient [9].

2.4 Prediction of Mechanical Properties

Mechanical properties are dependent on fiber length and orientation. The tensile strength and modulus of composites increase with an increase concentration of carbon fiber [82]. Elastic properties are calculated using fiber concentration, fiber length, and fiber orientation [83]. The Halpin-Tsai equation is the most widely used micromechanical model due to the ease of implementation and gives a reasonable estimate for stiffness [83] [84]. Chen [83] proves that the Mori-Tanaka model based on the Eshelby's equivalent inclusion method gave the best predictions. For modulus computation, the Halpin-Tsai (HT) equations were used to predict the compliance matrix, and the stiffness matrix was of course the inverse [83]. The EMT method combined Eshelby's equivalent inclusion method and Mori-Tanaka's back stress analysis [83]. This method was proven to be valid for large volume fractions of fibers. The EMT method resulted in the overall stiffness of the composite weakened by fiber-end cracks [83].

For this research, the EMT or HT method was used to calculate the stiffness of a unidirectional reference fiber composite with the experimental average fiber length ($L_{avg} = L_n$ or L_w):

$$C_{ijkl} = C^*_{ijkl}\left(\frac{L_{avg}}{d}\right) \tag{2-90}$$

C_{ijkl} is the stiffness matrix for specific fiber aspect ratio L_{avg}/d, where d is the diameter of a single fiber [83]. This reference composite stiffness was then averaged over the fiber orientation state using the **A** tensor [83]:

$$\begin{aligned}\bar{C}_{ijkl} = B_1 A_{ijkl} + B_2\left(A_{ij}\delta_{kl} + A_{ij}\delta_{kl}\right) + B_3\left(A_{ik}\delta_{jl} + A_{il}\delta_{jk} + A_{jl}\delta_{ik} + A_{jk}\delta_{il}\right) \\ + B_4\delta_{ij}\delta_{kl} + B_5\left(\delta_{ik}\delta_{jl} + \delta_{il}\delta_{jk}\right)\end{aligned} \tag{2-91}$$

δ_{jl} is the Kronecker delta and the B_is are scalar parameters that represent the invariants of the stiffness tensor of the unidirectional fiber composite defined as [83]:

$$\begin{aligned} B_1 &= C_{11} + C_{22} - 2 * C_{12} - 4 * C_{66} \\ B_2 &= C_{12} - C_{23} \\ B_3 &= C_{66} + \tfrac{1}{2}(C_{23} - C_{22}) \\ B_4 &= C_{23} \\ B_5 &= \tfrac{1}{2}(C_{22} - C_{23}) \end{aligned} \tag{2-92}$$

The composite was divided into thin layers and the orientation of each layer was calculated [83]. Classical lamination theory was used to determine the overall effective engineering stiffness of the composite [83]. The fiber diameter was also corrected to account for fiber bundling that occurred at large fiber concentrations [83]. These HT and EMT modulus models were tested for long glass fiber reinforced polypropylene and matched very well with experimental results [83]. Although this method was developed and tested for short fibers, further expansion to greater fiber lengths and flexibility could be reached by replacing the **A** tensor with the **R** used for the bead-rod model.

A similar approach was used to derive a model for the strength of a discontinuous fiber composite [85]. The longitudinal strength of a unidirectional composite was determined using the rule of mixtures, and the transverse strength of the unidirectional composite was assumed to equal that of the matrix [85]. The Kelly and Tyson stress distribution model was chosen which states that the applied load is transferred to the fibers by means of a shear force at the interface [85]. The fiber fractured at a critical length, l_c, when there was sufficient stress build-up [85]. When there was a strong interfacial bond, the interfacial shear strength, τ, was limited by the shear strength of the matrix (the matrix is assumed to be isotropic) [85]. Therefore, the longitudinal strength of the unidirectional composite is:

$$\begin{aligned} \sigma_{cL} &= V_f\sigma_f\frac{l}{2l_c} + \sigma'_m(1-V_f) = V_f\frac{\tau l}{d} + \sigma'_m(1-V_f) \qquad for\ l < l_c \\ \sigma_{cL} &= V_f\sigma_f\left(1-\frac{l}{2l_c}\right) + \sigma'_m(1-V_f) \qquad for\ l \geq l_c \end{aligned} \tag{2-93}$$

where l is the length of the fiber, V_f is the fiber volume fraction, σ'_m is the stress developed in the matrix, σ_f is the fiber strength, $l_c = \sigma_f d/2r$, and $\tau = \sigma_m/\sqrt{3}$ [85].

The tensile strength of carbon fibers depends significantly on their length, and the lengths of all fibers are not the same in an injection molded composite [85]. The unidirectional stress was adapted to account for fibers of varying strengths and lengths by using a fiber length distribution and a Weibull distribution function for the tensile strength [85]. The expression of the longitudinal tensile strength accounting for varying fiber strength is:

$$\sigma_{cL}(l) = V_f\frac{\tau l}{d} + \sigma'_m(1-V_f) \qquad for\ l < l_c \tag{2-94}$$

$$\sigma_{cL}(l) = V_f\sigma_f(l_c)\left(1 - \frac{l}{2l_c}\right) + \sigma'_m(1 - V_f) \qquad for\ l \geq l_c$$

with $l_c = \sigma_f(l_c)d/2r$ [85]. The properties were then weighted over the whole range of fiber lengths to account for the effects of the FLD, which resulted in the following length averaged longitudinal strength:

$$\bar{\sigma}_{cL} = \int_{l=0}^{l_c} \sigma_{cl}(l)\,\psi_l(l)dl + \int_{l=l_c}^{l_{max}} \sigma_{cl}(l)\psi_l(l)dl \tag{2-95}$$

l_{max} is the maximum length of the fibers in the distribution [85]. ψ_l is the probability distribution function defined as [85]:

$$\psi_l(l) = \frac{1}{\sqrt{2\pi\beta}} l^{-1} e^{-(\ln l - \alpha)^2/2\beta^2} \tag{2-96}$$

where α and β are related to the mean, $\bar{l}$, and standard deviation, sl, of the distribution [85]:

$$\alpha = \ln \frac{\bar{l}}{\sqrt{1 + \left(\frac{sl}{\bar{l}}\right)^2}} \qquad \beta = \sqrt{\ln\left[1 + \left(\frac{sl}{\bar{l}}\right)^2\right]} \tag{2-97}$$

The Tsai-Wu strength criterion, $F_i\sigma_i + F_{ij}\sigma_i\sigma_j = 1$, the σ_i's are the applied stresses and F_i and F_{ij} are second and fourth order strength tensors [85]. The elastic stiffness tensor, C_{ijkl}, was derived using the Halpin-Tsai equations [85]. The strength tensor for a unidirectional fiber composite was expressed as [85]:

$$F_{ij} = \begin{pmatrix} \frac{1}{\bar{\sigma}_{cL}{}^2} & \frac{-1}{2\bar{\sigma}_{cL}{}^2} & \frac{-1}{2\bar{\sigma}_{cL}{}^2} & 0 & 0 & 0 \\ \frac{-1}{2\bar{\sigma}_{cL}{}^2} & \frac{1}{\sigma_{cT}^2} & -\frac{1}{2}\left(\frac{2}{\sigma_{cT}^2} - \frac{1}{\bar{\sigma}_{cL}{}^2}\right) & 0 & 0 & 0 \\ \frac{-1}{2\bar{\sigma}_{cL}{}^2} & -\frac{1}{2}\left(\frac{2}{\sigma_{cT}^2} - \frac{1}{\bar{\sigma}_{cL}{}^2}\right) & \frac{1}{\sigma_{cT}^2} & 0 & 0 & 0 \\ 0 & 0 & 0 & \left(\frac{4}{\sigma_{cT}^2} - \frac{1}{\bar{\sigma}_{cL}{}^2}\right) & 0 & 0 \\ 0 & 0 & 0 & 0 & \frac{1}{\tau^2} & 0 \\ 0 & 0 & 0 & 0 & 0 & \frac{1}{\tau^2} \end{pmatrix} \quad (2\text{-}98)$$

Properties of the final composite were taken as an average of the unidirectional properties over all directions weighted by a fiber orientation distribution function [85]. The final orientation averaged strength tensor was given as:

$$\langle F_{ij} \rangle = \langle G_{mn} \rangle \langle C_{mi} \rangle^{-1} \langle C_{nj} \rangle^{-1} \quad (2\text{-}99)$$

$\langle G_{ijkl} \rangle$ is the strength tensor in terms of strain, but is the same as $\bar{C}_{ijkl}$ given in Equation (2-91) for modulus, and the B values remain the same as those in Equation (2-92) [85]. This method was developed and tested for short fiber composites. The predicted data was verified to be within 10% of measured results [85].

Works Cited

1. Hongyu Chen, M.C., Donald G. Baird, *Progress in Modeling Long Glass and Carbon Fiber Breakage during Injection Molding.* Proceedings of PPS-30, 2015.
2. Jay H. Phelps, A.I.A.E.-R., Vlastimil Kunc, Charles L. Tucker III, *A model for fiber length attrition in injection molded long-fiber composites.* Composites: Part A, 2013.
3. Huan-Chang Tseng, R.-Y.C., Chia-Hsiang Hsu, *Numerical prediction of fiber orientation and mechanical performance for short/long glass and carbon fiber-reinforced composites.* Composites Science and Technology, 2017. **144**.
4. Lambert, G., *Using Non-Lubricated Squeeze Flow to Obtain Empirical Parameters for Modeling the Injection Molding of Long-Fiber Composites*, in *Chemical Engineering*. 2018, Virginia Polytechnic Instititue and State University.
5. F. Garesci, S.F., *Young's modulus prediction of long fiber thermoplastics.* Composites Science and Technology, 2013. **85**.
6. S.-Y. Fu, B.L., E. Mader, C.-Y. Yue, X. Hu, *Tensile properties of short-glass-fiber- and short-carbon-fiber-reinforced polypropylene composites.* Composites: Part A, 2000. **31**.
7. Shan-Shan Yao, F.-L.J., Kyong Yop Rhee, David Hui, Soo-Jin Park, *Recent advances in carbon-fiber-reinforced thermoplastic composites: A review.* Composites Part B, 2018. **142**.
8. Ba Nghiep Nguyen, S.K.B., James D. Holbery, Mark T. Smith, Vlastimil Kunc, Barbara J. Frame, Jay H. Phelps, Charles L. Tucker III, *Fiber Length and Orientation in Long-Fiber Injection-Molded Thermoplastics- Part I: Modeling of Microstructure and Elastic Properties.* Composite Materials, 2008. **42**: p. 1003-1029.
9. Hongyu Chen, D.G.B., *Experimental Evaluation of Fiber Length Distribution and Modeling of Fiber Orientation and Elastic Properties for Long Glass Fiber Reinforced Thermoplastics*, in *Chemical Engineering*. 2017, Virginia Polytechnic Institute and State University.
10. A. Salinas, J.F.T.P., *Bending and Breaking Fibers in Sheared Suspensions.* Polymer Engineering and Science, 1981. **21**.
11. Leonard H. Switzer, D.J.K., *Rheology of sheared flexible fiber suspensions via fiber-level simulations.* Journal of Rheology, 2003. **47**.
12. M. Keshtkar, M.C.H., P.J. Carreau, *Rheological behavior of fiber-filled model suspensions: Effect of fiber flexibility.* Journal of Rheology, 2009. **53**.
13. O. L. Forgacs, S.G.M., *PARTICLE MOTIONS IN SHEARED SUSPENSIONS: IX. SPIN AND DEFORMATION OF THREADLIKE PARTICLES.* Journal of Colloid Science, 1959. **14**.
14. Stephen M. Dinh, R.C.A., *A Rheological Equation of State for Semiconcentrated Fiber Suspensions.* Journal of Rheology, 1984. **28**.
15. Phelps, J.H., *PROCESSING-MICROSTRUCTURE MODELS FOR SHORT- AND LONG-FIBER THERMOPLASTIC COMPOSITES*, in *Mechanical Engineering*. 2009, University of Illinois at Urbana-Champaign.

16. T. Vu-Khanh, J.D., P. Habib, A. Low *The Effects of Injection Molding on the Mechanical Behavior of Long-Fiber Reinforced PBT/PET Blends.* Composites Science and Technology, 1990. **40**.
17. R. K. Mittal, V.B.G., P. K. Sharma, *Theoretical and Experimental Study of Fibre Attrition during Extrusion of Glass-fibre-reinforced Polypropylene.* Composites Science and Technology, 1987. **31**.
18. Wolf, H.J., *Screw Plasticating of Discontinuous Fiber Filled Thermoplastics: Mechanisms and Prevention of Fiber Attrition.* Polymer Composites, 1994. **15**.
19. M. Doi, S.F.E., *The theory of polymer dynamics*. Vol. 73. 1988: Oxford University Press.
20. Jeffery, G.B., *The Motion of Ellipsoidal Particles Immersed in a Viscous Fluid.* Proceedings of the Royal Society of London. Series A, Mathematical and Physical Sciences, 1922.
21. Huan-Chang Tseng, R.-Y.C., Chia-Hsiang Hsu, *Numerical predictions of fiber orientation and mechanical properties for injection-molded long-glass-fiber thermoplastic composites.* Composites Science and Technology, 2017. **150**.
22. Paal Skjetne, R.F.R., Daniel J. Klingenberg, *Simulation of single fiber dynamics.* Journal of Chem. Phys., 1997. **107**.
23. S. G. Mason, R.S.J.M., *Particle Motions in Sheared Suspensions: Orientations and Interactions of Rigid Rods.* Proceedings of the Royal Society of London. Series A, Mathematical and Physical Sciences, 1956. **238**.
24. M. A. Nawab, S.G.M., *THE VISCOSITY OF DILUTE SUSPENSIONS OF THREAD-LIKE PARTICLES.* 1958. **62**.
25. Fransisco Folgar, C.L.T.I., *Orientation Behavior of Fibers in Concentrated Suspensions.* Reinforced Plastics and Composites, 1984. **3**: p. 98-119.
26. Jay H. Phelps, C.L.T.I., *An anisotropic rotary diffusion model for fiber orientation in short- and long-fiber thermoplastics.* Journal of Non-Newtonian Fluid Mechanics, 2008. **156**.
27. Suresh G. Advani, C.L.T.I., *The Use of Tensors to Describe and Predict Fiber Orientation in Short Fiber Composites.* Journal of Rheology, 1987. **31**.
28. Randy S. Bay, C.L.T.I., *Stereological Measurement and Error Estimates for Three Dimensional Fiber Orientation.* Polymer Engineering and Science, 1992. **32**(4): p. 240-253.
29. Meyer, K.J., *Improved Prediction of Glass Fiber Orientation in Basic Injection Molding Geometries*, in *Chemical Engineering*. 2013, VIrginia Tech.
30. Cieslinski, M.J., *Using a Sliding Plate Rheometer to Obtain Material Parameters for Simulation Long Fiber Orientation in Injection Molded Composites*, in *Chemical Engineering*. 2015, Virginia Polytechnic Institute and State University.
31. Gang Wang, W.Y., Chixing Zhou, *Optimization of the rod chain model to simulate the motions of a long flexible fiber in simple shear flows.* European Journal of Mechanics B/Fluids, 2005. **25**.
32. C.G. Joung, N.P.-T., X.J. Fan, *Direct simulation of flexible fibers.* Journal of Non-Newtonian Fluid Mechanics, 2001. **99**.
33. Wenzhong Tang, S.G.A., *Dynamic Simulation of Long Flexible Fibers in Shear Flow.* CMES, 2005. **8**.

34. Uldis Strautins, A.L., *Flow-driven orientation dynamics of semiflexible fiber systems.* Rheol Acta, 2007. **46**: p. 1057-1064.
35. Kevin Ortman, D.B., Peter Wapperom, Alex Aning *Prediction of Fiber Orientation in the Injection Molding of Long Fiber Suspensions.* Polymer Composites, 2012: p. 1360-1367.
36. Hand, G.L., *A theory of anisotropic fluids.* Flouid Mechanics, 1961. **13**.
37. Kyeong-Hee Han, Y.-T.I., *Modified hybrid closure approximation for prediction of flow-induced fiber orientation.* Journal of Rheology, 1999. **43**.
38. Gregorio M. Velez-Garcia, P.W., Donald G. Baird, Alex O. Aning, Vlastimil Kunc, *Unambiguous orientation in short fiber composites over small sampling area in a center gated disk.* Composites: Part A, 2011. **43**.
39. Bhisham N. Sharma, D.N., Ba Nghiep Nguyen, Charles L. Tucker, Michael D. Sangid, *Uncertainty quantification of fiber orientation distribution measurements for long-fiber-reinforced thermoplastic composites.* Journal of Composite Materials, 2017.
40. Hofmann, J.T., *Extension of the Method of Ellipses to Determining the Orientation of Long, Semi-flexible Fibers in Model 2- and 3-dimensional Geometries*, in *Macromolecular Science and Engineering*. 2013, Virginia Polytechnic Institute and State University.
41. N.C. Davidson, A.R.C., G. Archenhold, *Large-area, high resolution image analysis of composite materials.* Journal of Microscopy, 1997. **185**.
42. John T. Hofman, G.M.V.-G., Donald G. Baird, Abby R. Whittington, *Application and Evaluation of the Method of Ellipses for Measuring the Orientation of Long, Semi-Flexible Fibers.* Polymer Composites, 2013.
43. G.M. Velez-Garcia, P.W., V. Kunc, D.G. Baird, A. Zinc-Sharp, *Sample preparation and image acquisition using optical-reflective microscopy in the measurement of fiber orientation in thermoplastic composites.* Journal of Microscopy, 2012. **248**: p. 23-33.
44. P. J. Hine, N.D., R. A. Duckett, I. M. Ward, *MEASURING THE FIBRE ORIENTATION AND MODELLING THE ELASTIC PROPERTIES.* Composites Science and Technology, 1994. **53**.
45. Kevin J. Meyer, J.T.H., Donald G. Baird, *Initial conditions for simulating glass fiber orientation in the filling of center-gated disks.* Composites: Part A, 2013. **49**.
46. Kunji Chiba, K.Y., Kiyoji Nakamura, *Numerical solution of fiber suspension flow through a parallel plate channel by coupling flow field with fiber orientation distribution.* Journal of Non-Newtonian Fluid Mechanics, 2001. **99**.
47. Jan Teuwsen, S.G., Tim A. Osswald, *IMPACT OF THE PROCESS-INDUCED MICROSTRUCTURE ON THE MECHANICAL PERFORMANCE OF INJECTION MOLDED LONG GLASS FIBER REINFORCED POLYPROPYLENE.* SPE ANTEC, 2017.
48. Anthony J. Favaloro, H.-C.T., R. Byron Pipes *A new anisotropic viscous constitutive model for composite molding simulation.* Composites: Part A, 2018. **115**.
49. P.-C. Wu, C.F.H., C. G. Cogos, *Simulation of the Mold-Filling Process.* Polymer Engineering and Science, 1974. **14**.

50. Velez-Garcia, G.M., *Experimental Evaluation and Simulations of Fiber Orientation in Injection Molding of Polymers Containing Short Glass Fibers*, in *Chemical Engineering*. 2012, Virginia Polytechnic Institute and State University.
51. Donald G. Baird, D.I.C., *Polymer Processing Principles and Design*. Second ed. 2014, New Jersey: John Wiley & Sons, Inc.
52. Ihsane Modhaffar, K.G., Samir Men-La-Yakhaf, Hamid El-Tourroug, *Simulation study for prediction of short Fiber Orientation reinforced thermoplastics.* Materials today: Proceedings, 2015. **3**.
53. Sridhar Ranganathan, S.G.A., *A simultaneous solution for flow and fiber orientation in axisymmetric diverging radial flow.* Journal of Non-Newtonian Fluid Mechanics, 1992. **47**.
54. Brent E. VerWeyst, C.L.T.I., *Fiber Suspensions in Complex Geometries: Flow/Orientation Coupling.* The Canadian Journal of Chemical Engineering, 2002. **80**.
55. Du Hwan Chung, T.H.K., *Numerical studies of fiber suspensions in an axisymmetric radial diverging flow: the effects of modeling and numerical assumptions.* Journal of Non-Newtonian Fluid Mechanics, 2002. **107**.
56. Rose, W., *FLUID-FLUID INTERFACES IN STEADY MOTION.* Nature, 1961. **191**.
57. Luis Domenech, A.F., Victor Garcia, Fernando Sanchez, *Towards a 2.5D geometric model in mold filling simulation.* Journal of Computational and Applied Mathematics, 2014. **291**.
58. Y.K. Shen, P.H.Y., J.S. Wu, *NUMERICAL SIMULATION FOR THIN WALL INJECTION MOLDING OF FIBER-REINFORCED THERMOPLASTICS.* Int. Comm. Heat Mass Transfer, 2001. **28**.
59. Tucker, C.L., *Flow regimes for fiber suspensions in narrow gaps.* Journal of Non-Newtonian Fluid Mechanics, 1991. **39**.
60. Hongyu Chen, P.W., Donald G. Baird, *Simulation of Long Semi-flexible Fiber Orientation during Injection Molding.* SPE ANTEC Indianapolis 2016, 2016.
61. Xinghui Chen, Q.Y., Lixia Liu, Wenhua Ji, Li Yang, Dongli Fan, *Research on Mechanical Properties of Carbon Fiber/ Polyamide Reinforced PP Composites.* 2nd International Conference on Materials Science, Resource and Environmental Engineering, 2017.
62. Abdulkadir Gullu, A.O., Emin Ozdemir, *Experimental investigation of the effect of glassf fibres on the mechanical properties of polypropylene (PP) and polyamid 6 (PA6) plastics.* Materials and Design, 2004. **27**.
63. Huan-Chang Tseng, R.-Y.C., Chia-Hsiang Hsu, *Numerical Predictions of Fiber Orientation and Mechanical Properties for Injection Molded Long-Carbon-Fiber Thermoplastic Composites.* Polymer Composites, 2018.
64. N. Klein, G.M., E. Wachtel, *Microstructure of nylon 66 transcrystalline layers in carbon and aramid fibre reinforced composites.* Polymer, 1996. **37**.
65. Jahan, N., *Fiber Orientation Prediction and Strength Evaluation of Composite Spur Gears Reinforced by Discontinuous Fiber*, in *Mechanical Engineering*. 2016, South Dakota State University.

66. Peter H. Foss, H.-C.T., John Snawerdt, Yuan-Jung Chang, Wen-Hsien Yang, Chia-Hsiang Hsu, *Prediction of Fiber Orientation Distribution in Injection Molded Parts Using Moldex3D Simulation.* Polymer Composites, 2013.
67. Jin Wang, B.N.N., Raj Mathur, Bhisham Sharma, Michael D. Sangid, Franco Costa, Xiaoshi Jin, Charles L. Tucker III, Leonard S. Fifield, *FIBER ORIENTATION IN INJECTION MOLDED LONG CARBON FIBER THERMOPLASTIC COMPOSITES.* SPE ANTEC Orlando 2015, 2015.
68. Jin Wang, P.C., Alex Bakharev, Franco Costa, David Astbury, *Prediction of fiber orientation in injection-molded parts using three-dimensional simulations.* AIP Conference Proceedings, 2016. **1713**.
69. Vlastimil Kunc, S.W.C., Hector J. Santos-Villalobos, Srdjan Simunovic, *The stiffness tensor for composites with curved discontinuous fibers.* Composites: Part A, 2015. **72**.
70. Kevin J. Meyer, J.T.H., Donald G. Baird, *Prediction of short glass fiber orientation in the filling of an end-gated plaque.* Composites: Part A, 2014. **62**.
71. Ericksen, J.L., *Transversely Isotropic Fluids.* Kolloid-Zeitschrift, 1960. **173**.
72. G.G. Lipscomb, M.M.D., D.U. Hur, D.V. Boger, *THE FLOW OF FIBER SUSPENSIONS IN COMPLEX GEOMETRIES.* Journal of Non-Newtonian Fluid Mechanics, 1987. **26**.
73. Batchelor, G.K., *The stress generated in a non-dilute suspension of elongated particles by pure straining motion.* Journal of Fluid Mech., 1971. **46**.
74. Goddard, J.D., *TENSILE STRESS CONTRIBUTION OF FLOW-ORIENTED SLENDER PARTICLES IN NON-NEWTONIAN FLUIDS.* Journal of Non-Newtonian Fluid Mechanics, 1976. **1**.
75. Maw-Ling Wang, T.-C.C., *A constitutive approach for studying concentrated suspensions of rigid fibers in a non-Newtonian Ellis fluid.* Journal of the Chinese Institute of Engineers, 2011. **14**.
76. J. Thomasset, P.J.C., B. Sanschagrin, G. Ausias, *Rheological properties of long glass fiber filled polypropylene.* Journal of Non-Newtonian Fluid Mechanics, 2004. **125**.
77. Eberle, A.P.R., *The Dynamic Behavior of a Concentrated Composite Fluid Containing Non-Brownian Glass Fibers in Rheometrical Flows*, in *Chemical Engineering*. 2008, Virginia Polytechnic Institute and State University.
78. kevin Ortman, d.B., Peter Wapperom, Abby Whittington, *Using startup of steady shear flow in a sliding plate rheometer to determine material parameters for the purpose of predicting long fiber orientation.* Journal of Rheology, 2012. **56**.
79. Gregory Lambert, P.W., Donald G. Baird, *Obtaining short-fiber orientation model parameters using non-lubricated squeeze flow.* Physics of Fluids, 2017. **29**.
80. Ortman, K.C., *Assessing an Orientation Model and Stress Tensor for Semi-Flexible Glass Fibers in Polypropylene Using a Sliding Plate Rheometer: for the Use of Simulating Processes*, in *Chemical Engineering*. 2011, Virginia Polytechnic Institute and State University.
81. Mazahir, S.M., *Improvement in Orientation Predictions of High-Aspect Ratio Particles in Injection Mold Filling Simulations*, in *Chemical Engineering*. 2013, Virginia Polytechnic Institute and State University.

82. Shao-Yun Fu, B.L., Edith Mader, Chee-Yoon Yue, Xiao Hu, Yiu-Wing Mai, *Hybrid effects on tensile properties of hybrid short-glass-fiber-and short-carbon-fiber-reinforced polypropylene composites.* Journal of Material Science, 2001. **36**.
83. Hongyu Chen, D.G.B., *Prediction of Young's Modulus for Injection Molded Long Fiber Reinforced Thermoplastics.* Journal of Composite Sciences, 2018.
84. Peter J. Hine, H.R.L., Andrei A. Gusev, *Numerical simulation of the effects of volume fraction, aspect ratio and fibre length distribution on the elastic and thermoelastic properties of short fibre composites.* Composites Science and Technology, 2002. **62**.
85. F. W. J. Van Hattum, C.A.B., *A Model to Predict The Strength of Short Fiber Composites.* Polymer Composites, 1999. **20**.

Chapter 4: Predicting Long Fiber Orientation for Injection Molded Carbon Fiber Reinforced Nylon 6,6

Kennedy R. Boyce[1,2], Peter Wapperom[3], and Donald G. Baird[1,2]
Virginia Polytechnic Institute and State University
Blacksburg, VA USA
1) *Department of Chemical Engineering*
2) *Macromolecules Innovation Institute*
3) *Department of Mathematics*

4.1 Abstract

The goal of this work is to test material characterization techniques developed for measuring and predicting the orientation of fiber reinforced injection molded thermoplastics using long carbon fiber (LCF) reinforced nylon 6,6 (PA 6,6). The properties and behavior of the flow of a fiber reinforced polymer composite during molding are directly related to the mechanical properties of the completed part. Flow affects the orientation of the fibers within the polymer matrix and at locations within the mold cavity. Mechanical properties of fiber reinforced polymer parts, such as stiffness and strength, are controlled by the average length of the fibers and the fiber arrangement. The ability to predict, and ultimately control, flow properties allows for the efficient design of safe parts for industrial uses, such as vehicle parts in the automotive industry. Previous work focused on the development of a system of processes for accurately measuring and modeling material and flow properties for long glass fiber (LGF) reinforced polypropylene (PP). This led to the development of a simulation package that utilizes the finite element method to predict fiber orientation. The authors proved that these experimental and simulation techniques are valid for use with a different, more complex material than that which was previously used. A commercial grade nylon 6,6 reinforced with long carbon fibers was used to test experimental methods and model predictions.

4.2 Introduction

Current trends in the automotive industry show an increased focus on engineering new materials to create lighter vehicles. Like many trends in modern vehicles, carbon fiber composites began in limited production, high cost, and high-performance sectors of the industry. As legislation demands higher environmental standards and individuals become increasingly aware of their carbon footprint, fuel efficiency becomes an ever more important factor for mass production vehicles. Injection molded parts are commonly used in the automotive industry due to their low cost of production, the ability to make complex geometries, and the high speed of production. However, this process has limited material options. Composite materials provide the ability to produce lightweight plastic products with higher mechanical properties, such as modulus and strength, than polymers alone. This allows manufacturers to create lightweight, high performance parts.

In order to injection mold fiber reinforced materials, the fibers are combined with the matrix and chopped into pellets; smaller fiber lengths allow for more intricate part geometries than continuous reinforced materials. The pellets are fed into the injection molder where breakage and mixing occur, resulting in a final piece that has a distribution of fiber lengths arranged in different orientations throughout the part. The mechanical properties of the final part are dependent on the reinforcement length and orientation distributions. Long fiber thermoplastic (LFT) materials are pultruded, so the fibers are continuous throughout the length of the pellet, resulting in an initial fiber length of 10-13 mm as opposed to short fibers that are 0.2-0.4 mm long, regardless of the pellet length. The longer the fiber lengths, the better the material properties that can be expected from the final part. Long fibers are classified as over an aspect ratio of 100. This distinction is drawn because modulus continues to increase with fiber length until that point is reached and then plateaus, as you

can see in Figure 4.1. Strength and impact resistance continue to increase well into lengths that cannot be reached in injection molded parts. Figure 4.1 shows the mechanical properties for glass fiber reinforcement. Glass fibers have an average diameter of 0.010 mm and carbon fibers have an average diameter of 0.005 mm. Due to their different diameters, glass fibers are classified as long at 1 mm and above, and carbon fibers are considered long starting at 0.5 mm.

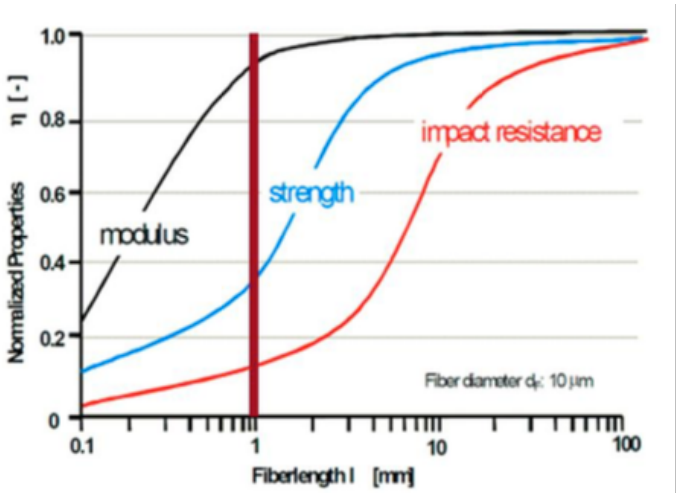

Figure 4.1: Mechanical properties of wet-laid glass reinforced composite dependent on fiber length [1]. Reproduced with permission from the author and Virginia Tech.

It is imperative to be able to understand the orientation evolution of the fiber reinforcement. The ability to model and predict fiber orientation during mold filling allows engineers to tailor mold design for preferred orientation and, therefore, mechanical properties. The proposed research aims to apply work previously conducted by Baird and coworkers [1-9] to new materials. Prior research has been conducted using glass reinforced polypropylene to predict the fiber length and orientation distributions in injection molded parts. The work was successful in center-gated disk (CGD) geometries, matching well the predicted orientation to experimentally obtained data [2]. Fiber orientation is dependent on the flow of the suspension and fiber interactions [10]. Material properties of an injection molded LFT part depend on the microstructures within the part. Therefore, it is important to be able to model

and predict the orientation throughout a final product. The Baird research group [11] has developed a system of equations that can predict orientation of injection molded glass fiber reinforced polypropylene center-gated disks with greater accuracy than the rigid models used by commercially available software. In order to verify the adaptability of the simulation efforts, the authors will be applying the model to a new composite and a new geometry. The system developed by these researchers has not been previously tested using nylon reinforced with carbon fiber.

The majority of the literature for orientation simulations is done with glass reinforced polypropylene composites. The purpose of this research is to investigate the ability to predict orientation and properties of a nylon 6,6 carbon fiber suspension. There are several differences between the two matrix materials. The two have comparable flow and melt properties, such that hybrid polymers have been investigated, PA 6,6 proves to be an effective copolymer to increase the mechanical properties of PP [11]. The chemical structure of PA contains nitrogen and is, therefore, moisture sensitive and requires drying and processing in an inert environment to prevent degradation [12]. PP is also a non-polar polymer, and PA is a polar one [11].

Tseng et al. [13] tested the orientation predictions for a center-gated plaque using Moldex3D which used the iARD-RPR model. They used a PA 6,6 and a PP matrix both reinforced with 40 wt% LGF [13]. They reported that the weight average length was longer in the PP matrix [13]. The injection molding temperature was higher for the PA 6,6 matrix [13]. The shear viscosity of the two suspensions was compared at 300°C, and the PP/LGF suspension shear thinned more than the PA 6,6/LGF [13]. The orientation curves for the two materials show the ability of the model to predict the orientation in the two matrices, and that

the orientation evolution was similar despite the differences in the matrix [13]. Another study by Tseng et al. [14] compares PP and PA 6,6 matrices reinforced with 50 wt% LGF in an injection molded EGP. The PA 6,6 is somewhat sensitive to shear rate and temperature, and the PP is very sensitive to temperature and contains a strong shear thinning slope [14]. The iARD-RSC model is shown to adequately predict the orientation for both composites [14].

Tseng et al. [15] also conducted a study with plaques of PA 6,6 reinforced with LGF and LCF. The average fiber lengths of the carbon fibers, whose diameter was half that of the glass fibers, were preserved to be twice as long as the glass [15]. It is important to note that the plaques of the different material were produced on different machines and by different companies [15]. The iARD-RPR model was used to predict the orientation for both materials [15]. The wall orientation matched for A_{11}, but the core was wider for the LCF material [15]. The predictions for the LGF were closer to experimental results than those for LCF [15]. The authors also note that adding a large number of carbon fibers is more effective in increasing mechanical properties than adding a large number of glass fibers [15].

These three studies conducted by the researchers with the commercially available Moldex software show that PA 6,6 and LCF materials can be modeled using the same techniques used for PP and LGF materials. However, the models are only reasonably accurate. As fiber aspect ratio increases, so does bending. The smaller diameter of carbon fibers makes fiber bending a much greater concern. The iARD-RPR and iARD-RSC models are both adaptations of the basic Folgar-Tucker model [16] of representing fiber orientation with a statistically averaged orientation tensor, a more in-depth explanation of fiber orientation models is continued in the theory portion of this paper. These models both assume that the fibers can be represented by a single “rigid-rod” tensor, empirical parameters

have been added to slow the orientation evolution and account for fiber-fiber interactions. These models present a variety of problems in modeling LFTs. Long fibers bend and are not well represented by a rigid rod. Fiber length is also not accounted for in the orientation equations used for these models, but orientation and mechanical properties are highly dependent on fiber length. Furthermore, these three studies use the bulk rheology of the composite for modeling purposes. It has been proven that a more accurate representation of the flow parameters during injection molding can be achieved by using the rheology of the pure matrix and then account for Brownian motion like fiber interactions using the empirical parameters [17]. Current prediction software uses optimally fit parameters that have been determined for the chosen material, and the rationale is not described [66]. Work by Tseng et al. [3] with Moldex3D reported the same iARD-RSC model parameters used for both carbon fiber and glass fiber suspensions. The work done by the Baird research group [1, 4, 7, 8] has been influential on the development of rheologically determined orientation parameters. Due to the connection of fiber orientation and flow patterns, research has been done to derive the empirical orientation model parameters from rheological flows.

4.2.1 Background for Fiber Orientation Theory

Traditional LFTs are reinforced with glass or carbon fibers and are cut into 10-13 mm long pellets. (The initial length of the pellets does not determine final average lengths for glass or carbon fibers [18].) Within the discontinuous fiber literature “short” refers to fibers that are less than 1 mm in length (usually around 0.2-0.4 mm), and “long” refers to fibers that are 1 mm or longer [15]. The 1 mm threshold was determined from the mechanical behavior of glass fibers. The modulus begins to plateau at 1 mm while the strength and impact resistance continue to rise with increasing fiber length. The diameters of carbon fibers range

from 5-10 microns, making them nearly half that of glass fibers. The aspect ratio (length/diameter) of carbon fibers is approximately twice that of glass fibers, so this modulus plateau happens at a lower length. For example, the plateau begins at the 1 mm mark for glass fibers and that corresponds to an aspect ratio of 100, so the length of glass fiber at the same aspect ratio would be 0.5 mm. This means that carbon fibers exhibit long fiber properties beginning at 0.5 mm.

As pellets undergo processing, the fibers experience a significant amount of breakage. This breakage has many causes: fiber-polymer, fiber-fiber, and fiber-machine interactions [19]. Due to the large number of fibers, tracking and measuring an individual fiber's length would be computationally expensive and unrealistic. Instead, a fiber length distribution is determined. The weight average and number average lengths (L_w and L_n) are used to represent the distribution. Details about the derivation can be found in a paper by Nguyen et al. [20]. When the fibers all have the same length L_w=L_n, for all other systems, L_w>L_n [21]. Equations 4-1 and 4-2 define L_w and L_n in terms of N_i, the number of fibers of length l_i.

$$L_n = \frac{\sum_i N_i l_i}{\sum_i N_i} \tag{4-1}$$

$$L_w = \frac{\sum N_i l_i^2}{\sum N_i l_i} \tag{4-2}$$

In commercial LFTs, the fiber count is too high to track every fiber's individual evolution, so a probability distribution function $\psi(\boldsymbol{p})$ is used. The probability of a fiber being oriented between **p** and **p**+d**p,** ψ, is a statistical representation of the orientation state for a population of particles or fibers in a suspension [22]. This orientation distribution is a complete and unambiguous description of the orientation state that can be calculated from processing conditions. The downside is that it is cumbersome to track, due to its dependence on both the orientation angles of **p** and position [23], which results in too much information for

a numerical simulation [23]. Advani and Tucker [23] developed a set of orientation tensors by taking the dyadic products of the vector **p** and integrating with $\psi(\boldsymbol{p})$ over all orientation directions. The distribution is even, so odd integrals are negated and, therefore, only the even-order tensors are left [23]. The second and fourth order tensors are [20]:

$$A_{ij} = \langle p_i p_j \rangle = \int \psi(\boldsymbol{p}) p_i p_j d\boldsymbol{p} \tag{4-3}$$

$$A_{ijkl} = \langle p_i p_j p_k p_l \rangle = \int \psi(\boldsymbol{p}) p_i p_j p_k p_l d\boldsymbol{p} \tag{4-4}$$

The higher the order of the tensor the more accurately the orientation state is represented [18,19]. The fourth order tensor is the orientation tensor equation. Closure approximations are used to find values for the fourth-order tensor.

Folgar and Tucker [16] developed a mathematic model to predict the orientation distribution function of rigid fibers in concentrated suspensions by adding an isotropic rotary diffusion term to Jeffery's model in which C_I is a phenomenological constant and $\mathbf{I}$ is the unit tensor:

$$\frac{D\mathbf{A}}{Dt} = \mathbf{W}\cdot\mathbf{A} - \mathbf{A}\cdot\mathbf{W} + \xi(\mathbf{D}\cdot\mathbf{A} + \mathbf{A}\cdot\mathbf{D} + 2\mathbf{D}\colon\mathbf{A_4}) + 2C_I\dot{\gamma}(\mathbf{I} - 3\mathbf{A}) \tag{4-5}$$

Their model makes some assumptions about the fibers, the matrix, and the suspension. The fibers are represented by rigid cylinders (uniform in length and diameter). They are large enough that Brownian motion is negligible, and their centers of mass are randomly distributed [16]. They found that the motion for an individual fiber in a concentrated suspension is dependent on its current angle, the flow field, the ability to reorient when interacting with other fibers, and their behavior, which is contingent on angle and flow field, until they interact with another fiber [16]. The isotropic rotary diffusion term C_I must be determined experimentally. As C_I increases, the steady state orientation is more disperse [16]. All of the empirical attempts to model C_I denote the term as a function of fiber size and concentration [17]. Bay et

al. [24] state that other C_I models assume that fiber length and diameter were constant throughout the suspension and proposed that a fiber length distribution would increase the accuracy of modeling C_I trends [24].

Stress growth experiments in the startup of simple shear flow, using glass fiber reinforced polypropylene, demonstrate that orientation kinetics in reality are slower than predicted [4]. A scaling factor, α, a slip parameter with a value between 0-1 is used to reduce the rate of evolution [4]. The right side of Equation 4-5 is multiplied by this factor resulting in the Strain Reduction Factor (SRF) model [4]. The addition of this strain reduction term improves the accuracy of the model, but results in a loss of material objectivity, meaning that the coordinate system cannot be changed, nor the frame rotated, or translated [4]:

$$\frac{D\mathbf{A}}{Dt} = \alpha[\mathbf{W}\cdot\mathbf{A} - \mathbf{A}\cdot\mathbf{W} + \xi(\mathbf{D}\cdot\mathbf{A} + \mathbf{A}\cdot\mathbf{D} + 2\mathbf{D}\colon\mathbf{A_4}) + 2C_I\dot{\gamma}(\mathbf{I} - 3\mathbf{A})] \quad (4\text{-}6)$$

Fibers will rotate, bend, and break in the processing of LFTs, and the configurations of the fibers have a direct relationship to the mechanical properties of the final parts. The longer the reinforcing fibers, the greater the mechanical properties because the discontinuous fibers approach the properties of continuous fibers. However, longer fibers come with more challenges, due to their flexibility, for modeling and predicting orientation [25]. Strautins and Latz [26] developed a system of equations to account for semi-flexible fibers. They concentrated on the effect of local flexibility on the orientation of the long fibers [26]. The long fiber is represented by three beads connected by ball and socket joints with two rigid rods, and, hence, it has been aptly named the bead-rod model, shown in Figure 4.2 [26]. There are two unit vectors **p** and **q** that point from the central bead out to the other two beads.

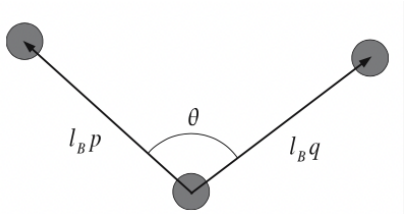

Figure 4.2: A two rod and three bead model of an elastic fiber. The two rods are represented by vectors **p** and **q** [26]. Reproduced with permission from Rheologica Acta journal.

The orientation was put in the familiar Folgar-Tucker notation, but the two vectors resulted in three moments, A, B, and C as defined [27]:

$$\mathbf{A}(t) = \iint \mathbf{pp}\ \psi(\mathbf{p}, \mathbf{q}, t) d\mathbf{p} d\mathbf{q} \tag{4-7}$$

$$\mathbf{B}(t) = \iint \mathbf{pq}\ \psi(\mathbf{p}, \mathbf{q}, t) d\mathbf{p} d\mathbf{q} \tag{4-8}$$

$$\mathbf{C}(t) = \iint \mathbf{p}\ \psi(\mathbf{p}, \mathbf{q}, t) d\mathbf{p} d\mathbf{q} \tag{4-9}$$

A full derivation and description can be found in the work by Strautins and Latz [26]. The **A** tensor is the second moment of any one of the rods with respect to the orientation tensor. The **B** tensor is a mixed second moment of the orientation tensor, and the trace of **B** describes the bending. The **C** tensor is the first moment of the orientation distribution function using either rod's orientation. The bead-rod model was extended to non-dilute suspensions by Ortman et al. [27] by the addition of the isotropic rotary diffusion term. The resulting equations show that the flexibility is induced by a combination of rotary diffusion and hydrodynamic effects, and provide the second moment of the orientation of the end to end vector [27]:

$$\begin{aligned} \frac{D\mathbf{A}}{Dt} &= \alpha((\mathbf{W}\cdot\mathbf{A} - \mathbf{A}\cdot\mathbf{W}) + (\mathbf{D}\cdot\mathbf{A} + \mathbf{A}\cdot\mathbf{D} - 2\mathbf{D}\colon\mathbf{A_4}) \\ &- 6C_I\dot{\gamma}\left(\mathbf{A} - \frac{1}{3}\mathbf{I}\right) + \frac{l_B}{2}[\mathbf{Cm} + \mathbf{mC} - 2(\mathbf{m}\cdot\mathbf{C})\,\mathbf{A}] - 2k[\mathbf{B} - \mathbf{A}\,tr(\mathbf{B})]) \end{aligned} \tag{4-10}$$

$$\frac{D\mathbf{B}}{Dt} = \alpha((\mathbf{W}\cdot\mathbf{B} - \mathbf{B}\cdot\mathbf{W}) + (\mathbf{D}\cdot\mathbf{B} + \mathbf{B}\cdot\mathbf{D} - (2\mathbf{D}\colon\mathbf{A})\mathbf{B}) - 4C_I\dot{\gamma}\mathbf{B} + \frac{l_B}{2}[\mathbf{Cm} + \mathbf{mC} - 2(\mathbf{m}\cdot\mathbf{C})\,\mathbf{B}] - 2k[\mathbf{A} - \mathbf{B}\,tr(\mathbf{B})]) \tag{4-11}$$

$$\frac{D\boldsymbol{C}}{Dt} = \alpha\left(\nabla v^t\cdot\boldsymbol{C} - (\boldsymbol{A}\colon\nabla v^t)\boldsymbol{C} + \frac{l_B}{2}[\boldsymbol{m} - \boldsymbol{C}\,(\boldsymbol{m}\cdot\boldsymbol{C})] - k\boldsymbol{C}[1 - tr(\boldsymbol{B})] - 2C_I\dot{\gamma}\boldsymbol{C}\right) \tag{4-12}$$

$$\boldsymbol{m} = \sum_{i=1}^{3}\sum_{j=1}^{3}\sum_{k=1}^{3}\frac{\partial^2 v_i}{\partial x_j \partial x_k}A_{ijk}e_i \tag{4-13}$$

In these equations, k is the resistive bending potential, and the **m** vector accounts for melt flow induced fiber bending [27]. Note also that the fourth order tensor still needs a closure approximation.

An end-to-end vector, **r,** is drawn from each of the end beads and is used to define a dimensional end-to-end orientation tensor:

$$\boldsymbol{r} \equiv \iint l_B^2(\boldsymbol{p}-\boldsymbol{q})\psi(\boldsymbol{p},\boldsymbol{q},t)\,d\boldsymbol{p}d\boldsymbol{q} = 2l_B^2(\boldsymbol{A}-\boldsymbol{B}) \tag{4-14}$$

$$\mathbf{R} = \frac{\mathbf{r}}{\mathrm{tr}(\mathbf{r})} = \frac{\mathbf{A}-\mathbf{B}}{1-\mathrm{tr}(\mathbf{B})} \tag{4-15}$$

in which l_B is the half fiber length. The degree of bending can then be defined as the reduction in this end- to- end distance. The **R** tensor is shown to predict the orientation evolution for a center-gated disk molded from glass fiber reinforced polypropylene with more accuracy than the basic Folgar-Tucker model [27].

4.3 Experimental Methods

Numlab, a lab developed C-language software package, is the system that was used by the previous researchers and was tested for this work [17, 28]. Numlab requires a Linux/Unix system to operate and was used to conduct the finite element analysis for flow and orientation simulation using the Folgar-Tucker model and the bead-rod model. The accuracy of these simulations was verified by comparison with experimental orientation and tensile data. Several inputs were required for the simulation: fiber length distribution in the part, rheology of the base matrix, and empirical parameters [10]. The bulk of the experimental effort was in collecting the orientation and fiber length data required to input into the code and for verification.

Center-gated disks were injection molded using 13 mm pellets from BASF of nylon 6,6 reinforced with carbon fiber (BASF A3WC8 LFX). The pellets were dried under vacuum at 85°C for four hours before use. Injection molding was conducted in an inert atmosphere using the conditions listed in Table 4.1 (melting point is 265°C). The disks were then cut, as shown in Figure 4.3, to evaluate the orientation and fiber length at multiple locations: 10, 40, and 90 percent of the flow direction. These three locations represent the entrance, Hele-Shaw, and advancing front regions of flow [17]. Fiber length was measured by the needle method per prior research efforts [18, 29, 30]. Test regions were cut from the injection molded parts, the matrix was then removed by pyrolysis, a needle coated in epoxy was pushed through the bed of fibers to extract a plug sample of fibers, and the resin was then removed by pyrolysis which left a sample of loose fibers. The loose fibers were spread on a document scanner and scanned at a resolution of 4,800 dpi. Image j, an image processing program from the National Institutes of Health, was then used to measure the length of the fibers. Currently, carbon fibers must be measured manually because automatic measurement tools will not accurately and consistently detect them due to their small diameters and dull appearance, in comparison to glass fibers [17] . Number and weight averages of the length distribution were then calculated.

Table 4.1: Injection molding parameters for carbon fiber reinforced nylon 6,6. Includes literature suggested parameter ranges and those used in this research [31].

	Suggested [31]	**Used**
Rear Temperature	282-299°C	290.5°C
Center Temperature	288-305°C	296.5°C
Front Temperature	293-310°C	301.5°C
Mold Temperature	93°C	113°C
Injection Speed	51-76 mm/s	63.5 mm/s
Injection Pressure	Medium to max	150 bar
Back Pressure	1.7-3.5 bar	2.6 bar
Screw Speed	30-50 rpm	40 rpm
Shot Size		22.0 mm
Cushion	6.2 mm	1.5 mm

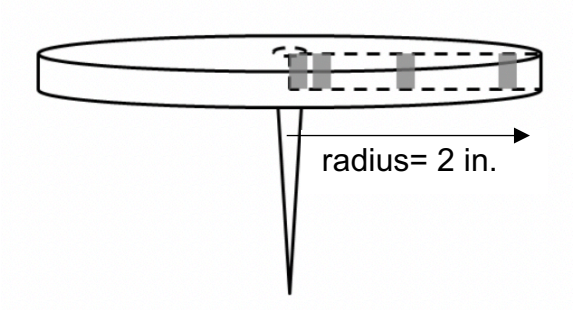

Figure 4.3: Locations of interest for orientation sampling in an injection molded center-gated disk (10%, 40%, 90% of flow direction). Reproduced and altered with permission from Polymer Composites journal.

Orientation data was collected by cutting out samples from the locations of interest and then resin was cured around the samples to hold them in place so that the cross sectional area was visible for imaging. The samples were cut at least 5 mm away from the location of interest on all sides to prevent damage to the fibers that were imaged. A process of gradual sanding and polishing was used to prepare the image surface. This method was detailed by Hofmann and Velez-Garcia [6, 32-35]. An optical microscope was then used to collect micrographs of the cross-sectional area. The micrographs showed the fibers as a series of ellipses and lines; fibers perpendicular to the surface created a circle, fibers parallel to the surface were in the form of a line, and the fibers in between were ellipses. The axes of the ellipses were used to calculate the fibers orientation, this process is called the method of ellipses [6, 32-35]. Analysis was conducted using a combination of image manipulation software and Matlab to measure ellipses and calculate the components of the **A** tensor.

The matrix rheology was needed for the simulation. This was determined using a cone-and-plate rheometer and pure nylon 6,6 from BASF. Steady shear tests were run from 0.1 to $2s^{-1}$, and dynamic oscillatory tests were run from 1 to 100 Hertz. The data were then fit to the Carreau-Yasuda viscosity model.

Non-lubricated squeeze flow (NLSF) was used to collect the empirical parameters required for modeling, α and C_I. This process is an effort to use rheological properties to

determine orientation parameters, greater detail can be found in the work by Lambert [1]. Samples were created by collecting nozzle purge from the injection molder to ensure that the material had undergone the same processing conditions and fiber breakage. The nozzle purge was compression molded to create plaques for testing. The samples underwent non-lubricated squeeze flow at a constant Hencky strain. The orientation was measured from initial compression molded samples and from samples after testing. NLSF was an adequate flow type for testing due to the presence of both shear and elongational regions, similar to the flow patterns present in injection molding.

4.4 Results

The viscosity of the pure Nylon 6,6 resin is shown in Figure 4.4. The viscosity is shown at two temperatures, 285°C and 301.5°C. Figure 4.5 shows the data at 301.5°C fit to the Carreau-Yasuda model, as follows:

$$\eta = \eta_\infty + (\eta_o - \eta_\infty)[1 + (\lambda\dot{\gamma})^a]^{\frac{n-1}{a}} \quad (16)$$

The viscosity of the pure polypropylene resin at 200°C is shown in Figure 4.5, along with the Carreau-Yasuda model. The model fit constants are provided in Table 4.2.

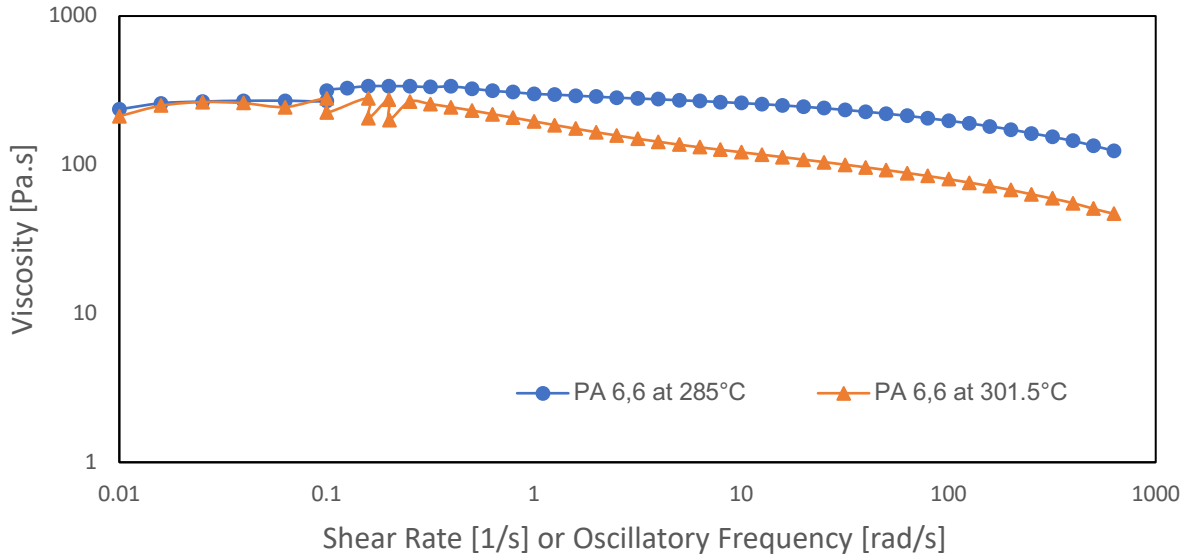

Figure 4.4: Viscosity of pure nylon 6,6 at 285°C and 301.5°C. Steady shear sweep from 0.01-0.20 s^{-1} and oscillatory test from 0.1-628.3 rad/s. Test conducted in an inert atmosphere using a 25 mm cone and plate geometry.

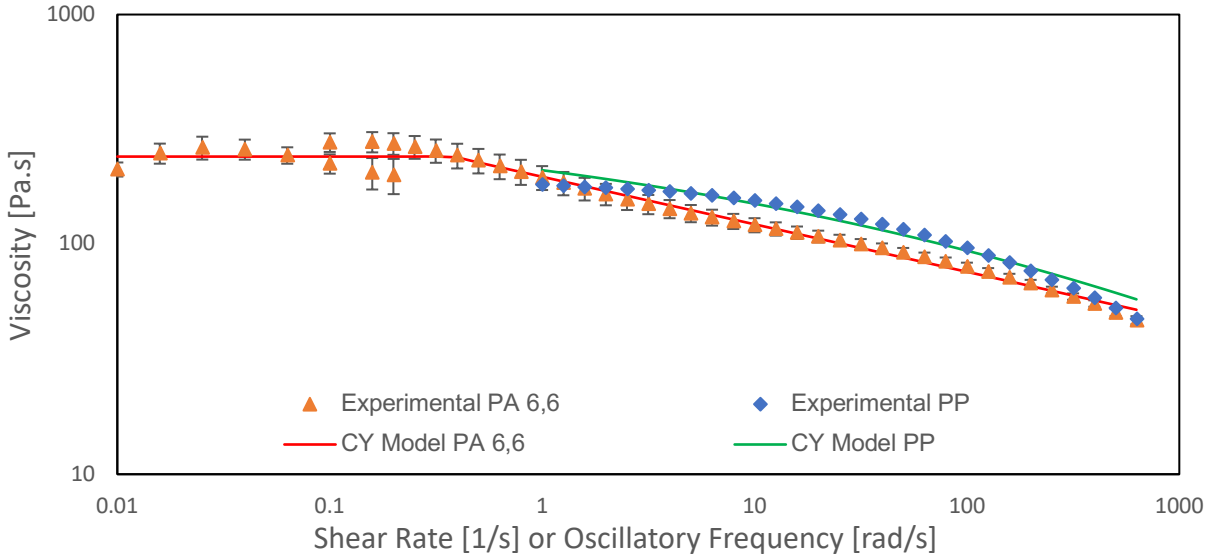

Figure 4.5: Viscosity of pure nylon 6,6 at 301.5°C and pure polypropylene at 200°C, experimental results and the predicted values from the Carreau-Yasuda model. Steady shear sweep from 0.01-0.20 s^{-1} and oscillatory test from 0.1-628.3 rad/s. PA 6,6 test conducted in an inert atmosphere using a 25 mm cone and plate geometry. Error bars represent a 95% confidence interval.

Table 4.2: Carreau- Yasuda viscosity model parameters for pure nylon 6,6 (PA 6,6) at 301.5°C and pure polypropylene (PP) at 200°C.

Carreau Model Parameters	PA 6,6	PP
n	0.793	0.401
a	64.310	0.208
η_0	240.997	402.060
η_∞	0	0
λ	2.657	0.001

Center-gated disks were injection molded using the LCF reinforced PA 6,6. The samples of interest were extracted for fiber length and fiber orientation analysis. Figure 4.6 shows the fiber length distribution for the disks. As one can see, there is a large peak in the short fiber region with a tail toward the more preserved fiber lengths. The number average fiber length was 0.483 mm and the weight average fiber length was 1.242 mm. For glass filled polypropylene the number average length was 0.8 mm and the weight average length was 1.2 mm [17]. Averages are shown in Table 4.3 along with the minimum lengths required to be characterized as a long fiber for each material. Table 4.3 also contains the aspect ratios associated with each length.

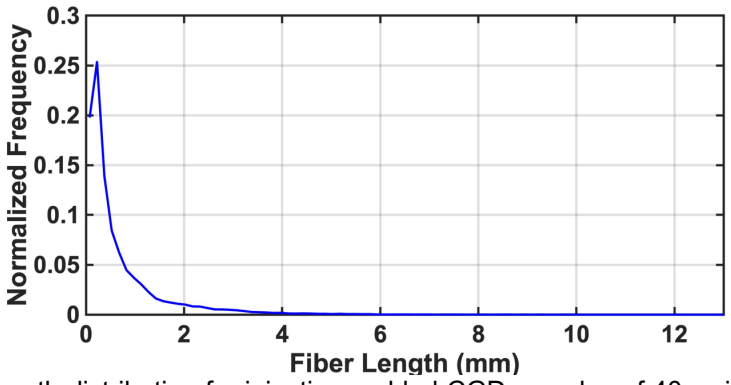

Figure 4.6: Fiber length distribution for injection molded CGD samples of 40 weight percent LCF reinforced nylon 6,6.

Table 4.3: Fiber length comparison for LCF and LGF including aspect ratio. Aspect ratio calculations used the carbon fiber diameter of 0.005 mm and glass fiber diameter of 0.010 mm. Glass fiber length data from Chen [17].

	LCF	Aspect Ratio	LGF	Aspect Ratio
l_n (mm)	0.483	96.6	0.8	80
l_w (mm)	1.242	248.4	1.2	120
Min. length for long fiber (mm)	0.5	100	1.0	100

Figure 4.7 demonstrates the simulation's ability to model the orientation for the LCF reinforced PA 6,6 injection molded center gated disk, three components of the orientation tensor are shown, A_{rr}, A_{zz}, and $A_{\theta\theta}$. Samples were analyzed at 10, 40, and 90% of the flow direction and compared to the results using the strain reduced factor (SRF) model. The empirical model parameters used are α=0.7 and C_I=0.0005. The model parameters for this material were chosen by fitting orientation data to simulated orientation using a non-lubricated squeeze flow (NLSF) [36]. NLSF is a simpler flow to simulate that is still a combination of shear and extensional flows and induces fiber bending.

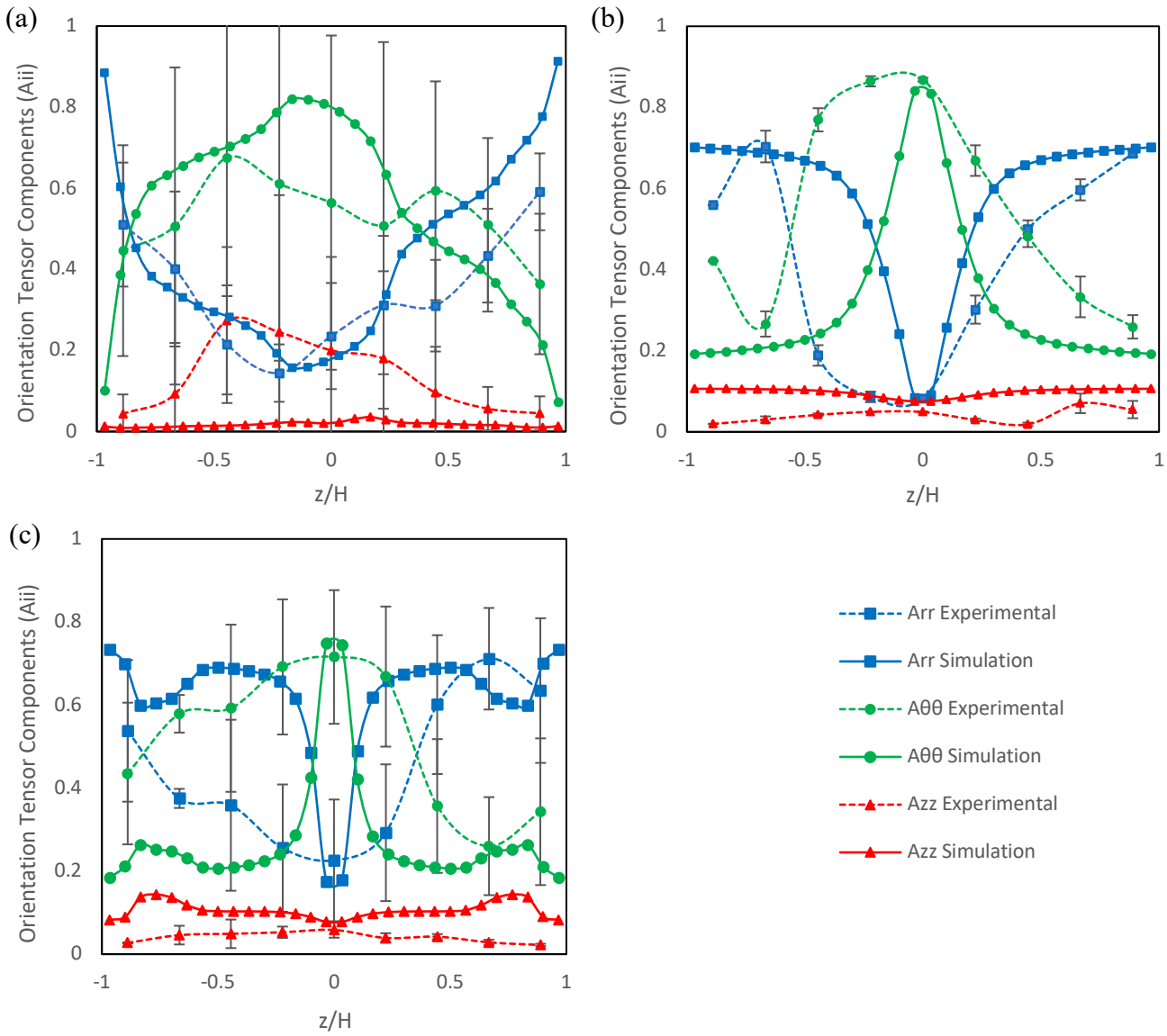

Figure 4.7: Fiber orientation for 40 weight percent long carbon fiber reinforced nylon 6,6 injection molded center gated disk at (a) 10% of the fill direction, (b) 40% of the fill direction, and (c) 90% of the fill direction. The orientation tensor components (A_{rr}, $A_{\theta\theta}$, and A_{zz}) for experimental data are represented by the dotted lines, and SRF model simulation data with the solid lines. The SRF model parameters used are α=0.7 and C_I=0.0005. Error bars represent a 95% confidence interval.

Figure 4.8 shows the A_{rr} orientation tensor component at 40% of the flow direction for the LCF/PA 6,6 injection molded CGD. The experimental data is compared to the SRF model predictions using 5 sets of empirical parameters listed in Table 4.4. The parameters for simulation 1 were used by Chen [17] for 40 weight percent (wt%) LGF/PP. Simulations 2-3 use the C_I value chosen by Chen [17], and increasing α values. The α value for simulation 2

was used by Tseng et al. [13, 14] for 40 wt% LGF/PP, 40 wt% LGF/PA 6,6, 50 wt% LCF/PA 6,6, and 50 wt% LCF/PP. The fourth simulation shown in this figure uses the parameters determined by Boyce [36] by optimizing NLSF simulation results, the α value is the same as the most accurate results comparing the constant C_I tests (1-3) and the C_I value is the same as that used by Tseng et al. for the 50 wt% LCF/PA 6,6 [14]. The fifth simulation tests the same α value as 3 and 4 with a large C_I value.

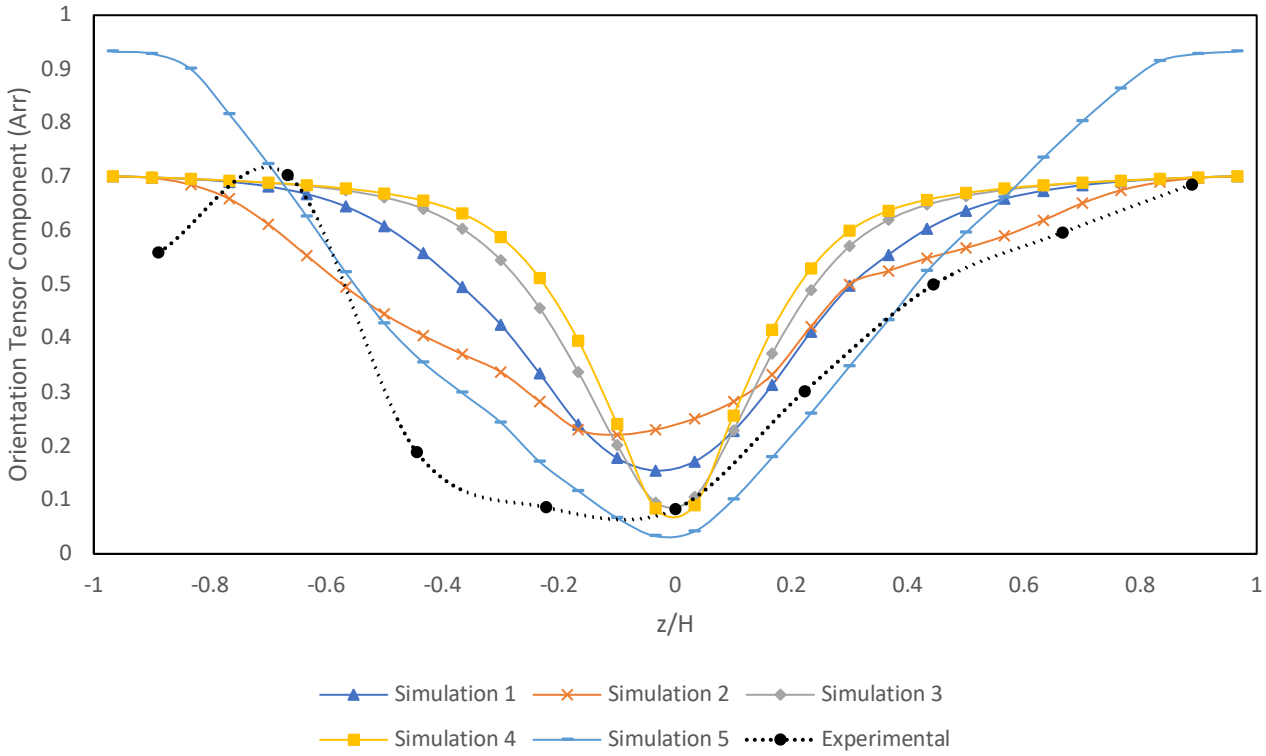

Figure 4.8: Exploration of alternate SRF model simulation parameters for optimization of accurate through-thickness orientation predictions for long carbon fiber reinforced nylon 6,6. Five sets of α and C_I values, listed in Table 4.4, are compared at the Hele-Shaw region of the center gated disk (40% of the flow direction) for the A_{rr} orientation tensor component.

Table 4.4: SRF model simulation parameters considered for optimization of accurate CGD orientation predictions.

Simulation Number	C_I	α
1	0.0200	0.25
2	0.0200	0.10
3	0.0200	0.70
4	0.0005	0.70
5	0.1000	0.70

Figure 4.9 is used to compare the accuracy of the predictions for the LCF/PA 6,6 material to the predictions by Chen et al. [10] for the LGF/PP material. Through thickness orientation profiles are compared for the A_{rr} component in the Hele-Shaw region (40% of the fill direction) of an injection molded center gated disk. The 50 weight percent LGF/PP material was simulated using the rigid Folgar Tucker model with α=0.25 and C_I=0.005 [10]. The 40 weight percent LCF/PA 6,6 material was simulated using the SRF model with α=0.07 and C_I=0.0005.

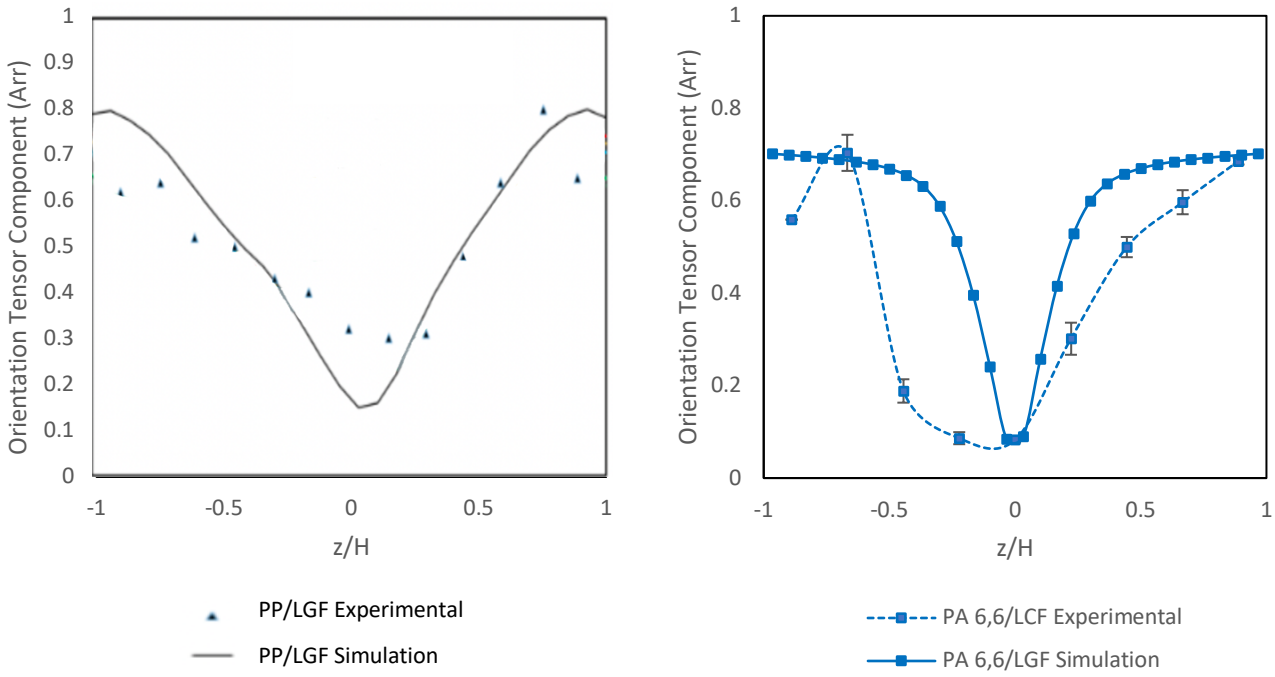

Figure 4.9: (a) Through thickness orientation for 30 weight percent long glass fiber reinforced polypropylene injection molded center gated disk. Experimental and simulation data for the A_{rr} orientation tensor component at 40% of the flow direction. Simulation data was predicted using the rigid Folgar Tucker model with α=0.25 and C_I=0.005. Data from Chen et al [10]. Figure altered with permission from the author and Virginia Tech. (b) Through thickness orientation for 40 weight percent long carbon fiber reinforced nylon 6,6 injection molded center gated disk. Experimental and simulation data for the Arr orientation tensor component at 40% of the flow direction. Simulation data was predicted using the SRF model with α=0.07 and C_I=0.0005. Error bars represent a 95% confidence interval.

4.5 Discussion

The rheological data shown in Figures 4.4 and 4.5 indicate that the polypropylene matrix used by previous researchers [1, 17] is more shear thinning than the nylon 6,6 used for current testing at the processing temperatures used. Although nylon does not shear thin, the onset of degradation is a higher concern than when processing polypropylene. The lack of shear thinning behavior may contribute to the core region being less aligned in the PA 6,6 transverse orientation than the PP. The differences in flow behavior will contribute to a difference in fiber orientation evolution. The viscosity data of both materials are fit well by the Carreau-Yasuda model.

The LCF/PA 6,6 material exhibits the expected fiber length distribution pattern, Figure 4.6, with a large peak of short fiber lengths and a tail into the long fiber region (greater than 0.5). The initial pellet length was 13 mm and a very small number of fibers remained with lengths greater than 5 mm. Table 4.3 lists the number and weight averages, along with the corresponding aspect ratios, for the LCF/PA 6,6 material used in this study and the LGF/PP material that is used for comparison. The carbon fiber experienced greater breakage during processing than the glass fiber at the same concentration and identical initial length. However, as mentioned in the introduction, the carbon fiber demonstrates long fiber behavior at shorter lengths due to its smaller diameter and greater flexibility. These two attributes also contribute to the greater level of fiber attrition. Fibers are classified as long when the aspect ratio is greater than 100. The aspect ratio using both the number average and weight average lengths are greater for the LCF/PA 6,6 material than the LGF/PP material. Therefore, the carbon fiber should exhibit more long fiber behavior.

The LCF/PA 6,6 through-thickness orientation evolution follows the expected pattern. There is a shell-core-shell configuration with the core narrowing as it moves outward in the

flow direction. In the entry region (Figure 4.7a) the pattern is beginning to form with a very wide core region because the fibers have not begun to heavily align in the center from the extensional flow. The SRF model was able to predict the orientation evolution for all three tensor components well in this region, but there was a large amount of variation between the experimental samples. In the Hele-Shaw region (Figure 4.7b), the pattern was well developed with a small variation between experimental samples. The SRF model was able to predict the orientation in the center and wall regions due to the large alpha value. The center and the wall are dominated by extensional flow, and the alpha value is 1 for true extensional flow [1]. Therefore, when the alpha value was optimized at 0.7, the predictions will be more accurate in extensional regions than the shear dominated zones. Greater experimental variation was observed in the advancing front region (Figure 4.7c) than the Hele-Shaw but significantly less than the entry region. The SRF model was able to predict the orientation in this region with reasonable success.

The A_{rr} component in the Hele-Shaw region was used to explore the effects of changing the empirical parameters on the accuracy of the SRF model predictions for the LCF/PA 6,6 through thickness orientation in the CGD, Figure 4.8. Table 4.4 lists the combinations of α and C_I values shown in Figure 4.8. The parameters used by Chen [17] (Simulation 1) predicted the A_{rr} component as more aligned than the experimental data. Using the C_I from Chen [17] and the α from Tseng et al. [13, 14] (Simulation 2) produced a prediction that did not model the experimental data to an acceptable level of accuracy, increasing the α value while keeping the C_I constant (Simulation 3) improved the predictions by narrowing the core region and lowering the alignment. Using the C_I value from Tseng et al. [13, 14] and the large α value (Simulation 4) produced the best SRF model values which verifies the optimized parameters determined by fitting NLSF data to simulation results [36].

Figure 4.9 compares the through thickness orientation data for an injection molded CGD of 30 wt% LGF/PP and 40 wt% LCF/PA 6,6. The A_{rr} component at the Hele-Shaw region is used for comparison. The LGF/PP material was modeled using the rigid Folgar Tucker model and the LCF/PA 6,6 material was modeled using the SRF model. The simulation was able to model the orientation of the LCF/PA 6,6 material to a similar degree of accuracy. Due to the larger alpha values the predictions are better for the LCF/PA 6,6 material in the core region and along the wall because the flow is extension dominated. The simulation work for the LGF/PP material used a smaller alpha value which had better predictions in the area around $z/H=\pm 0.5$ due to this being a shear flow dominated region.

4.6 Conclusions and Recommendations for Future Work

The two long fiber composites compared in this paper, long carbon fiber reinforced nylon 6,6 and long glass fiber reinforced polypropylene, have different properties. The nylon carbon fiber composite is favored by the automotive industry due to its superior mechanical properties, but it is much more difficult to process and requires an added level of care when handling. The LGF/PP material has given researchers the ability to analyze a discontinuous fiber reinforced material efficiently and without the added challenges of a complex material.

The experimental methods set in place to collect and analyze the length and orientation of samples were initially developed using the LGF/PP material. The same experimental techniques have been proven to work for understanding the LCF/PA 6,6 material when the appropriate material preparation, temperature, and atmospheric considerations are made. The simulation package developed by the authors has also been proven to be able to adequately be adjusted to account for the new material. Inputs were adjusted for the change in processing conditions, the different material properties, and

updated empirical parameters. With the changes that were made the simulation package was able to use the strain reduced factor method to predict the orientation for the LCF/PA 6,6 material.

Future studies of this material will need to include testing the simulation using the bead-rod long fiber model. The bead-rod model was previously proven to increase the accuracy of the orientation predictions for LGF/PP [17]. The bead-rod model accounts for the length and bending potential of long fibers. The aspect ratios for the LCF/PA 6,6 material are significantly longer than those reported for LGF/PP [17] and, therefore, it can be predicted that using the bead-rod model will significantly increase the accuracy of the orientation predictions for the LCF/PA 6,6 material. Further studies should also include the use of a variable alpha parameter. Chen et al. [37] began the process of using an alpha parameter that was a function of a flow type parameter. By accounting for the shear and extensional flow regions, this was able to adjust the alpha value throughout the thickness of the part with smaller values in the shear dominated regions and larger values in the extensional flow regions. This variable parameter was able to drastically increase the orientation predictions for the LGF/PP material [37]. If this model can be updated for use with the LCF/PA 6,6 material it will greatly improve the material predictions. The results of this study showed the dependency of the model predictions on the alpha parameter. The different simulations conducted using different values were each closer to the experimental data in different regions (Figure 4.8). Therefore, the implementation of the variable alpha would allow for the correct alpha value for each region of the orientation evolution.

4.7 Acknowledgements

The authors thank Ford Motor Company for their support and partial funding of this project.

Works Cited

1. Lambert, G., *Using Non-Lubricated Squeeze Flow to Obtain Empirical Parameters for Modeling the Injection Molding of Long-Fiber Composites*, in *Chemical Engineering*. 2018, Virginia Polytechnic Instititue and State University.
2. Hongyu Chen, D.G.B., *Prediction of Young's Modulus for Injection Molded Long Fiber Reinforced Thermoplastics.* Journal of Composite Sciences, 2018.
3. Harrington, K.D., *Factors Affecting Fiber Orientation and Properties in Semi-Flexible Fiber Composites: Including the Addition of Carbon Nanotubes*, in *Chemical Engineering*. 2015, Virginia Polytechnic Institute and State University.
4. Meyer, K.J., *Improved Prediction of Glass Fiber Orientation in Basic Injection Molding Geometries*, in *Chemical Engineering*. 2013, VIrginia Tech.
5. Ortman, K.C., *Assessing an Orientation Model and Stress Tensor for Semi-Flexible Glass Fibers in Polypropylene Using a Sliding Plate Rheometer: for the Use of Simulating Processes*, in *Chemical Engineering*. 2011, Virginia Polytechnic Institute and State University.
6. Velez-Garcia, G.M., *Experimental Evaluation and Simulations of Fiber Orientation in Injection Molding of Polymers Containing Short Glass Fibers*, in *Chemical Engineering*. 2012, Virginia Polytechnic Institute and State University.
7. Eberle, A.P.R., *The Dynamic Behavior of a Concentrated Composite Fluid Containing Non-Brownian Glass Fibers in Rheometrical Flows*, in *Chemical Engineering*. 2008, Virginia Polytechnic Institute and State University.
8. Cieslinski, M.J., *Using a Sliding Plate Rheometer to Obtain Material Parameters for Simulation Long Fiber Orientation in Injection Molded Composites*, in *Chemical Engineering*. 2015, Virginia Polytechnic Institute and State University.
9. Herrington, K.D., *Factors Affecting Fiber Orientation and Properties in Semi-Flexible Fiber Composites: Including the Addition of Carbon Nanotubes*, in *Chemical Engineering*. 2015, Virginia Polytechnic Institute and State University.
10. Hongyu Chen, P.W., Donald G. Baird, *Simulation of Long Semi-flexible Fiber Orientation during Injection Molding.* SPE ANTEC Indianapolis 2016, 2016.
11. Xinghui Chen, Q.Y., Lixia Liu, Wenhua Ji, Li Yang, Dongli Fan, *Research on Mechanical Properties of Carbon Fiber/ Polyamide Reinforced PP Composites.* 2nd International Conference on Materials Science, Resource and Environmental Engineering, 2017.
12. Abdulkadir Gullu, A.O., Emin Ozdemir, *Experimental investigation of the effect of glassf fibres on the mechanical properties of polypropylene (PP) and polyamid 6 (PA6) plastics.* Materials and Design, 2004. **27**.
13. Huan-Chang Tseng, R.-Y.C., Chia-Hsiang Hsu, *Numerical predictions of fiber orientation and mechanical properties for injection-molded long-glass-fiber thermoplastic composites.* Composites Science and Technology, 2017. **150**.

14. Huan-Chang Tseng, R.-Y.C., Chia-Hsiang Hsu, *Numerical Predictions of Fiber Orientation and Mechanical Properties for Injection Molded Long-Carbon-Fiber Thermoplastic Composites.* Polymer Composites, 2018.
15. Huan-Chang Tseng, R.-Y.C., Chia-Hsiang Hsu, *Numerical prediction of fiber orientation and mechanical performance for short/long glass and carbon fiber-reinforced composites.* Composites Science and Technology, 2017. **144**.
16. Fransisco Folgar, C.L.T.I., *Orientation Behavior of Fibers in Concentrated Suspensions.* Reinforced Plastics and Composites, 1984. **3**: p. 98-119.
17. Hongyu Chen, D.G.B., *Experimental Evaluation of Fiber Length Distribution and Modeling of Fiber Orientation and Elastic Properties for Long Glass Fiber Reinforced Thermoplastics*, in *Chemical Engineering*. 2017, Virginia Polytechnic Institute and State University.
18. Hongyu Chen, M.C., Donald G. Baird, *Progress in Modeling Long Glass and Carbon Fiber Breakage during Injection Molding.* Proceedings of PPS-30, 2015.
19. S.-Y. Fu, B.L., E. Mader, C.-Y. Yue, X. Hu, *Tensile properties of short-glass-fiber- and short-carbon-fiber-reinforced polypropylene composites.* Composites: Part A, 2000. **31**.
20. Ba Nghiep Nguyen, S.K.B., James D. Holbery, Mark T. Smith, Vlastimil Kunc, Barbara J. Frame, Jay H. Phelps, Charles L. Tucker III, *Fiber Length and Orientation in Long-Fiber Injection-Molded Thermoplastics- Part I: Modeling of Microstructure and Elastic Properties.* Composite Materials, 2008. **42**: p. 1003-1029.
21. Jay H. Phelps, A.I.A.E.-R., Vlastimil Kunc, Charles L. Tucker III, *A model for fiber length attrition in injection molded long-fiber composites.* Composites: Part A, 2013.
22. Jay H. Phelps, C.L.T.I., *An anisotropic rotary diffusion model for fiber orientation in short- and long-fiber thermoplastics.* Journal of Non-Newtonian Fluid Mechanics, 2008. **156**.
23. Suresh G. Advani, C.L.T.I., *The Use of Tensors to Describe and Predict Fiber Orientation in Short Fiber Composites.* Journal of Rheology, 1987. **31**.
24. Randy S. Bay, C.L.T.I., *Stereological Measurement and Error Estimates for Three Dimensional Fiber Orientation.* Polymer Engineering and Science, 1992. **32**(4): p. 240-253.
25. Gang Wang, W.Y., Chixing Zhou, *Optimization of the rod chain model to simulate the motions of a long flexible fiber in simple shear flows.* European Journal of Mechanics B/Fluids, 2005. **25**.
26. Uldis Strautins, A.L., *Flow-driven orientation dynamics of semiflexible fiber systems.* Rheol Acta, 2007. **46**: p. 1057-1064.
27. Kevin Ortman, D.B., Peter Wapperom, Alex Aning *Prediction of Fiber Orientation in the Injection Molding of Long Fiber Suspensions.* Polymer Composites, 2012: p. 1360-1367.
28. Mazahir, S.M., *Improvement in Orientation Predictions of High-Aspect Ratio Particles in Injection Mold Filling Simulations*, in *Chemical Engineering*. 2013, Virginia Polytechnic Institute and State University.
29. Sebastian Goris, T.B., Angel Yanev, Dave Brands, Dietmar Drummer, Tim A. Osswald, *A Novel Fiber Length Measurement Technique for Discontinuous Fiber-Reinforced Composites: A Comparative Study with Existing Methods.* Polymer Composites, 2017.

30. Vlastimil Kunc, B.F., Ba Nghiep Nguyen, Barbara Frame, Charles L. Tucker, *Fiber Length Distribution Measurement for Long Glass and Carbon Fiber Reinforced Injection Molded Thermoplastics.* 2007.
31. Plasticomp, *Molding guidelines and processing conditions for Complet long fiber composite pellets.* 2018.
32. Hofmann, J.T., *Extension of the Method of Ellipses to Determining the Orientation of Long, Semi-flexible Fibers in Model 2- and 3-dimensional Geometries*, in *Macromolecular Science and Engineering*. 2013, Virginia Polytechnic Institute and State University.
33. G.M. Velez-Garcia, P.W., V. Kunc, D.G. Baird, A. Zinc-Sharp, *Sample preparation and image acquisition using optical-reflective microscopy in the measurement of fiber orientation in thermoplastic composites.* Journal of Microscopy, 2012. **248**: p. 23-33.
34. Gregorio M. Velez-Garcia, P.W., Donald G. Baird, Alex O. Aning, Vlastimil Kunc, *Unambiguous orientation in short fiber composites over small sampling area in a center gated disk.* Composites: Part A, 2011. **43**.
35. John T. Hofman, G.M.V.-G., Donald G. Baird, Abby R. Whittington, *Application and Evaluation of the Method of Ellipses for Measuring the Orientation of Long, Semi-Flexible Fibers.* Polymer Composites, 2013.
36. Boyce, K., *Modeling Fiber Orientation using Empirical Parameters Obtained from Non-Lubricated Squeeze Flow for Injection Molded Long Carbon Fiber Reinforced Nylon 6,6* in *Chemical Engineering*. 2021, Virginia Polytechnic Institute and State University.
37. Hongyu Chen, P.W., Donald G. Baird, *A model incorporating the effects of flow type on fiber orientation or flows with mixed flow kinematics.* Journal of Rheology, 2019. **63**.

Chapter 5: Conclusions and Recommendations for Future Work

5.1 Conclusions

The research conducted for the compilation of this dissertation accomplished the goals outlined in Chapter 1. The following conclusions were drawn based on the use of long carbon fiber reinforced polyamide 6,6 material for orientation simulations. A cone and plate rheometer was used to measure the matrix rheology for pure PA 6,6 and produced adequate viscosity data for simulation of the injection molded orientation. The process of using the matrix rheology in simulation of the flow produced sufficient predictions for the orientation of the LCF/PA 6,6 composite confirming the use of this decoupled approach. The LCF/PA 6,6 material and LGF/PP material had viscosities of similar magnitude at their respective processing temperatures, but the LGF/PP was significantly more shear thinning (shown in Figure 3.5). The variations in viscosity led to a significant difference in the orientation evolution between the two materials (Figure 3.9).

The process of obtaining experimental orientation and fiber length data outlined in Chapters 3 and 4 produced repeatable and reliable values for both the injection molded center gated disk and the rectangular compression molded sample. The aspect ratio (a_r) for the previously tested LGF/PP material was 120, and the LCF/PA 6,6 material, used for this study, had an a_r value of 248. Using the LCF/PA 6,6 allowed the researchers to test the simulation package for an aspect ratio range that was not possible with glass fiber materials. The strain reduction factor (SRF) model was used to predict the fiber orientation for the center gated disk geometry with reasonable levels of accuracy.

The SRF model empirical parameters, α and C_I, were determined using non-lubricated squeeze flow (NLSF) as a simplified processing method that contained both shear and extensional flows. The injection molder nozzle purge was compression molded with a controlled initial fiber orientation. The methodology developed by Lambert et al. [1] (outlined in Chapter 2) was modified for this work. Previous researchers [1] used a mold that contained a punch and die that were the same thickness and therefore generated excess flash. The author designed a new mold that had a deeper mold cavity and produced a specimen that was near net shape [1]. This allowed for less initial plies needed to create a final part with the desired thickness of 8 mm. The new mold design incorporated an 8 mm difference between the depth of the cavity and thickness of the punch. The initial plies were then weighed and inserted into the mold and pressed to the final thickness. Using the density and size of the desired specimen controlled the amount of material that was loaded into the mold cavity. The void created between the mold cavity and the punch, along with the proper charge weight, allowed for less flash to be produced. This improved mold design was required for the moisture sensitive PA 6,6 material and decreased the amount of time at the processing temperature thus leading to less degradation. The nozzle purge that was extruded from the injection molder was loaded into the mold cavity by aligning the cut pieces in the transverse direction, shown in Figure 3.2. The transversely aligned initial orientation resulted in greater fiber movement. Therefore, the resulting fiber alignment was greater than what the simulation predicted.

The SRF model simulation was initially tested for the NLSF using a SGF/PP material (a_r=53) [1]. The long carbon fibers (a_r=248) aligned more greatly in the flow

direction during testing than the model accounted for, due to the large aspect ratio difference. The rheological behavior of the PP matrix was previously simplified to be represented as a Newtonian fluid in the simulation. Successful adaptations were made to account for the viscosity behavior of the PA 6,6 matrix more accurately being represented by the Carreau-Yasuda model. Despite the increase in fiber aspect ratio, the greater fiber movement, and the differences in matrix viscosity, empirical parameters for the SRF model were able to be determined using this methodology. The use of these model parameters ultimately produced fiber orientation predictions for the LCF/PA 6,6 composite in an injection molded center gated disk that corresponded well to the measured experimental orientation.

5.2 Recommendations for Future Work

It is the understanding of the researchers that if the following studies are conducted, they will build upon the findings of this work and increase the ability to accurately predict the material and mechanical properties of long fiber reinforced thermoplastics. The recommendations can be classified into a three step process:

1.) Improving fiber orientation predictions;

2.) Obtaining empirical parameters using rheology;

3.) Predicting the mechanical properties.

5.2.1 Improving Fiber Orientation Predictions

The first recommendation is to expand the use of the bead-rod model to be able to use the LCF/PA 6,6 material. The bead-rod model more accurately accounts for the bending and flexing that long fibers will experience [2]. This model has only been able to

be tested with LGF/PP, but significantly increased the accuracy of those orientation predictions [3]. Based on the current understanding of long fiber simulations, it can be expected that the use of the bead-rod model for LCF/PA 6,6 predictions will have an even greater impact on the accuracy of the predictions than it had on the LGF/PP material due to the scale of the aspect ratios. It is also recommended that future studies be invested in modeling NLSF using the bead-rod method based upon the same logic.

Future work is also needed in the development of a flow-dependent α parameter. Chen et al. [4] began the process of using an alpha parameter that was a function of a flow type parameter. By accounting for the shear and extensional flow regions, it was possible to adjust the alpha value throughout the thickness of the part with smaller values in the shear dominated regions and larger values in the extensional flow regions. This variable parameter was able to drastically increase the orientation predictions for the LGF/PP material [4]. If this model can be updated for use with the LCF/PA 6,6 material, it will greatly improve the material predictions. The results of this study showed the dependency of the model predictions on the alpha parameter. The different simulations conducted using different parameter values were each closer to the experimental data in different regions (Figure 4.8). Therefore, the implementation of the variable alpha would allow for the correct alpha value for each region of the orientation evolution.

The final recommendation for this step is to extend the simulation package developed for the two-dimensional center-gated disk geometries to the prediction of the orientation and stiffness of three-dimensional end-gated plaque geometries. Orientation modeling is often started with a center-gated disk (CGD) due to its radial symmetry and

two-dimensional geometry. The end-gated plaque (EGP) is used to test orientation predictions in a three-dimensional flow. The EGP flow front is flat and the flow is unidirectional and dominated by simple shear in most of the cavity [5]. The radial flow pattern in the CGP causes a combination of shear and elongational flow leading to the wider core [5]. The flow length in the CGP is also half the length of the EGP, and, thus, the shell layers are thinner because the fibers have less time to align [5]. Meyer et al. [6] analyzed EGPs injection molded from short and long glass fiber reinforced PP. In the EGP prediction of LGF reinforced PP, a non-isothermal decoupled approach was used to determine the accuracy of the rigid and semi-flexible models [6]. Once again, parameters determined from simple shear rheology that had been tested for CGD could not be used for sufficient prediction of EGP orientation evolution [6]. Some effort was investigated into the exploration of an EGP geometry with the LCF/PA 6,6 material for this study, but it was determined that the CGD should be used for simulation first for the new material.

5.2.2 Obtaining Empirical Parameters Using Rheology

Experimentally measuring fiber orientation is an extremely time consuming and tedious process. Using NLSF to determine empirical parameters provides a testing method that includes both shear and extensional flows, but is isothermal, has a controllable initial orientation, has faster convergence for simulation purposes. These properties make the NLSF prime for a parameter fitting test. However, the ultimate thrust of this work is to be able to couple the fiber orientation to the stress-growth data. The work of Cieslinski [7] proved that the Lipscomb [8] stress tensor was insufficient for predicting the stress growth during startup of shear. The stress model was unable to

predict the experimentally observed stress overshoot when using measured values for the fourth order orientation tensor. The rheological behavior could be accurately predicted if the stress model used the theoretical values (predicted by orientation models) for the orientation tensor. This led to the assumption that the stress model had the ability to predict the correct behavior, but was using an incorrect mechanism [9]. Another technique attempted by Cieslinksi [7] was a stress model that utilized the direct interactions between fibers, but the conclusion was that this still would not increase the model's accuracy. The stress overshoot during the startup of shear behavior was not observed for a pure resin [9]. This is a characteristic that appears to be driven by fiber-matrix interactions. Further exploration of this phenomena is needed to be able to determine the appropriate mechanism to predict orientation data.

The work of Lambert [9] also explored the use of the Lipscomb model in NLSF. The parameters determined from the startup of shear stress data over predicted the stress growth during NLSF [9]. Once again, the predicted stress did not represent the pattern of the transient behavior well. The purely viscous Lipscomb model is not sufficient for capturing elastic behavior which is observed during NLSF. Future work should be conducted to explore the use of a viscoelastic stress tensor model that has the capacity to account for the elastic behavior of the polymer and fibers.

5.2.3 Predicting the Mechanical Properties

Mechanical properties are dependent on fiber length and orientation. The ultimate goal of predicting material properties is to be able to use them for the prediction of mechanical properties. Future work is needed to expand the processes used in this study for measuring and predicting the properties of the LCF/PA 6,6 to be able to

predict the mechanical properties of a final part. The tensile strength and modulus of composites increase with an increase concentration of carbon fiber [10]. Elastic properties are calculated using fiber concentration, fiber length, and fiber orientation [11]. The Tsai-Halpin equation is the most widely used micromechanical model due to the ease of implementation and gives a reasonable estimate for stiffness [11, 12]. Chen et al. [11] proved that the Mori-Tanaka model based on the Eshelby's equivalent inclusion method gave the best predictions. For modulus computation, the Tsai-Halpin equations were used to predict the compliance matrix, and the stiffness matrix was, of course, the inverse [11]. The EMT method combined Eshelby's equivalent inclusion method and Mori-Tanaka's back stress analysis [11]. This method was proven to be valid for large volume fractions of fibers. The EMT method resulted in the overall stiffness of the composite weakened by fiber-end cracks [11]. These methods use a reference composite stiffness that is averaged over the fiber orientation state using the **A** tensor (greater details can be found in Chapter 2).

The model for the strength of a discontinuous fiber composite uses a similar approach. The strength model is not formatted for the orientation tensor (**A**). The tensile strength is greatly dependent on the length of the fibers, and, therefore, the unidirectional strength was adapted to account for a fiber length distribution resulting in a length averaged longitudinal strength [13]. The properties of the final composite were taken as an average of the unidirectional properties over all directions weighted by a fiber orientation distribution function.

Future work should be performed to utilize the fiber length and orientation properties determined in this study for the LCF/PA 6,6 material. The predicted orientation tensor can be used to calculate the predicted modulus. The author predicts that by taking the steps outlined in 5.2.1 to improve the orientation predictions model will in turn improve the modulus predictions. More studies will need to be conducted in order to adapt the fiber orientation distribution function used for strength modeling to a format that can be used with the current orientation tensor nomenclature.

Works Cited

1. Gregory Lambert, P.W., Donald G. Baird, *Obtaining short-fiber orientation model parameters using non-lubricated squeeze flow.* Physics of Fluids, 2017. **29**.
2. Ortman, K.C., *Assessing an Orientation Model and Stress Tensor for Semi-Flexible Glass Fibers in Polypropylene Using a Sliding Plate Rheometer: for the Use of Simulating Processes*, in *Chemical Engineering*. 2011, Virginia Polytechnic Institute and State University.
3. Hongyu Chen, P.W., Donald G. Baird, *Simulation of Long Semi-flexible Fiber Orientation during Injection Molding.* SPE ANTEC Indianapolis 2016, 2016.
4. Hongyu Chen, P.W., Donald G. Baird, *A model incorporating the effects of flow type on fiber orientation or flows with mixed flow kinematics.* Journal of Rheology, 2019. **63**.
5. Jin Wang, B.N.N., Raj Mathur, Bhisham Sharma, Michael D. Sangid, Franco Costa, Xiaoshi Jin, Charles L. Tucker III, Leonard S. Fifield, *FIBER ORIENTATION IN INJECTION MOLDED LONG CARBON FIBER THERMOPLASTIC COMPOSITES.* SPE ANTEC Orlando 2015, 2015.
6. Meyer, K.J., *Improved Prediction of Glass Fiber Orientation in Basic Injection Molding Geometries*, in *Chemical Engineering*. 2013, VIrginia Tech.
7. Cieslinski, M.J., *Using a Sliding Plate Rheometer to Obtain Material Parameters for Simulation Long Fiber Orientation in Injection Molded Composites*, in *Chemical Engineering*. 2015, Virginia Polytechnic Institute and State University.
8. G.G. Lipscomb, M.M.D., D.U. Hur, D.V. Boger, *THE FLOW OF FIBER SUSPENSIONS IN COMPLEX GEOMETRIES.* Journal of Non-Newtonian Fluid Mechanics, 1987. **26**.
9. Lambert, G., *Using Non-Lubricated Squeeze Flow to Obtain Empirical Parameters for Modeling the Injection Molding of Long-Fiber Composites*, in *Chemical Engineering*. 2018, Virginia Polytechnic Instititue and State University.

10. Shao-Yun Fu, B.L., Edith Mader, Chee-Yoon Yue, Xiao Hu, Yiu-Wing Mai, *Hybrid effects on tensile properties of hybrid short-glass-fiber-and short-carbon-fiber-reinforced polypropylene composites.* Journal of Material Science, 2001. **36**.
11. Hongyu Chen, D.G.B., *Prediction of Young's Modulus for Injection Molded Long Fiber Reinforced Thermoplastics.* Journal of Composite Sciences, 2018.
12. Peter J. Hine, H.R.L., Andrei A. Gusev, *Numerical simulation of the effects of volume fraction, aspect ratio and fibre length distribution on the elastic and thermoelastic properties of short fibre composites.* Composites Science and Technology, 2002. **62**.
13. F. W. J. Van Hattum, C.A.B., *A Model to Predict The Strength of Short Fiber Composites.* Polymer Composites, 1999. **20**.